INFORMATION TO USERS

This manuscript has been reproduced from the microfilm master. UMI films the text directly from the original or copy submitted. Thus, some thesis and dissertation copies are in typewriter face, while others may be from any type of computer printer.

The quality of this reproduction is dependent upon the quality of the copy submitted. Broken or indistinct print, colored or poor quality illustrations and photographs, print bleedthrough, substandard margins, and improper alignment can adversely affect reproduction.

In the unlikely event that the author did not send UMI a complete manuscript and there are missing pages, these will be noted. Also, if unauthorized copyright material had to be removed, a note will indicate the deletion.

Oversize materials (e.g., maps, drawings, charts) are reproduced by sectioning the original, beginning at the upper left-hand corner and continuing from left to right in equal sections with small overlaps. Each original is also photographed in one exposure and is included in reduced form at the back of the book.

Photographs included in the original manuscript have been reproduced xerographically in this copy. Higher quality 6" x 9" black and white photographic prints are available for any photographs or illustrations appearing in this copy for an additional charge. Contact UMI directly to order.

UMI

A Bell & Howell Information Company
300 North Zeeb Road, Ann Arbor MI 48106-1346 USA
313/761-4700 800/521-0600

SPECTROSCOPY OF MASS-SELECTED TRANSITION METAL CLUSTERS IN ARGON MATRICES

by

HANAE HAOUARI

A dissertation submitted to the Graduate Faculty in Chemistry in partial fulfillment of the requirements for the degree of Doctor of Philosophy, The City University of New York.

1996

This manuscript has been read and accepted for the Graduate Faculty in Chemistry in satisfaction of the dissertation requirement for the degree of Doctor of Philosophy.

7/30/96
date

Chairman of Examining Committee

7/31/96
date

Executive Officer

Supervisory Committee

The City University of New York

ABSTRACT

SPECTROSCOPY OF MASS-SELECTED TRANSITION METAL CLUSTERS IN ARGON MATRICES

by

HANAE HAOUARI

Advisors: Derek M. Lindsay and John R. Lombardi.

The chemistry of metal clusters is a fascinating and expanding area of research. During the last three decades, the study of metal clusters and in particular transition metal clusters has been the subject of numerous experimental and theoretical investigations. The desire to understand the frontier between molecular chemistry and solid state physics, as well as gaining new insight into the chemical properties of the metal surfaces used in heterogeneous catalysis are one of the motivations for the extensive work done on metal clusters.

The deposition " soft-landing " of size selected nickel dimer, tantalum dimer, rhodium dimer, ruthenium dimer, zirconium trimer, niobium trimer and tantalum tetramer in solid argon matrices has been done. Neutralized

clusters samples deposited on argon matrices were interrogated in-situ by an equivalent of optical absorption referred to as "scattering depletion spectroscopy", and also resonance Raman spectroscopy. The Raman spectra of all above transition metal clusters have been assigned. The information about the geometry, electronic and vibrational structures, dissociation energies and force constants are determined from resonance Raman spectroscopy, absorption and Raman excitation profiles which turned out to be a very useful and fruitful method to assign all the optical transitions involved in each metal clusters. In fact Raman excitation profiles might even be a more sensitive method for obtaining cluster absorption spectra than direct measurements. For instance Raman excitation profiles helped us tremendously assign the optical transitions in both Zr_3 and Nb_3.

ACKNOWLEDGMENT

Without the help of my fellow coworkers, this thesis wouldn't have been completed. First of all I am very lucky and grateful to have two great mentors, Dr.Derek M. Lindsay and Dr. John R. Lombardi. Their advice and guidance during all my graduate studies were beneficial, enriching and very useful. Also they have always been friendly and very understanding. Special thanks to Dr.Huaming Wang for his assistance, helpful discussions and for making research look very simple and straightforward. Doing research wouldn't have been enjoyable without the presence of my cclleague and friend Robert Craig. I also appreciate the help of Jian-Guo Dong, Dr.Joseph G.Eaton, Shelley Deosaran and Yifei Liu.

I really could not have done it without my family behind me. Especially my brother Hicham Haouari for his encouragement, support and most of all he has never failed to be there for me. My grandparents Fatma and Mohammed Meggarou for their continuos blessing. My father Mohammed Haouari for giving me the opportunity to live here in the US.

At last but not the least I dedicated this thesis to my mother Zaineb Meggarou who is an extraordinary women. She has been my first mentor. In fact Her unconditional love and prayers have always helped me achieve my goals.

TABLE OF CONTENTS

LIST OF FIGURES

CHAPTERS **PAGE**

LIST OF TABLES

CHAPTERS **PAGE**

CHAPTER I. INTRODUCTION

I.1 Spectroscopy of metal clusters.

Clusters are aggregates of atoms or molecules, generally intermediate in size between individual atoms and aggregates large enough to be called bulk matter. We can study clusters as small as dimers, trimers and tetramers or even something containing more than a few hundred or possibly a thousand particles. Clusters differ from conventional molecules and solids because of their composition and structure and for this reason they can have very specific properties.

Clusters are sufficiently small that they remain theoretically tractable and can be studied by using sophisticated molecular beam and laser spectroscopic techniques. At the same time, they are sufficiently complex that they provide insight into the forces that govern physics and chemistry of condensed phases.

Large number of investigators working in diverse areas of research are attracted by metal cluster because of their potential applications in many field like small-particle physics, nucleation phenomena, the photographic process, surface reaction intermediates, cluster theory, chemisorption models, alloy and bimetallic clusters and heterogeneous catalytic phenomena. Indeed, there have been several symposia[1-5] and review articles[6-9] in which

contribution has been from for instance nuclear and solid state physics, to material science and chemical synthesis. There are many different ways of making clusters in laboratory. One is by making a vapor of the elementary component particles and letting them aggregate or sputtering them directly out of a solid. Since late 1960's a big explosion of interest dealing with gaseous clusters raised. Especially laser vaporization method which consists of making clusters by using a pulsed laser vaporization and pulsed supersonic expansion. Bondybey[10,11] and Smalley[12,13] pioneered these techniques. Another effective means to generate clusters is the "gas aggregation source". Other sources are direct laser ablation, without a cooling gas and sputtering. In this last technique the impact of high kinetic energy particles on a solid target results in sputtering of a wide variety of neutral and ionic species. The projectile particles are typically either high energy rare gas or fast atoms generated by charge neutralization of an anion beam. Clusters ions are produced directly in the sputtering process. Sputtered cluster ions are both translationally and internally hot, as shown by both their chemical reactivity and by observations of metastable decay after leaving the ion source. Cooling of the nascent ions is therefore essential in chemical studies. Sputtering appears to be able to generate clusters ions from a wide variety of metals, semimetals, and insulators. Charged

clusters can be sorted out easily by using mass analyzers such as an electrostatic and magnetic analyzer, quadrupole analyzer or time of flight mass spectrometer[14].

Mass selection of metal clusters has been a very rewarding and beneficial way to study monodispersed metal clusters. Indeed there is less ambiguity in assigning the spectra and also in giving the structure of monodispersed clusters.

Moreover the use of cryogenic temperatures of matrix isolation is crucial because it insures that the clusters are in their lowest electronic and vibrational energy states. While it is relatively easy to produce and mass analyze cluster beams, direct structural information has been much harder to obtain. With some important polyatomic exceptions (e,g.Li_3[1], Na_3[1], Cu_3[7-8], Ni_3[8], Al_3[15], Ag_3[16], Y_3[58], Sc_3[58], Pd_3[59], Pt_3[59], Rh_3[60], Au_3[53], Ge_3[65]), vibrationally resolved spectra have only been obtained for a relatively few diatomic metal molecules[7] and lately some trimer metals.

Most early spectroscopic studies of metal clusters employed the matrix isolation technique. It is a well established method where-by low temperature environments are used to stabilize high-temperature or reactive species. For the past three decades the technique of matrix absorption and Raman spectroscopy has been extensively utilized to investigate transition metal dimers[17] and has been extended to investigate transition

metal trimers and larger clusters as well[18] in order to study the physical properties of molecules by means of electron spin resonance, Infrared, electronic absorption[19,20,21], laser fluorescence, MÒssbauer, resonance Raman and Raman spectroscopy.

The matrix isolation spectroscopy of a number of mass selected transition metal clusters has been studied comprehensively through Raman[22-31] and Electron Spin Resonance (ESR)[6-7,32-35]. By and large these techniques are most successful in determining cluster structures and spectroscopic constants. Thus from these studies we could also explain how the bonding in transition metals go from d-d bonding to s-s bonding when going from the early transition metals to the the late transition metals in the periodic table.

The matrix isolation technique refers to the technique where molecules, atomic, or ionic species are trapped in a solid inert environment such as the rare gas solids. These compositions can then be studied spectroscopically. A large number of papers have appeared that report on the use of various spectroscopic techniques to determine the ground and excited states electronic structures, vibrational frequencies, and reactivaties of small metal particles isolated in argon matrices. With the CCNY cluster deposition apparatus we have, in the last five years, successfully investigated V_2, Co_2, Zr_2, Nb_2, Hf_2, Ta_2, W_2, Re_2, Ni_2, Rh_2, Ru_2, Zr_3, Nb_3 and Ta_4 through

absorption, Resonance Raman spectroscopy and recently Raman excitation profiles which by and large has been a very useful method in assigning optical transitions, and by that determining electronic state symmetry. However one has to take many Raman scans to be able to obtain a good Raman excitation profile and hence the right assignment of optical transitions. Nevertheless the study of transition metal clusters is not simple especially when assigning the electronic state, because there are so many that it become complicated. Besides we have to take into account spin orbit coupling and magnetic effect which might quench the Jahn-Teller effects when dealing with heavy metals like the case of the third row transition metal clusters.

Furthermore, The presence of the unfilled d shell in transition metal elements has a number of important consequences. Still these elements are much more difficult to understand than for instance the alkali metal clusters where the electronic shell model provides a simple picture of the electronic structure.

The ionization potential of a cluster changes with its size. The experimental measurement can be compared with theoretical calculations and can be related to the properties of the condensation state. In principle, as a cluster increases in size, its ionization potential should approaches the work function w_{∞} of the bulk material. In any event among the distinctive features of cluster systems are their size dependent structural and electronic

properties, characteristics which are best probed by a variety of spectroscopic techniques.

No other matrix or gas-phase spectroscopic data have been published for tantalum tetramers, zirconium trimers, niobium trimers rhodium dimers or ruthenium dimers. However, very little is known (either experimentally or theoretically) about the properties of any of the second and third row transition metal trimers or tetramers. Nonetheless, in the gas phase, detailed spectroscopic studies using for example resonant two photons ionization or photoelectron spectroscopy have been performed for some transition metal trimers:Cu_3[36], Ni_3[37], Ag_3[38] and Au_3[53] ; and a few larger clusters:Cu_4^+[39], $Fe^-_{n,n-24}$[61]. Cu_3 and Ag_3 have been the most widely studied so far. But UV-visible absorption spectra have been assigned to trimers of Cr, Co, Ni, Cu, Mo, Rh, Ag, and Au, as well as a few larger clusters[40]. Raman or Resonance Raman studies have been performed on Cr_3[55], Ni_3[56], Cu_3[57], Mn_3[54] , Zr_3[66], Nb_3[67] and Ag_3[41,42]. However, almost all dimers of the transition metals have been thoroughly studied either in the gas phase or trapped in matrices. Thus the current literature contains examples of useful matrix data involving about 50% of all transition metals[43]. The matrix isolation method has a major disadvantage which arises from the unavoidable interaction between the matrix and the trapped species. Furthermore the inhomogeneous broadening and perturbations induced by the matrix might obscure some of

the finer details of spectroscopic structure. However, the use of inert gas like argon seems to minimize enormously this interaction but unfortunately cannot eliminate it. And this has been proven in our work with matrices since we have witnessed some interaction of the metals cluster with the matrix in the case of tantalum dimers sample(see Chap.IV.1). But in overall, most of our Raman spectra have not really been affected by the rare gas matrices where the samples are embedded.

Experimental work is always complemented by theoretical studies like ab initio effective core potential calculations[44-48], the local-spin-density method[49-50] or the complete-active-space self-consistent-field (CASSCF) followed by multireference singles+doubles configuration interaction (MRSDCI)[62-64] computations which can assist us in determining the energy levels and the symmetry of each state. Besides the tremendous efforts that have been done experimentally, theoretical progress is still hampered due to the large number of electrons, relativistic effects[51-52] and electron correlation effects present in such heavy molecule clusters, making calculations more difficult.

Nevertheless theoretical investigations of transition metal clusters are still very challenging task. But without any doubt they do provide us with information regarding low-lying electronic states of clusters, their binding energies, ionization potentials, electron

affinities, dissociation energies and other important properties and constants.

At any rate the ultimate goal of Raman spectroscopy of transition metal clusters in argon matrices will be to develop a comprehensive understanding of the bonding properties of small clusters, particularly as these results may have a big impact on both experimental and theoretical studies of larger clusters, surfaces and ultimately the bulk phase.

Last but not least, the nature of the bonding in such metal clusters, is still a broad area in which experiment and theory are always continuously challenging and complementing each other. Besides cluster theory is a field of science where the advantage of quantum chemical approaches, solid-state theory, and models and methods of nuclear physics can be compared, tested and analyzed.

The magic behind metal clusters

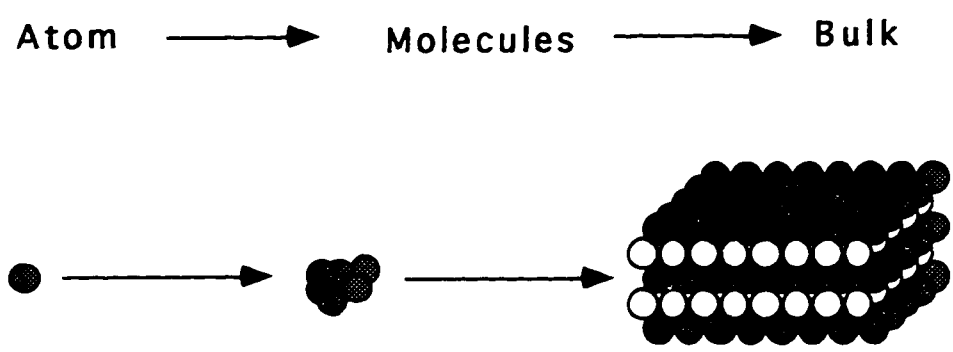

I.2 Overall view of the apparatus

The apparatus for depositing an intense beam of neutral clusters was constructed specifically to mass select metal clusters and deposit (soft landing) them in rare gas matrices on a solid surface like CaF_2, silver, titanium sapphire or aluminum. Until recently matrix studies have involved measurements in samples containing a large distribution of cluster sizes. As is known the matrix isolation technique permits the preparation of stable samples containing large numbers of clusters at low temperature. However the main idea behind the building of this apparatus was to be able to study metal clusters by using Raman, absorption, and fluorescence spectroscopy, because almost all the information about the structure and bonding of small metal clusters could be obtained by using the matrix isolation (MI) technique. In fact matrix-isolation Raman spectroscopy has also proven to be a powerful method to assist in determining the geometry and structure of large metal clusters. In addition the resulting sharpness of observed bands in Raman spectrum tend to resolve closely related bands.

Moreover the MI of vibrational spectra are similar to those of the gaseous phase, which means neither intermolecular interactions are present nor lattice modes are observed. However absorption spectra are different from those of the gas phase. Nonetheless the most

important aspect is that MI spectra tend to be simpler than gas-phase spectra because no rotational transitions are observed.

The CCNY cluster deposition apparatus will be described thoroughly in ChapII. Essentially there are three major components of this apparatus: the ion source, mass selection (Wien filter) and the deposition chamber. The ion source is a sputtering chamber where the metal target is located. An intense (Typically 15mA at 25KeV) argon ion beam from a "CORDIS" ion source sputters metal clusters from a water cooled metal target maintained at about 300V. Secondary ions are extracted with a modified Colutron model 200-B lens system. Mass selection is achieved by a Wien filter (Colutron 600-B). In fact the most important part of the beam is its mass-selection capabilities which enable us to study monodispersed metal clusters. The secondary beam which includes extraction lens, Wien filter, drift space, etc...is floated at about -1KV. The temperature in the deposition chamber is measured with a silicon diode in conjunction with a scientific instruments model 5500 temperature controller.

The deposition region consists of a substrate usually CaF_2 where the matrices are embedded, a closed cycle cryostat to obtain cryogenic temperature, a Faraday cage to define potential for the arriving ions by applying a retarding potential to the Faraday plate, an electron source to neutralize the ions, because the deposition

chamber was designed as to be able to deposit neutral clusters in argon matrices. Since The mixing ratio of the gas to metal is around 10^4:1 or higher, then the sample (solute) molecules are completely isolated from each other in the frozen gas matrix. Thus the spectra not only will reflect the molecule properties but also will be easier to interpret.

Matrix samples are interrogated in-situ using both absorption and Raman spectroscopy. For the former measurements we employ a tungsten or deuterium lamp, dispersed by a (computer controlled) Spex 1/4m monochromator (calibrated with a Hg lamp), reflected off a plane mirror and then focused onto the matrix sample. The mirror is mounted on a stepping motor, which allows the focused light to be scanned (in several steps) across the 8 mm wide sample.

Almost any metal can be used as a target in this apparatus. However here are some characteristics of good cluster candidates for Raman spectroscopy.

- The material should have a large sputtering yield.
- Secondary currents should not fall off too rapidly with cluster size.
- (The cluster ionization potential should be relatively low.)
- (The cluster bond strength should be relatively large.)
- There should be visible absorption bands which overlap with Ar^+ laser line(s) or a "good dye" or Ti-sapphire.

- Raman spectra should not be too obscured by fluorescence otherwise it will hinder the weak Raman signals and make the assignment a bit difficult.

CHAPTER II. THEORY

II.1 Scattering Depletion Spectroscopy (SDS)

When a sample consists of a number of absorbers embedded in a matrix which itself may scatter light (e.g. through microcrystallites), the intensity of light scattered at right angles to the incident light may be depleted by absorption. Under proper conditions, therefore, dispersion of the scattered light provides an alternative means of detecting absorption. The ratio of scattered light in the absence of an absorber to that in the presence of an absorber is given by the " SDS response function":

$$R^{SDS} = \left\{ 1 + \alpha_a / \alpha_s \left(\frac{1 - \exp(-\alpha_s)}{1 - \exp(-\alpha_s - \alpha_a)} \right) \right\}$$

where α_a and α_s are absorption and scattering coefficients, proportional to the number of absorbers/ scatters and the sample thickness.

The absorption measurements were made by collecting the light scattered at 90° to that incident. Thus, if the sample absorbs at a particular wavelength, the scattered light will be depleted at this wavelength and so (at least in principal) also contains the absorption spectrum of the sample.

Matrices prepared by the mass-selected ion deposition technique are, however, fairly dilute and often highly scattering. Then to partially overcome these disadvantages we employ a variation on the usual absorption process, which we term "Scattering Depletion Spectroscopy" (SDS). We find that the SDS technique is in fact somewhat more sensitive than the usual absorption measurements made by detecting the light transmitted by the sample. In Figure.II.1.1.a and b are shown the SDS of tantalum trimers and tantalum atoms. In our experiment the absorption tends to be more intense in the center of the substrate than in the edge because the center of the substrate is sample rich. However, the reference also contains absorption information but to a lesser degree than the signal. As shown in Figure.II.1.2 the maximum absorption is indeed in the center of the substrate. It is generally found that the sample is non uniform. In any case prior to recording scattering depletion spectra, the optical density profile of the sample is obtained by recording single beam spectra as a function of lateral position on the sample.

Figure II.1.1.a Scattering Depletion Spectrum (SDS) of tantalum trimer(127nA-h).

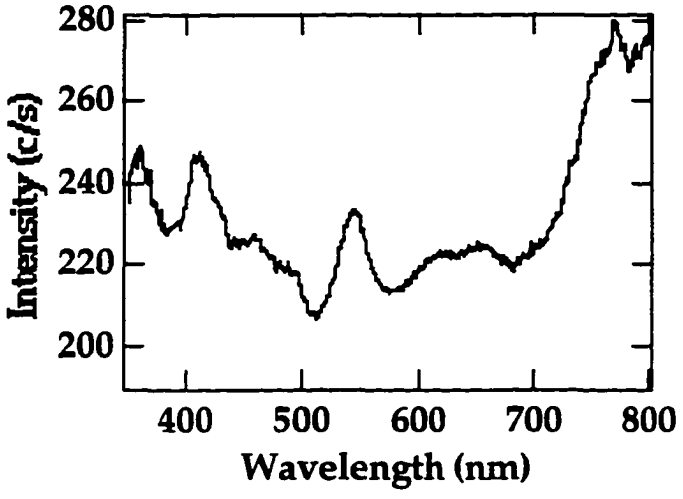

Figure II.1.1.b Scattering Depletion Spectrum (SDS) of tantalum atoms (107nA-h)

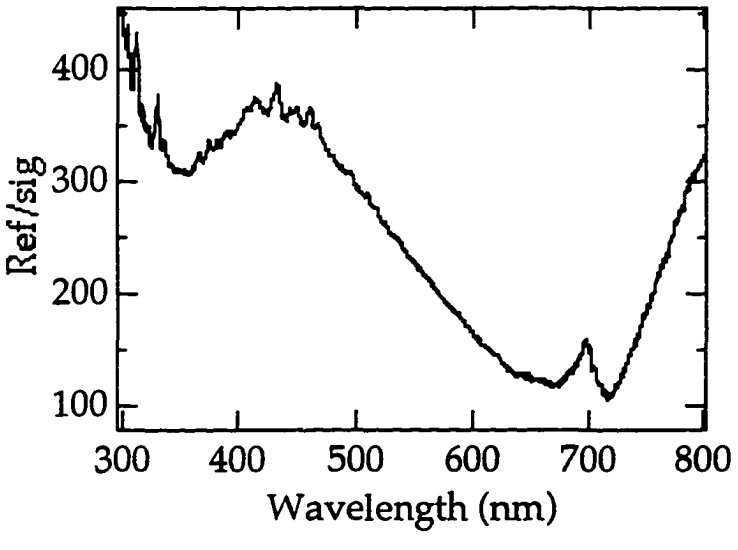

Figure II.1.2 Optical Density Profile for Ta_4 on CaF_2.

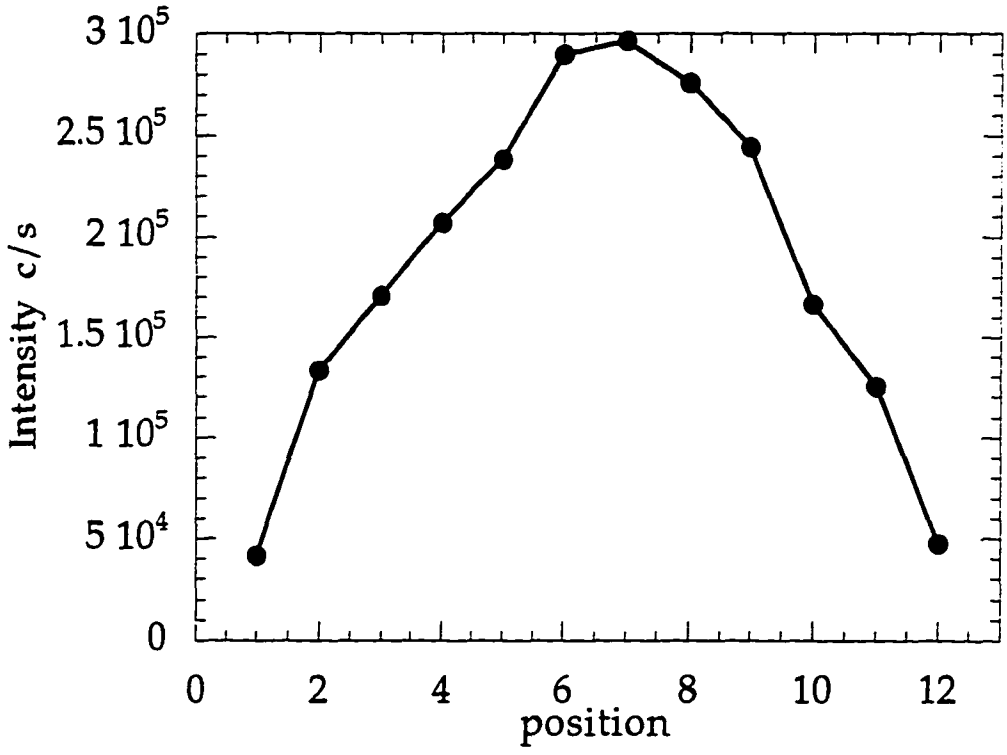

II.2 The Jahn-Teller Effect

The Jahn-Teller theorem is extremely important when considering the electronic states of polyatomic molecules. Recently there has been much interest in a special case of Jahn-Teller effects in trimer metal clusters systems with a D_{3h} symmetry.

Examples of these cases will be treated in Chap V.2 and Chap VI. To discuss the Jahn-Teller effect in detail it will take more than a paragraph to do so and the purpose of including this paragraph concerning Jahn-teller effect is to give the definition regarding this effect and its impact on the spectroscopy of small transition metal clusters. In any event I tried to summarize from references 1, 2 and 3 the most important and crucial points regarding this theorem.

Jahn & Teller (1937) proved that if a symmetrical non-linear molecule has a spatially degenerate electronic state then in this state it will tend to distort in such a way as to remove the electronic degeneracy. However in order to appreciate the nature of the coupling between electronic and nuclear motions it is easiest to begin by studying the usual situation in which the electrons adapt themselves more or less instantaneously to the nuclear configuration. Born and Oppenheimer were the first authors to examine this situation in detail, but their approach, though elegant, often presents difficulties of comprehension.

In 1934, L.D.Landau in a discussion with E.Teller first formulated the idea of instability and spontaneous distortion of the nuclear configuration of a molecule in an orbitally degenerate electronic term formed by two or more orbital states with the same energy. This idea was later verified by Jahn and Teller and shown to be true for all nonlinear molecular systems including those with spin degeneracy. In the presence of the Jahn-Teller effect, the electrons do not adiabatically follow the motions of the nuclei, and the nuclear states are determined not only by the averaged field of the electrons, but also by the details of the electronic structure and their changes under nuclear displacements.

If stationary electronic states (ground, first excited, etc.) are obtained as solutions of the Schrödinger equation for fixed nuclei, an accounting of the vibronic interaction terms in the Hamiltonian (interaction of electrons with nuclear displacements) mixes these electronic states, and this mixing is especially strong in the cases of electronic degeneracy. Vibronic mixing of electronic states is an important starting point in the systematic analysis of the origin of molecular properties. An example of E⊗e interaction and the resulting energy levels is shown in Figure.II.2.1. The theoretical background for this concept lies in the successive account of vibronic mixing of electronic state by nuclear displacements. Vibronic effects directly influence the

structure and properties of molecules and crystals, and should be taken into account not only in any investigation of the origin of their properties but also in the prediction of new properties.

For vibronic problems, limiting cases as weak and strong vibronic coupling (with relatively small and large vibronic constants, respectively) can be solved analytically. A quantitative criterion of weak and strong coupling can be defined by comparing the Jahn-Teller stabilization energy E with the energy of zero-point vibrations of an n-fold degenerate vibration. Then, if λ(λ is the dimensionless vibronic coupling)$<<1$ the vibronic coupling will be regarded as weak, and if $\lambda>>1$ the coupling is strong. In the limiting case of weak coupling the depths of the adiabatic potential minima, formed by the vibronic interactions, are much smaller than the zero vibration energies, and therefore there are no local states in the minima. In the strong coupling case, however, such local states exit. Nevertheless, in both cases the system is delocalized into all the equivalent minima, provided stationary states of the free system are considered.

If we consider the approximation solutions of the vibronic equations for weak coupling, when $\lambda<<1$ general considerations show that in this case the angular momenta of the electrons and nuclei are not preserved separately but as their vector sum.

Further more there is the effect of electron spin on Jahn-Teller instability. Jahn and Mulliken and Teller have considered the effect of electron spin. The general result is that spin-orbit interaction tends to reduce the effect of Jahn-Teller instability. This phenomena will be more broadly and comprehensively understood with more investigations of larger clusters.
with the help, of course, of theoretical calculation which are in some cases the backbones of experimental studies.

Figure II.2.1 Cross-section of the adiabatic potential for the linear E⊗e problem with corresponding vibronic energy levels(A), and the same levels in indication of the quantum numbers and symmetries(B), for three cases of the dimensionless coupling parameters: (a) λ_e=0.1; (b) λ_e=0.5; λ_e=2.5. Energy levels with same vibrational quantum number n are linked by dashed lines. All levels with a given value m(total vibronic angular momentum) have the same symmetry indicated at the lowest level.(Ref.3)

B

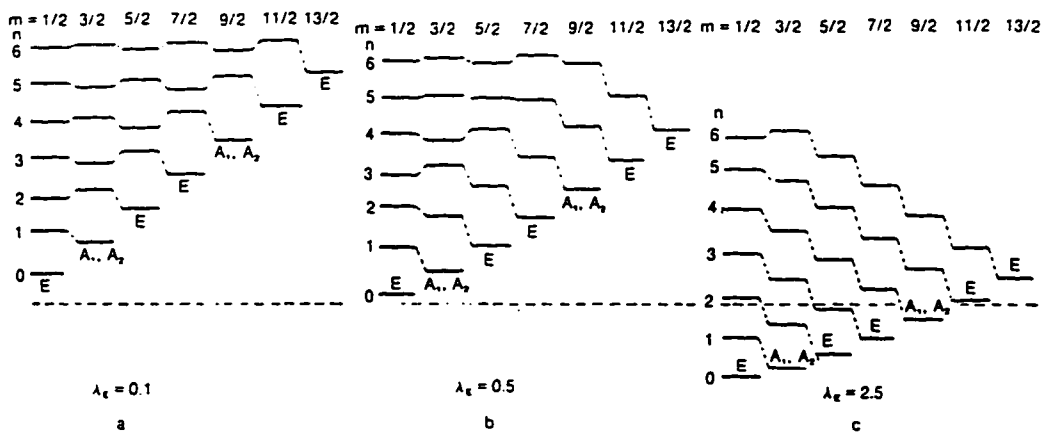

A

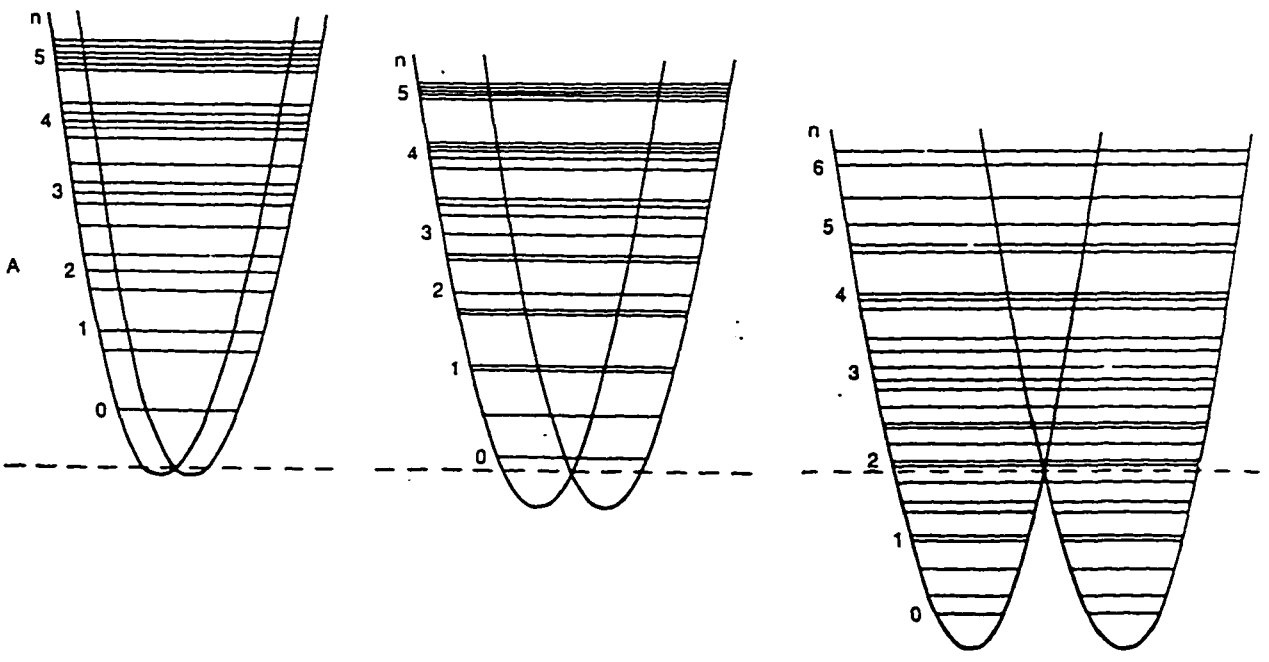

II.3.RAMAN spectroscopy

II.3.1 Instrumentation

The history of Raman spectroscopy has been significantly influenced by the developments in the available instrumentation. In fact it has become now a routine experiment. And this is due to commercial laser excited Raman spectrometers, with high quality triple monochromators, and photodiode array detectors or charge couple detectors (CCD).

A commercially available Raman spectrometer consists of five major components, which are the following:

- Excitation source, which is generally a continuous wave (CW) gas laser
- Sample illumination and scattered light collection system.
- Sample holder
- Monochromator or spectrograph
- Detection system, consisting of a detector, an amplifier and an output device.

I will describe briefly some of the components since they are relevant to our experiment.

In our experiment, the spectrograph used is a triple monochromator which is specially tailored to provide low-stray light and a flat, undistorted focal plane ideal for sensitive work with multichannel detectors like diode

arrays or CCDs. This multichannel technology has been used in Raman spectroscopy for almost a decade now. The CCD is appropriate for applications requiring low or very low light levels such as Raman and fluorescence spectroscopies. For the past few years, charge-coupled device(CCD) detectors have been used for scattering experiments and have contributed to improvements in this spectroscopic techniques. A CCD is a solid device and multichannel detector made of silicon. The advantage is that it can measure intensity, and spectral differences projected along the length of the slit. Moreover it offers the advantages of a rectangular detector, with resolution in two perpendicular directions. In contrast a photomultiplier tube(PMT) which is a single channel detector can measures only intensity. In general multichannel detector can acquire entire spectra much faster than conventional monochromator detector. CCDs come in standard sizes of 1152x298 pixels, 512x512 pixels, and 578x578 pixels with the individual pixel sizes about 22μmx22μm. A CCD detection element can be from as small as 20 μ to up to 6.7 mm in height. Besides it has a quite reasonable quantum efficiency about 45%. However cosmic rays can wipe out the spectrum. Cosmic Rays are high energy particles from the sun. To decrease the effects of cosmic rays, one can use the smallest section of the chip that the experiment allows, and use the least time possible. In addition recent use of a nitrogen-cooled CCD has considerably reduced the

thermal noise generated by this detector at near room temperature conditions.

For the excitation source we use an Ar^+ laser (Spectra-Physics Model 2045) which is a continuous wave (CW) laser. This gas laser operates mainly in the visible region of the electromagnetic spectrum. Also Argon ion laser is a source for exciting a dye laser in order to produce laser beams in a wide wavelength range by combining dye lasers and other devices.

Regarding dye lasers, they are used to extend the wavelength range for Raman excitation. There exist three types of dye lasers: those that are pumped by a CW gas laser, those pumped by a pulsed laser and finally those pumped by a flash lamp. The dye laser used in our experiment is a Coherent Model CR599. When exciting in the Blue-Green region two dyes were used, Rhodamine110(535-600nm) and Rhodamine 6G(565-640nm). When exciting in the red region, we use a recently developed solid-state laser, which utilizes a titanium-sapphire crystal (Lexel 479). It is tunable in the 700 to 1030nm range and can provide 3.25W output power when pumped for instance with a 20W Ar^+ laser. In short the Lexel 479 is a tunable, standing-wave Ti:Sapphire laser system capable of being pumped by a small or large frame ion laser system. It incorporates a birefringent tuning filter (1,2, or 3 plates) and the three standard optic sets in the 710-975 nanometer tuning range. All things considered, simplicity, efficiency, and

ease-of-use make this Ti:sapphire laser one of the best choices for experimentation in the near-infrared.
In any event lasers are the ideal excitation source for resonance Raman spectroscopy, and this is due mainly to some of the characteristics of the laser beam: they are highly monochromatic and are almost completely linearly polarized.

To achieve a better recording and higher resolution of our spectra, a very good spectrometer is a necessity. The typical recording spectrometer for the Near and Mid-infrared, visible, and Near-ultraviolet regions and perhaps the most common type of spectrometer that we encounter in the laboratory is the double-beam spectrometer. However there exist two other kinds of spectrometer which are a double monochromator and a triple monochromator (triplemate). But with a double monochromator it is not possible to obtain a good spectra because extraneous light that bounces around the spectrometer overlaps the weak Raman scattered light. This is mostly due to undiffracted light scattered from the face of the grating. However such stray light can be reduced by using a double-beam monochromator. In it two spectrometers are arranged in tandem so that the output of one is purified by the second. An even better reduction of this stray light is obtained by using a triple monochromator. It actually allows us to observe Raman bands located very close to the Rayleigh line. But nevertheless the resolution of a spectrometer

depends on the grating to a large extent. Then the more grooves per millimeter, the better the dispersion and the greater the resolution. In addition to compensate for the signal loss caused by improved resolution, the slit width has to be widened. Another important point to obtain a maximum resolution is by varying the slit width and monochromator speed (increments between data point). In our laboratory a Spex 1877 Triplemate is used. With a triplemate a multichannel detector is needed, e.g a charge-coupled device(CCD).

Our (0.5m) triple monochromator plus CCD detector have enormously enhanced our sensitivity and resolution while at the same time further suppressing the Rayleigh line thus allowing us to completely characterize and interpret the vibrational spectrum. This permit fruitful and rewarding studies of Resonance Raman spectroscopy of metal clusters.

Undoubtedly the developments in commercial Raman instrumentation brought the present state of the art Raman measurements. In other words, the future of Raman spectroscopy combined with matrix isolation techniques appears to be promising, very bright and most of all a very exciting field of investigation.

II.3.2 Theory

The Raman effect studies the vibrations of a molecule. However for a vibration to be Raman active, there

must be a change in the molecular polarizability. In other words the Raman effect is related to the phenomenon called Rayleigh scattering, which is caused when a molecule experiences a nonresonant oscillating electric field, which bring us to say that Raman spectroscopy is a scattering or emission phenomenon. A stream of photons from a light source (usually a laser) impinge on the sample. The photons scattered by the sample contain spectral information. Changes in molecular states can also be caused by inelastic scattering of high-energy visible photons. The energy (or frequency) shifts in the scattered radiation are then a direct measure of the vibrational frequencies of the molecule. Although the intensity of this scattered light is quite low, Raman was able to observe such scattering in 1928 and the effect was later named after him. By determining the Raman shifts with respect to the Rayleigh line, we may measure both vibrational and rotational frequencies. The Raman intensity is proportional to the square of the susceptibility $\chi^{(1)} = \alpha_{0n}$. The quantum expression for this quantity is

$$\alpha_{0n} = \hbar^{-1} \sum_{m} |\langle 0|\mu|m\rangle\langle m|\mu|n\rangle|(\omega_{mn} - \omega)^{-1} + |\langle 0|\mu|m\rangle\langle m|\mu|n\rangle|(\omega_{mn} + \omega)^{-1}$$

Here the sum over *m* runs over all excited molecular states. Note that the selection rules depend on two different dipole moment matrix elements both of which must

simultaneously be non-zero. These are sometimes refered to as two-photon selection rules. Thus most molecules exhibit a Raman effect, since it is not necessary for the molecule to have either a permanent electric dipole moment or dipole moment derivative. Raman spectroscopy thus provides a suitable probe of the properties of non polar molecules. The information we obtain from Raman spectra is in principle the same as that contained in an infrared spectrum. However the selection rules for infrared spectroscopy and Raman spectroscopy are different, in the Raman spectrum it is the polarizability that governs the symmetry. This has the same symmetry properties as the product of the Cartesian vectors x^2, y^2, z^2, xy, xz, yz. The Raman active vibrations will thus include those that are themselves totally symmetric, transforming as x^2, y^2, z^2. It should be noted that some vibrations may be inactive. In any case, group theoretical procedures allow one to derive selection rules for Raman scattering by molecules and crystals. In fact many texts give these procedures in detail. In the case of IR, infrared spectroscopic transitions originate from the dipole moment operator, with symmetry the same as vectors along x,y,and z.

The Raman scattered intensity is given by

$$I \propto \nu^4 I_O N f(\alpha^2)$$

Where I_o is the intensity of the exciting light (usually a laser), N is the number of scattering molecules in a given

state, ν is the frequency [in s^{-1}] of the exciting light, and α is known as the polarizability of the sample. In Fig.II.3.2 is shown a schematic representation of the Raman scattering process. The scattering phenomena are two photon processes, where an incident photon $h\bar{\nu}_1$ is momentarily absorbed into a virtual state, indicated by the dashed energy level. A new photon is created and scattered from this virtual level. Then the final state can be either the ground state (Rayleigh scattering) or a vibrationally excited state (Stokes-Raman scattering). The scattering process can also originate from the vibrational excited state. In this case the process is known as antiStokes-Raman scattering. Thus the scattered photons may have the energy $h\bar{\nu}_1$, $h(\bar{\nu}_1 - \bar{\nu}_m)$, or $h(\bar{\nu}_1 + \bar{\nu}_m)$, where $\bar{\nu}_m$ is a molecular vibrational transition frequency, expressed in cm^{-1}.

Raman measurements have the obvious advantage of giving cluster vibrational frequencies and force constants, parameters that are only little influenced by the matrix host. Most of all those parameters are very useful in determining the structure of metal clusters. Since Raman spectroscopy is relatively insensitive, these measurements can only be made in cases where the Raman signal is resonantly enhanced. They mean that the scattering occurs when the Raman spectra are excited with a frequency of

light that is within the molecular absorption bands of the sample. Excitation of this type is said to be in "resonance" with the electronic transition and yields Raman scattering that is said to be "resonance enhanced". This resonance excitation, which occurs at the natural frequency of electronic aborption, results in an increased oscillation charge displacement. An increased induced dipole moment directly results in a significantly increased scattering efficiency. The enhancement factor or resonance Raman scattering compared to normal Raman scattering can be as high as 10^4. Although resonance Raman spectra are obtained with standard Raman instrumentation, special attention must be paid to the consequences of illuminating an absorbing sample. Moreover when we use normal Raman spectroscopy in our experiment, it is more difficult to apply to low-temperature matrices for the following reasons: Since Raman signals are inherently weak, relatively high concentrations of the sample or relatively wide slit widths are required. However, These obstacles can be circumvented if Raman spectra are obtained under resonance conditions.

The intensity enhancement observed in resonance Raman (RR) spectroscopy has enormously benefited the vibrational spectroscopy field of transition metal clusters. RR has mainly two advantages. One lies in the fact that several members of a progression are so often seen in RR spectroscopy. Therefore the anharmonicity and so an

estimate of the bond dissociation energy as well as vibrational frequency may be obtained especially for diatomic molecules. Most of all the presence of a large progression helps determined the geometry of larger clusters. Secondly, the isotopic fine structure, if any exists, may be resolved hence the structure and geometry of the polyatomic may be quite easy to determine. This is because in RR the exciting line is chosen so that its energy intercepts the manifold of an electronic excited state of a molecule. However in normal Raman the transitions do not coincide with one of the molecular transitions. Furthermore we noticed that the splitting of Raman lines due to isotopes is not observed in clusters of the third row transition metals. This is because of the heavy weight of these elements. However the splitting has been observed in Raman line of Ni_2 and Ru_2 (see Chap.IV.2 and Chap.IV.4). Another important advantage of RR is the intensity enhancement observed in both fundamentals and overtones. However one of the disadvantages that RR causes is the unequal enhancement of all the fundamentals of a molecule in its RR spectrum. One problem is that usually only totally symmetric vibrations are RR active, yet with vibronic coupling this rule breaks down. They mean that for allowed electronic transitions the dominant resonance effect is seen for those normal modes which have appreciable origin shifts in the excited state, and for which the Franck-Condon overlaps are therefore large. These

modes are totally symmetric. Non-totally symmetric modes do not experience origin shifts and are usually absent in resonance Raman spectra. They can, however, be enhanced if they are effective in coupling the resonant state with a nearby excited state. Nevertheless RR is one of the best methods used so far to investigate transition metal clusters in argon matrices. By and large the advantages of RR still outnumber the disadvantages. Hopefully by combining RR spectroscopy and matrix isolation techniques we can investigate thoroughly more trimer and tetramer metal clusters. Recently RR spectroscopy has been extended from the structural chemistry area to biochemistry. For instance it has been possible to obtain structural information from deep within complex biological surfaces. Also RR has been applied in other fields. The shapes of potential surfaces and molecular geometries in excited states have been determined. Spectra of species with half-lives on the microsecond level have been recorded. It is also possible to study reactions taking place at the surface of electrodes (SERS).

Figure II.3.2 Schematic representation of Rayleigh, Stokes and anti-Stokes-Raman scattering.

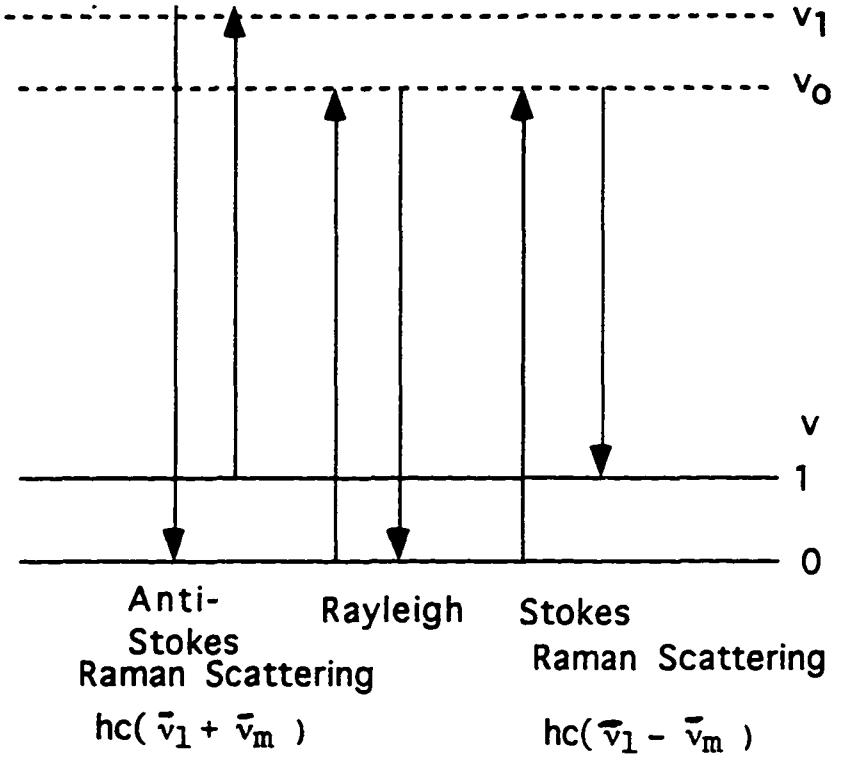

II.3.3 Raman Excitation Spectroscopy

Raman excitation profiles turned out to be a valuable tool because they did help us tremendously to assign the nature of the electronic and vibrational transition when we were assigning the origin of Raman signals of metal trimers. Raman scans must be taken throughout a broad region of the spectrum which means that a wide range of laser wavelengths should be available. Thus it has been shown that a wealth of vibronic details may be revealed. In any case the excitation profiles follow the electronic states vibrational progressions, and can also be approximated by evaluating the Franck-Condon overlaps.

By measuring the intensity of each Raman line and taking the ratio of it to the laser power we can easily obtain a plot of an excitation profile which in other words is simply a Raman intensity vs laser wavelength. It is similar to a fluorescence excitation spectrum. The only difference is that different vibrational normal modes can be separately monitored. The majority of profiles have been constructed from individual spectra obtained with the various Ar^+ laser lines. However with the advent of dye lasers it is possible to increase the desired area that has to be covered by scanning different laser wavelengths at very small intervals. Yet the most important information we can obtain from these profiles is that when we superimpose these plots on the absorption spectra. That is why it is

necessary first to map out the cluster absorption spectrum. After that, identifying the symmetry of the electronic transition (which means the nature of the ground as well as that of the excited state) is made easier. But nevertheless some selection rules should be taken into account.

In the absence of vibronic coupling, resonance Raman spectra should only be observed for totally symmetric ground state vibrations thus the presence of non totally symmetric vibrations give information as to vibronic coupling. This, together with Jahn-Teller effect and some theory enables assignment of optical transitions.

In both the Zr_3 and Nb_3 investigations we relied mostly on the Raman excitation profiles to determine all the allowed electronic transitions. Without this highly valuable information we could not have been able to determine either the nature of the ground and excited states nor the allowed electronic transitions involved. Also even without having a decent absorption spectrum, which was the case of Zr_3, we were able to draw some conclusions regarding some of the electronic transitions involved in Zr_3. More details will be given in ChapV.2. It has been shown that the shape of the excitation profile is influenced by interference effects. In fact the shapes depend in detail on the scattering amplitudes and level separations. Spiro[1] proved that vibrational Raman scattering can also experience interference from different electronic states. The case of

interference effects will be treated in Chap V.3 regarding Nb_3.

CHAPTER.III Experimental

III.1 Mass selected cluster beam

Figure III.1 outlines the experimental arrangement for the continuous wavelength mass selected beam. The cluster apparatus gives continuous, mass selected "fluxes" as high as 10^{12} sec^{-1} corresponding to currents of over 100nA as shown in Figure III.3.3.

Although the apparatus has many different parts, its ability to mass-selected metal clusters by using Wien filter is the central feature of this equipment.

III.2 Ion source

The cluster ion source is shown schematically in Figure III.1. It is similar in several aspects to that described by Harbich, Lindsay et al.in refs.[1,2].

An intense, high energy (typically 15 mA at 25 KeV) primary beam of Ar^+ ions is produced by a Cold Reflex Discharge Ion Source ("CORDIS") designed and manifactured by Rokion Ionenstrahl-Technologie (Darmstadt, Germany)[3]. This ion beam relies on the principle of a magnetic multipole/reflex discharge. The ion source is formed by a single-aperture accel/decel extraction-system which can be aligned independently of other source parts. The ion beam sputters metal clusters ions from a water cooled, metal target.

The primary beam is collimated by an 8 mm aperture (denoted A1 in Figure.III.1) which also separates the ion source from the rest of the apparatus. The ion source is pumped indirectly, through and around A1, by a 500 l/s turbomolecular pump (Balzers TPU 510) which supports the specially designed sputtering chamber (MDC Vacuum products). The 50° inclination between the primary and secondary beam lines corresponds closely to the optimum ejection angle for material sputtered from a metal surface[4].

Cluster ions sputtered from the target (normally maintained at 350V) were extracted with a modified colutron 200-B lens system. It consists of an extraction lens in combination with an einzel lens. The lens system can easily be attached to any of the Colutron Velocity Filters models 300, 600, and 600-B.

III.3.The velocity filter

The secondary ions are mass selected by a Wien filter (Colutron 600-B) see Figure III.3.1. This velocity filter consists of a magnet and a pair of deflection plates. The plates are mounted between the magnet poles to produce an electric field E perpendicular to the magnetic field B (crossed E and B fields). The velocity $v=\sqrt{(2qV/m)}$ of charged beams are obtained by accelerating the particles of mass m, and charge q across a constant electric potential

V. Different masses in the beam will be dispersed by the filter since they have different velocities.
The model 600-B is liquid cooled and is capable of higher magnetic fields. The Wien filter is in conjunction with an approximately 175 mm long drift space and a 6.5 mm diameter aperture (A3) shown in Figure III.1. A fairly high resolution is obtained M/ΔM is approximately 4-6, i.e., sufficient to separate for example dimers from atoms and trimers and to ensure that oxides are not present.

After mass separation, the ion beam is bent by 10° in order to eliminate neutral sputtered products and then guided to the deposition region by two eizenl-like lenses L3 and L4. The secondary beam line (extraction lens, Wien filter, drift space, etc...) was floated at about -1KV. This modification significantly increases the extractable ion current which is measured on a Faraday plate in the deposition region. All electrostatic lenses are shown in Figure III.3.2

A typical mass scan is obtained by applying a non linear voltage ramp to the power supply controlling the Wien filter magnetic field. Although the mass scales can be estimated from the known parameters of the Wien filter and the beam energy, we generally refine these scale using assigned cluster masses. Figure III.3.3 shows the current of some transition metal elements sputtered from a target. In this case the current on the Faraday plate is recorded as a function of the magnetic field on the Wien filter

III.4 The deposition chamber

The deposition chamber is quite similar to that described elsewhere[2] see Figure III.4.1. It consists of an 8 in. conflat cube, (MDC Vacuum Products) and is pumped by a second 500 l/s turbomolecular pump. Ions were co-deposited (at about 14K) with argon and electrons on a polished CaF_2 substrate(dim 1x8x45 mm) mounted (using Wood's metal and an In gasket) on a closed cycle cryostat[8](APD Displex, 204SL/DMX-6) shon in Figure III.4.4 to achieve low temperature. Further more the substrate is electrically insulated.

The cryostat temperature was measured by a Si diode in conjunction with a Scientific Instruments model 5500 temperature controller. The cryostat provides a sample holder, a refrigeration to cool the sample, a vacuum shroud to thermally insulate the sample, and an optical path for observation and excitation. Very cold temperatures plus highly dilute matrices will inhibit aggregation during deposition. The partial pressure of H_2O (the dominant background gas) in the cryostat chamber was generally about $5x10^{-8}$ torr, as measured on a residual gas analyzer (Leybold-Inficon, Quadruvac Q100). This translates into a higher probability that clusters will have argon atoms, which constitute the matrix, as nearest neighbors as opposed to water.

Matrices were grown on a CaF_2 plate which is largely enclosed by a "Faraday cage"(denoted FC in Figure III.1) composed of two sides plates (with openings for optical measurements) the lower half of the cryostat radiation shield, the electron source, and the last lens element of L4 which was closed by a 90% transmitting Ni mesh. This same lens element also incorporates a coaxial injector ring for the matrix gas (99.9995% Ar, Alphagaz). The potential in the deposition region is controlled by the voltage applied to the surrounding Faraday cage. The difference in voltage (Vdep) between the target and Faraday cage determines the ion deposition energy. A typical graph of the ion current vs. voltage difference between the target and the sputtering chamber is shown in Figure III.4.2. Since the matrix-isolated products are generally examined spectroscopically, the substrate for example CaF_2 on which the matrix is formed must be transparent in the appropriate wavelength region and a good thermal conductor[5]. However when using Al and Ag as substrates the condition of transparency in the appropriate wavelength region is not necessary. Because the cryostat is rotatable then the Faraday plate and the substrate may easily be adjusted in order to measure ion currents, to prepare matrix samples, or to record optical spectra. Figure III.4.3 show the dependence of the current intensity on the cryostat angle. Here,as elsewhere, ion currents are measured on a Faraday plate situated in the deposition region.

The kinetic energy distribution of the arriving ions, is measured by applying a retarding potential to the Faraday plate. Since the kinetic energy is about 2 orders of magnitude larger than the rare gas binding energy, such a process will also involve the displacement of a large number of matrix particles, this will minimize interactions between metal clusters. Size selected cluster ions can be neutralized as well as soft landed in rare gas matrices. The simplest, and perhaps most effective strategy is to neutralize the clusters either simultaneously with deposition or after the matrix has been formed. Thus cation clusters could be co-deposited with both a matrix gas and a swarm of low energy electrons. In fact some of the excess energy of neutralization will be dissipated by the matrix gas, thus decreasing the fragmentation. In any case we still do not have a physically convincing model for the deposition process.

It is clear that for fragmentation to be minimized, the cluster translational energy should be as low as is feasible. The term soft landing should be understood as probably involving a series of soft collisions which efficiently transfer this energy to the matrix as long as translational energies are ten times greater than bond strengths. But nevertheless even with some fragmentation, matrix samples would be significantly "enriched" in the selected cluster size.

We use units of nA-h (product of the current times the deposition time in hours, 1nA-h=$2.25x10^{13}$ particles) to measure the concentration of the sample and by that we can have an idea of "rich" is the sample. The density of neutrals in the matrix(N cm^{-2}) may be estimated from the gas-phase expression

$$N = 2.6x10^{19} \frac{1}{f\lambda^2} \int A(\lambda)d\lambda$$

where $A(\lambda)$ is the measured absorbance, f is the absorption oscillator strength for the transition and λ is the wavelength in nm.

III.5 The electron source

The electron source consisted of a Philips electron microscope filament (0.13 mm tungsten) on a ceramic base (Ladd Research Indusstries). This assembly was enclosed by a stainless steel box having an 8x1 mm slit positioned so that the electrons were introduced 1-2 mm in front of the CaF_2 substrate. In order for sufficient, low-energy electrons to reach the matrix target and hence to neutralize the positively charged clusters ions, the filaments were biased at -3V with respect to the Faraday cage. Because the ionization potential of a cluster is generally larger than its bond energy we suppose that the matrix surface plays an important role in suppressing fragmentation during the neutralizing step. We have

observed for example that the deposition of the dimer ions without electrons led to Raman spectra which are approximately 10 times weaker (when scaled for equivalent conditions) than that obtained with electrons added. This indeed shows the necessity of cluster ion neutralization.

III.6.Matrices

matrices are usually formed by condensation of a gas beam on a cold substrate usually at around 14K. The use of matrices was introduced by Pimental and his co-workers (Whittle,1954)[7]. The matrix to guest (or radical) ratio, M/R, is between 10^2 and 10^5 or higher ratio in order to assure lower guest-guest interaction. In Figure III.6 is shown the Ta_4 embedded on argon matrices, each tantalum clusters is surrounded by argon and not by another clusters. The sample thickness can actually be tested when taking absorption spectra, because the thickness of the sample depends on the oscillator strength of the optical transition that is to be observed. However, any material that vaporizes without decomposition can be embedded in matrix. Matrices are usually made of a condensed rare gas, neon, argon, krypton, and xenon. These are chemically inert and optically transparent, and their intermolecular forces are small. X-ray diffraction studies[6] have shown that the rare gases normally crystallize in cubic close-packed (ccp) structures with a face-centered cubic (fcc) unit cell. In

this geometry, the lattice can be pictured as consisting of layers of atoms stacked one on the other. The average density of vapor-deposited solids is about 1% less than the solid grown from the liquid[6], which indicates that the vapor-deposited solids are porous. Thus from this observation, we can say that matrices contain unoccupied sites and imperfections which might affect the molecules embedded in it. Matrix site effects will be discussed thoroughly in Chap IV, with tantalum dimers as an example.

Figure III.1

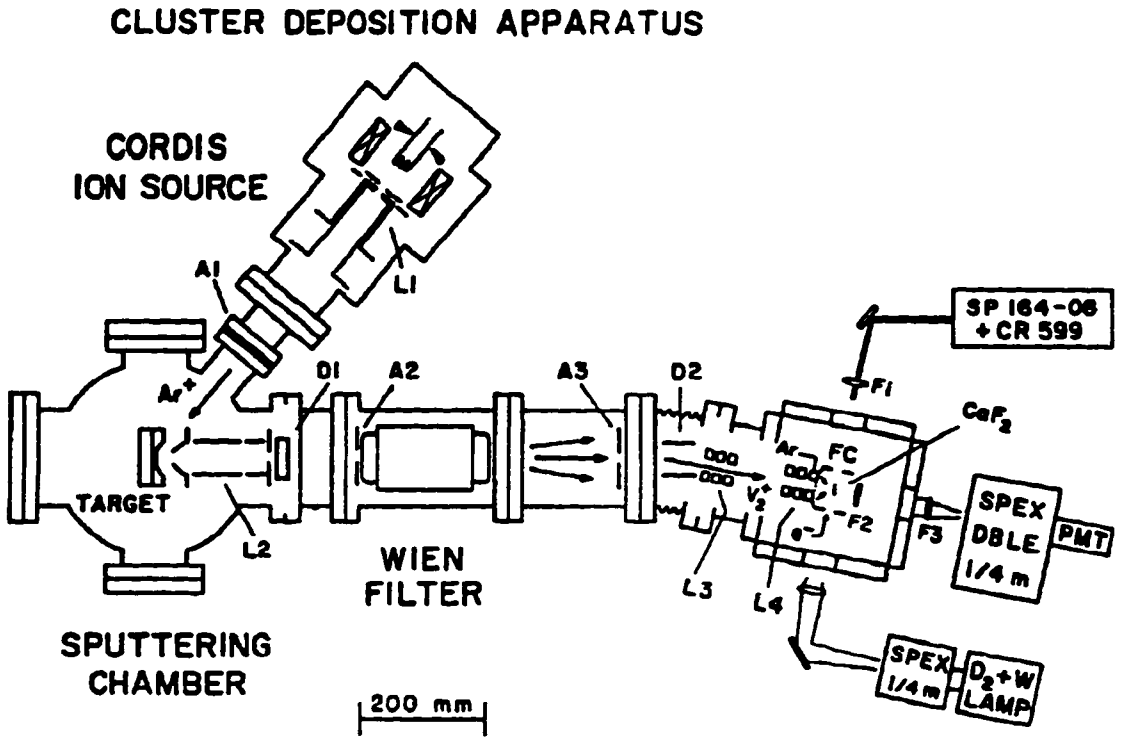

Figure III.4.1

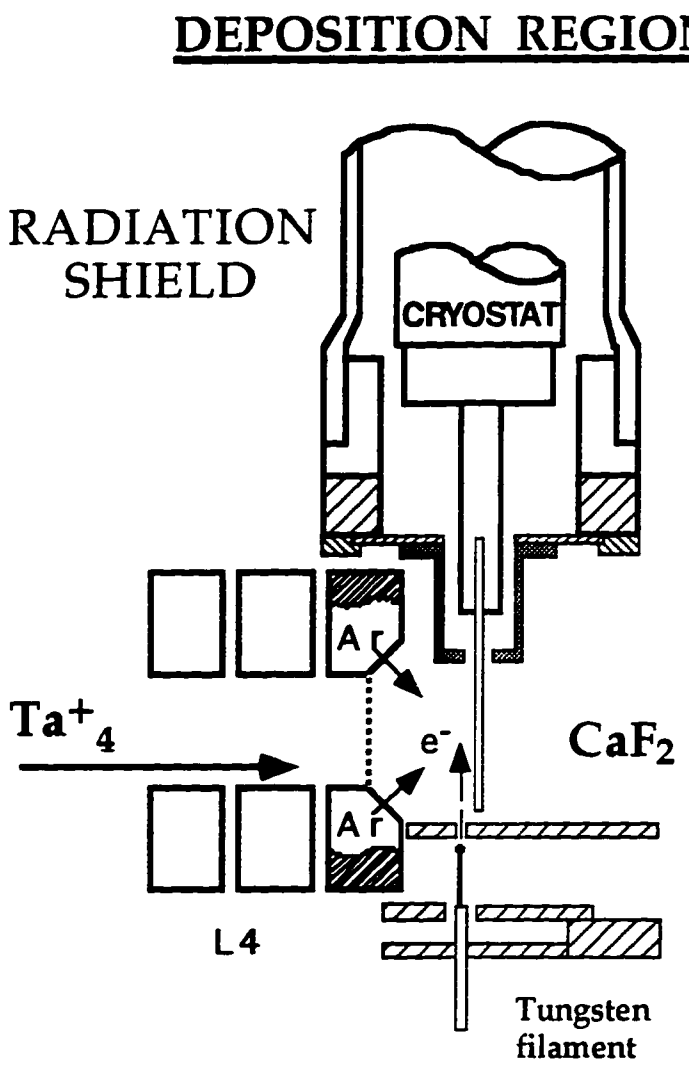

Figure III.4.4 Closed cycle cryostat(Ref.8)

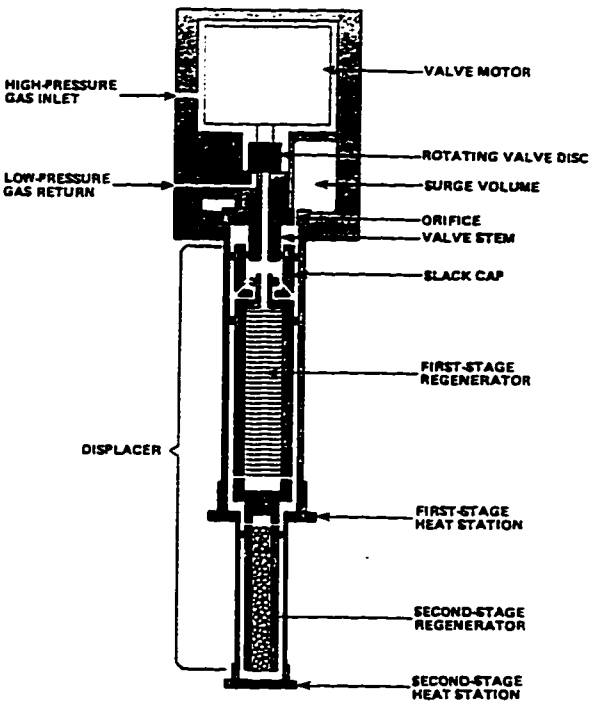

Figure III.4.3 Current Intensity as a function of Cryostat angle.

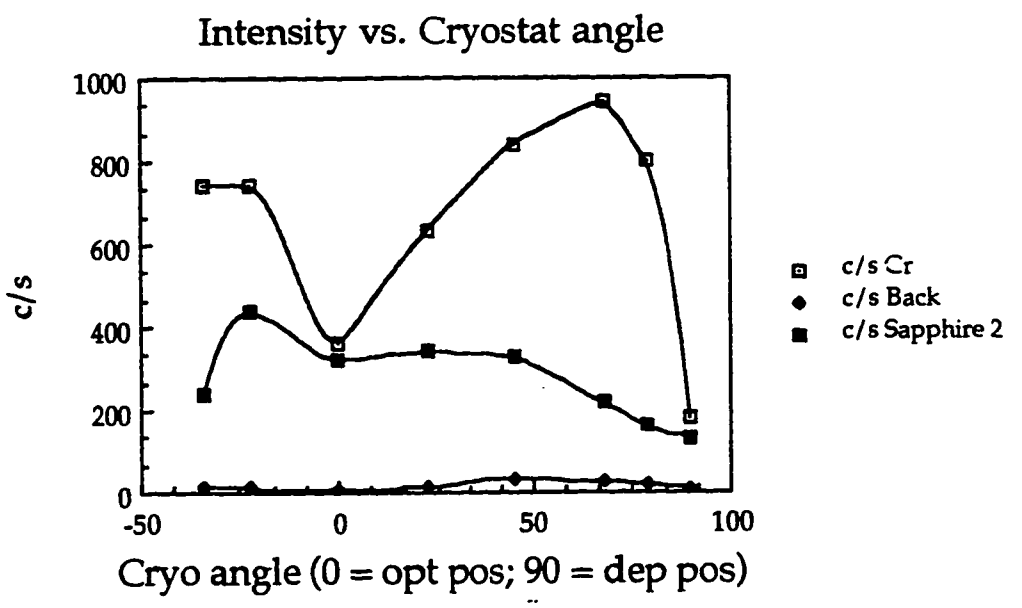

Figure III.3.1

Wien Filter (Velocity filter)

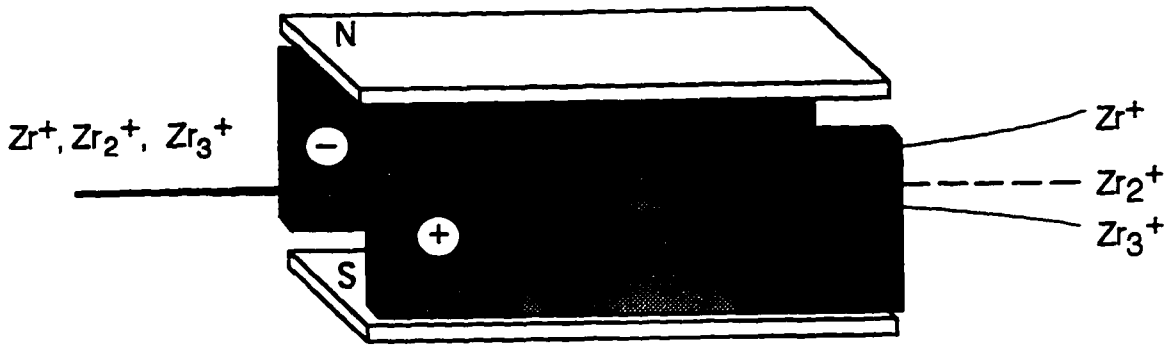

Figure III.3.2 Electrostatic lenses.

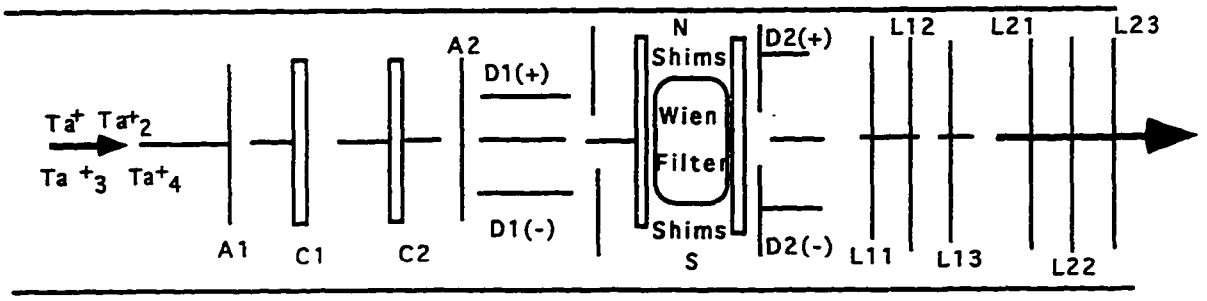

Figure III.6 The solvation and neutralization of tantalum clusters on the surface of argon matrix.

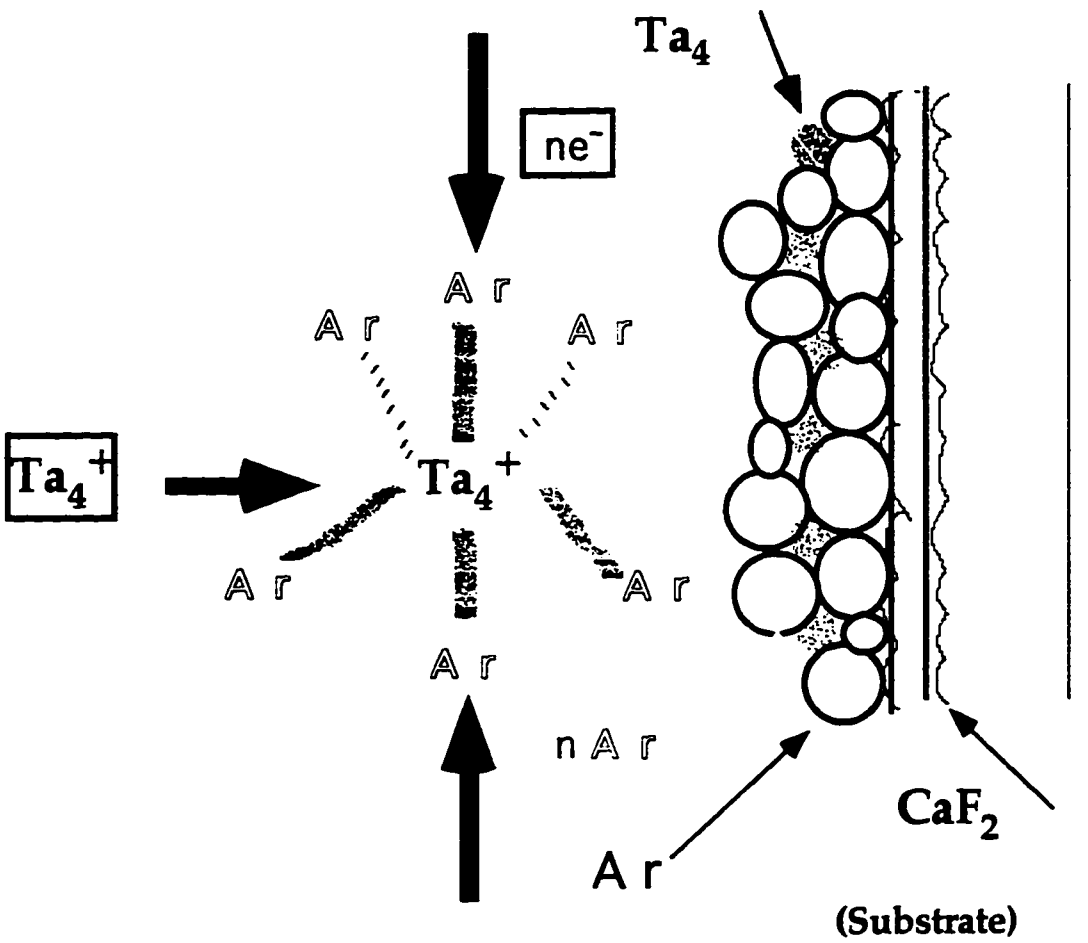

Figure III.4.2 **Ion current of tantalum clusters measured on a Faraday plate.**

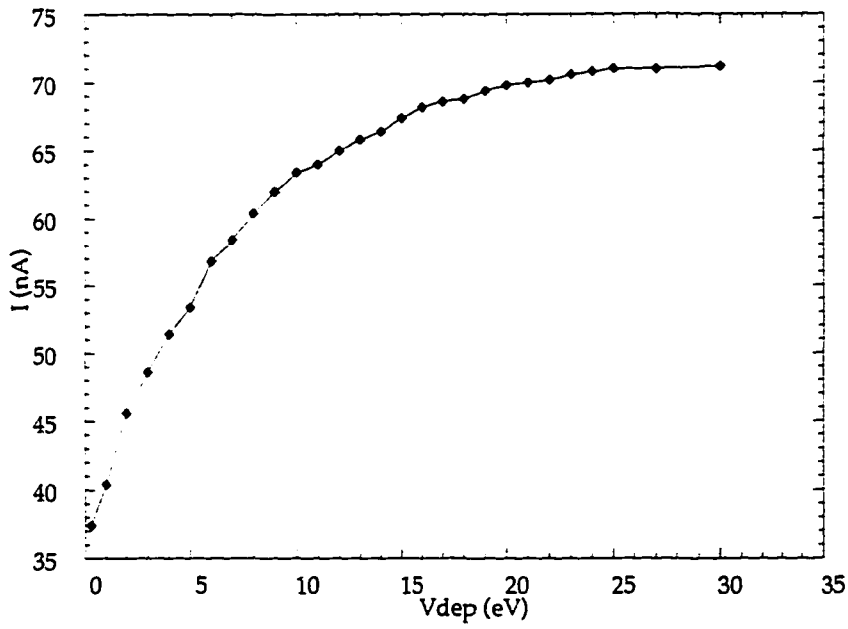

Figure III.3.3 Mass spectrum of some transition metal elements from sputtering target,by recording the current on the Faraday plate as a function of magnetic field on the Wien filter.

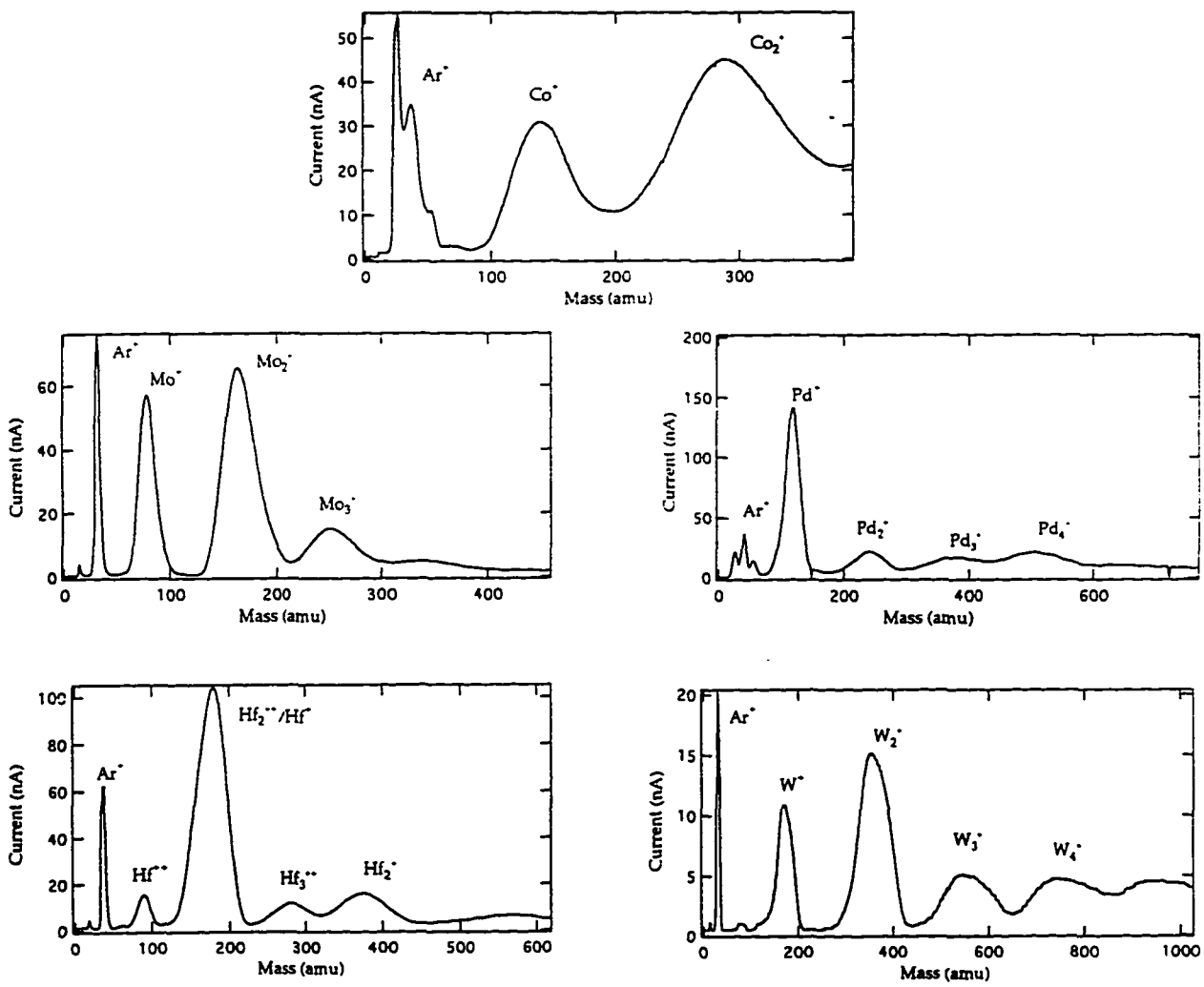

CHAPTER IV.Transition metal dimers

IV.1 Raman spectra of mass-selected tantalum dimers in argon matrices: Site effects

First of all it is worthwhile to note that because of the spectral simplification that results from working with cold systems, many investigators have turned to the matrix isolation technique for the study of high temperature molecules by freezing them to cryogenic temperature once deposited in a matrix. By all means this technique has the additional advantage that significant concentrations of molecules can be easily accumulated for leisurely study. However there are some disadvantages which are the sites effects caused by the matrix environments. In fact it has been shown that there is a shift in the wavelength of electronic and vibrational transitions of the species isolated in a cold host compared to the same species investigated in the gas phase, though this shift tends to be small. Anyhow the shift arises because the excited states of the species interact with the matrix to a different extent than does the ground state of the species.

The study of site[1] effects has been undertaken for the last three decades, but it is already known that the transition energy, lifetime, and other optical properties are strongly affected By the existence of the sites in

matrix. Multiple sites arise when molecules of a given host assume different environmental arrangements in a sample. This can be due to variations in the host structure in the guest environment, such as site symmetry, vacancies, or surface boundaries. A large number of ill-defined multiple sites occurs in almost all vapor-deposited matrices as was explained in Chap III.6. At very slow deposition rates on cold surfaces, the number of different sites is so large that very broad spectra result. In addition, matrices often contain vacancies and gross lattice defects with host molecules occupying distorted sites on the surface of the bulk crystal.

Our first observation matrix effects was in the tantalum dimer sample. In fact, it is the only sample that showed this effect so far besides Zr_2[3]. In the resonance Raman spectrum of tantalum dimers (see Figure IV.1.1 and Figure.IV.1.2) we saw four different sites. We calculated the vibrational frequencies taking into consideration the four sites observed (see Figure IV.1.3 and Figure IV.1.4). Also the results are summarized in Table IV.1.1 Analysis of Raman lines by standard techniques results in a determination of ω_e=296.3±1 cm^{-1} $\omega_e x_e$=0.53 cm^{-1} for site 2. The absorption (SDS) spectrum of tantalum dimers is shown in Figure IV.1.5. We have already done a resonance Raman study of tantalum dimers[2]. However, no sign of any sites were found. In fact ω_e was equal to 300.2 cm^{-1}. The only difference between the two experiments is that in the

recent one we have improved our spectrometer and detection system. Other than that all the experiment conditions are equal. Probably the charge Couple Detector makes it easier to detect the site effects in Raman lines than a photomultiplier tube.

It has been demonstrated that annealing has an effect on sites. In fact they can be reduced to one or a few stable arrangements through annealing. But nevertheless, annealing fulfills its purpose only if the guest is heavier than the host otherwise guest diffusion occurs, resulting in dimer formation and aggregates until such products are heavier than the host and remain trapped in their cage[1].

As mentioned before matrices are often annealed or tempered. For this purpose, the sample is heated up until local site rearrangement becomes efficient, but long-range diffusion is still slow. Tantalum dimer samples have been annealed to different temperatures 40K, 35K, 30K, 25K, 20K (see Figure.IV.1.6.a and Figure.IV.1.6.b). At 40K we start to loose the sample. We will expect that some peaks will disappear otherwise the observed peaks are not from sites but from some impurities or isotope effects. However in our case we can confirm that the splitting observed in Raman peaks were due to sites and not from impurities or transitions to different states as was first thought before annealing. Thus annealing the sample is one method of testing the presence of sites if some splitting is observed in Raman peaks. However often the splitting is due to isotope effects. This means

that this hypothesis should always be taken in consideration instead of being ruled out.

Figure IV.1.5 Scattering Depletion Spectroscopy (SDS) of tantalum dimers (245 nA-h).

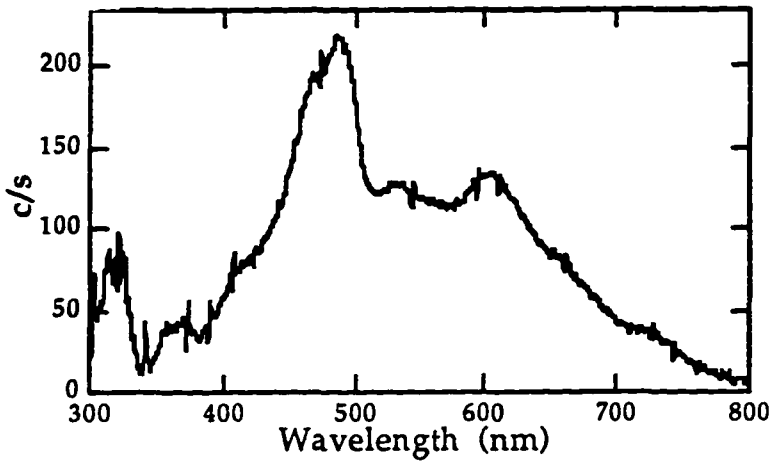

Figure IV.1.1 Raman signals of tantalum dimers λ_{ex}=465.74 nm

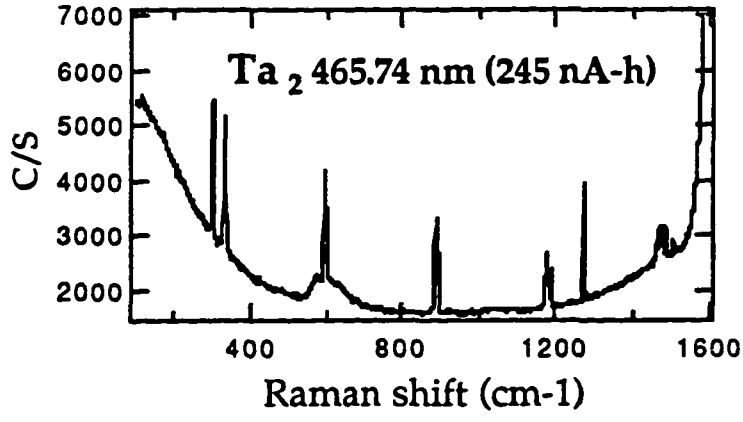

Figure IV.1.2 Raman signals of tantalum dimer, λ_{ex}=476.44 nm.

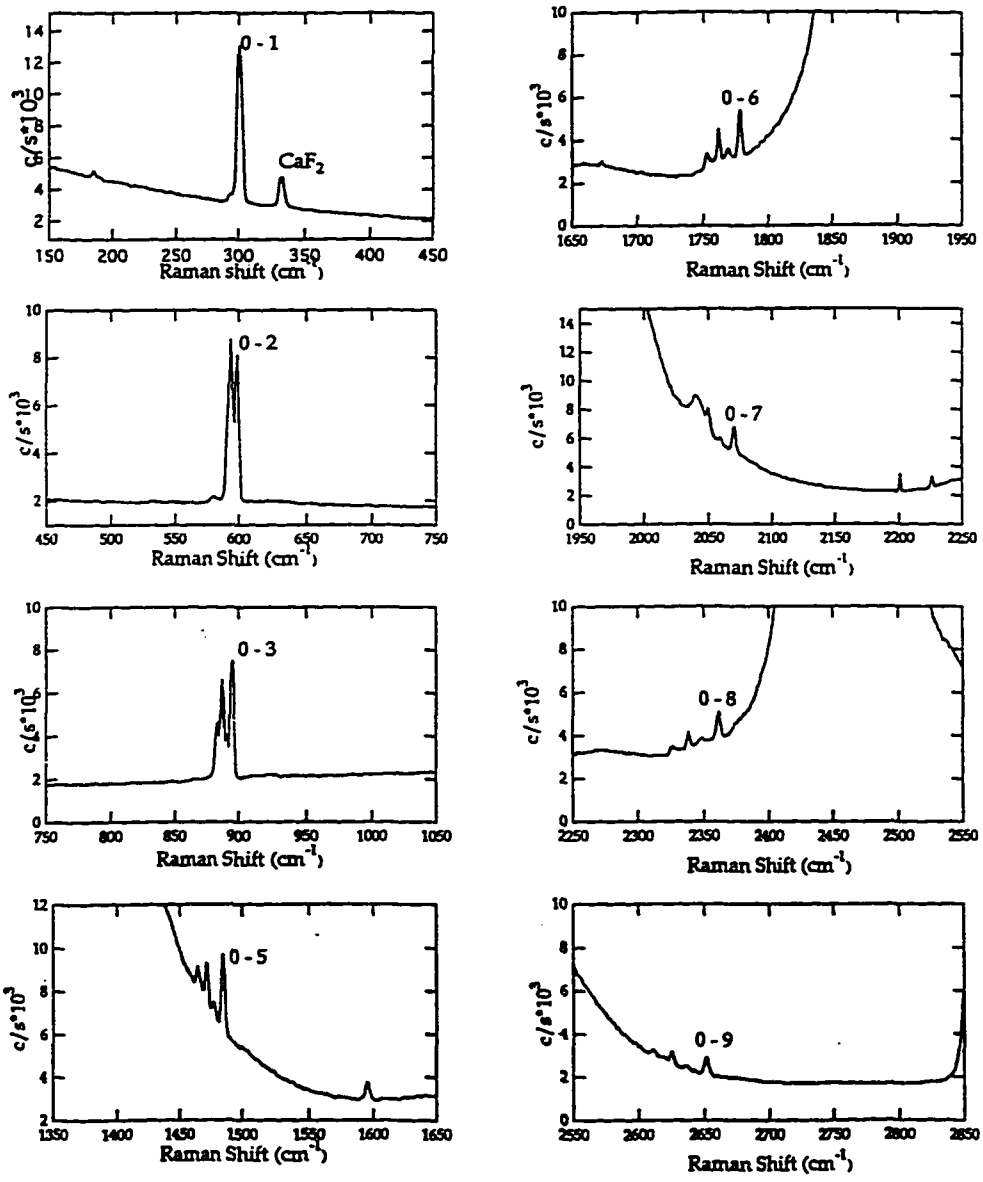

Figure IV.1.3 ω_e and $\omega_e x_e$ of the four sites of Ta_2.

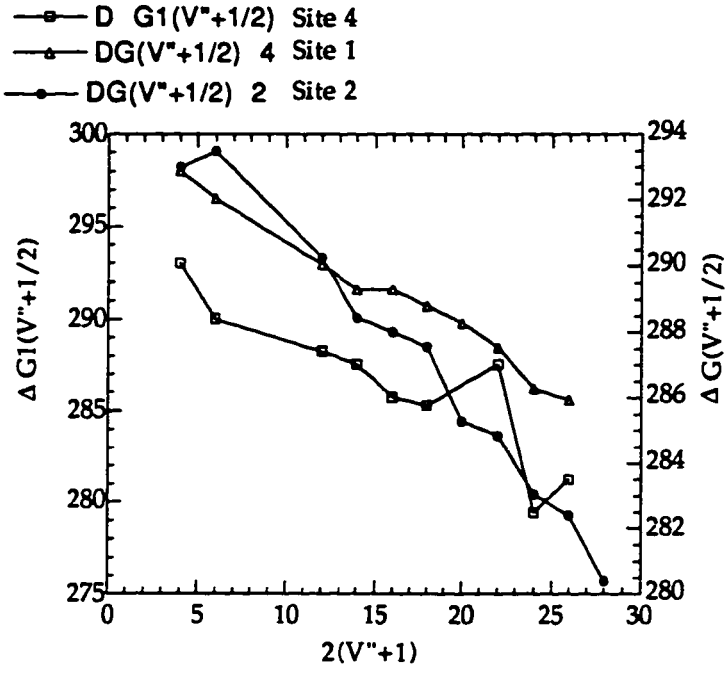

Figure IV.1.4 ω_e and $\omega_e x_e$ of Ta_2 site 2.

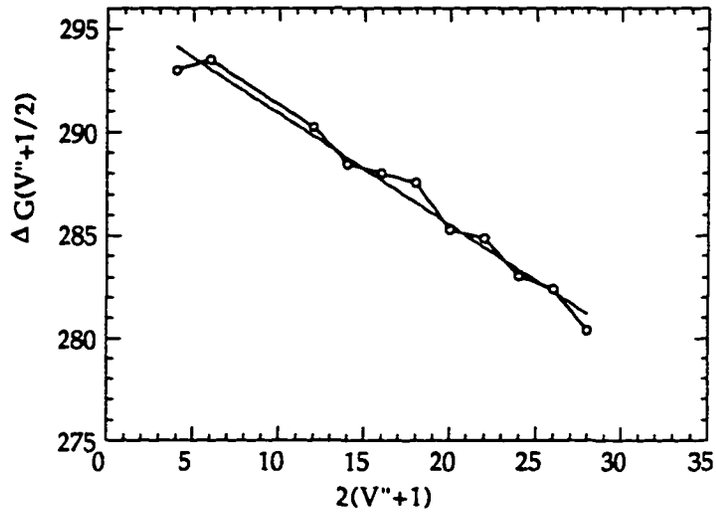

Table IV.1.1 Observed resonance Raman transitions (in cm^{-1}) for the four sites of Ta_2.

G(V")	DG1(V"+1/2)	G(V")2	DG(V"+1/2) 2	G(V")3	DG(V"+1/2) 3	G(V")4	DG(V"+1/2) 4
301.000	293.000	301.000	293.000			301.000	298.000
594.000	290.000	594.000	293.500			599.000	296.500
883.500		887.500		891.500		895.500	
1465.00	288.250	1471.50	290.250	1477.50	291.450	1485.00	292.950
1753.20	287.550	1761.75	288.450	1768.95		1777.95	291.600
2040.30	285.750	2050.20	288.000			2069.55	291.600
2326.50	285.300	2338.20	287.550	2059.20		2361.15	290.700
2611.35		2625.75	285.300	2348.55	289.350	2651.85	289.800
2898.90	287.550	2911.05	284.850	2635.65	287.100	2941.65	288.450
3178.35	279.450	3195.90	283.050			3230.10	286.200
3459.60	281.250	3478.95	282.400			3516.30	285.600
3456.00		3761.35	280.400			3801.90	
		4041.75					

Figure IV.1.6.a Annealing Ta_2 Raman signals to different temperature from 12K to 40K.

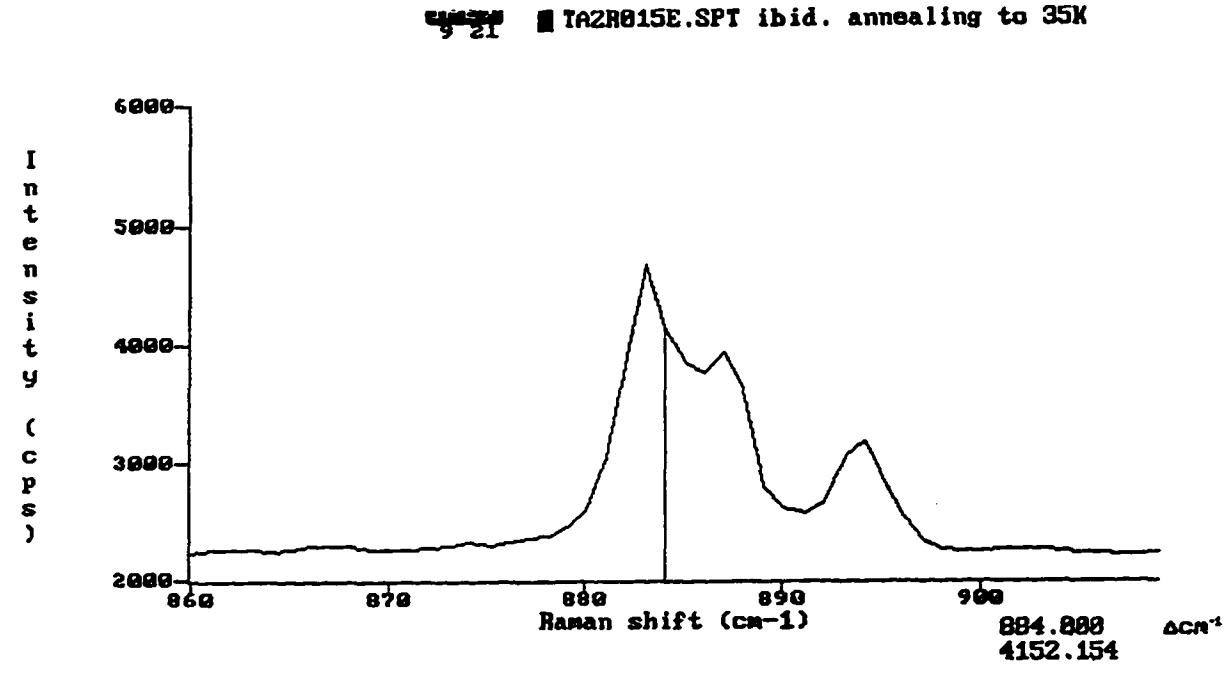

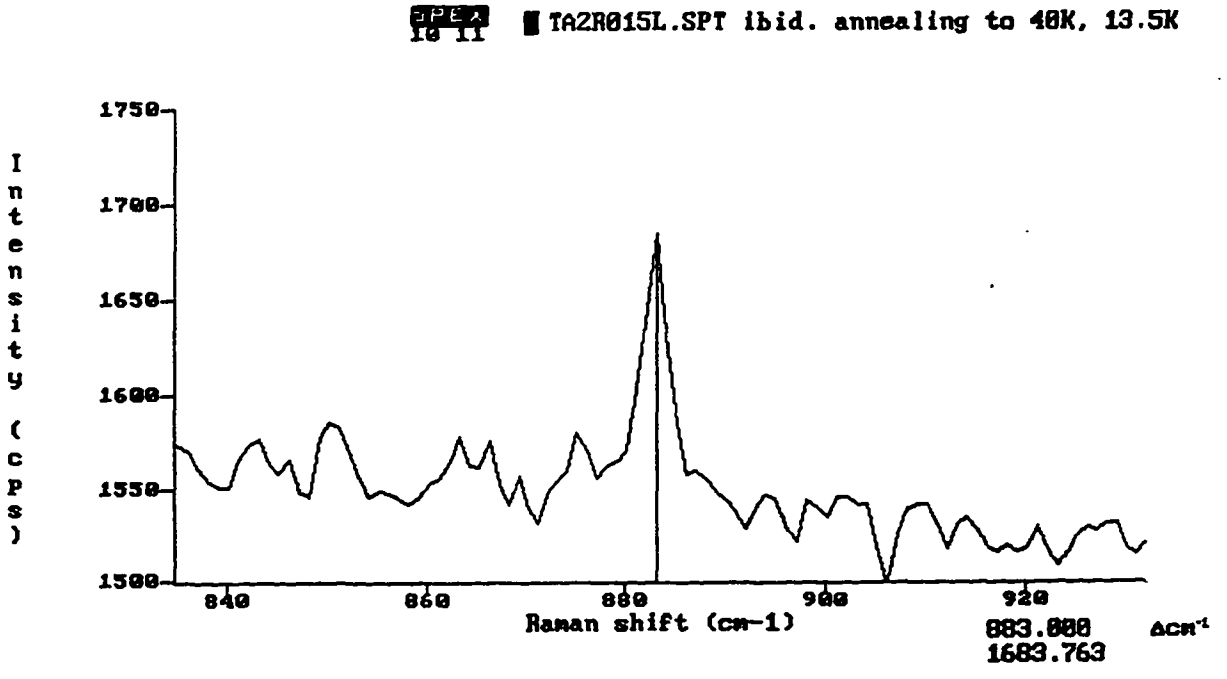

Figure IV.1.6.b Annealing Ta_2 Raman signals to different temperatures from 13.5K to 30K.

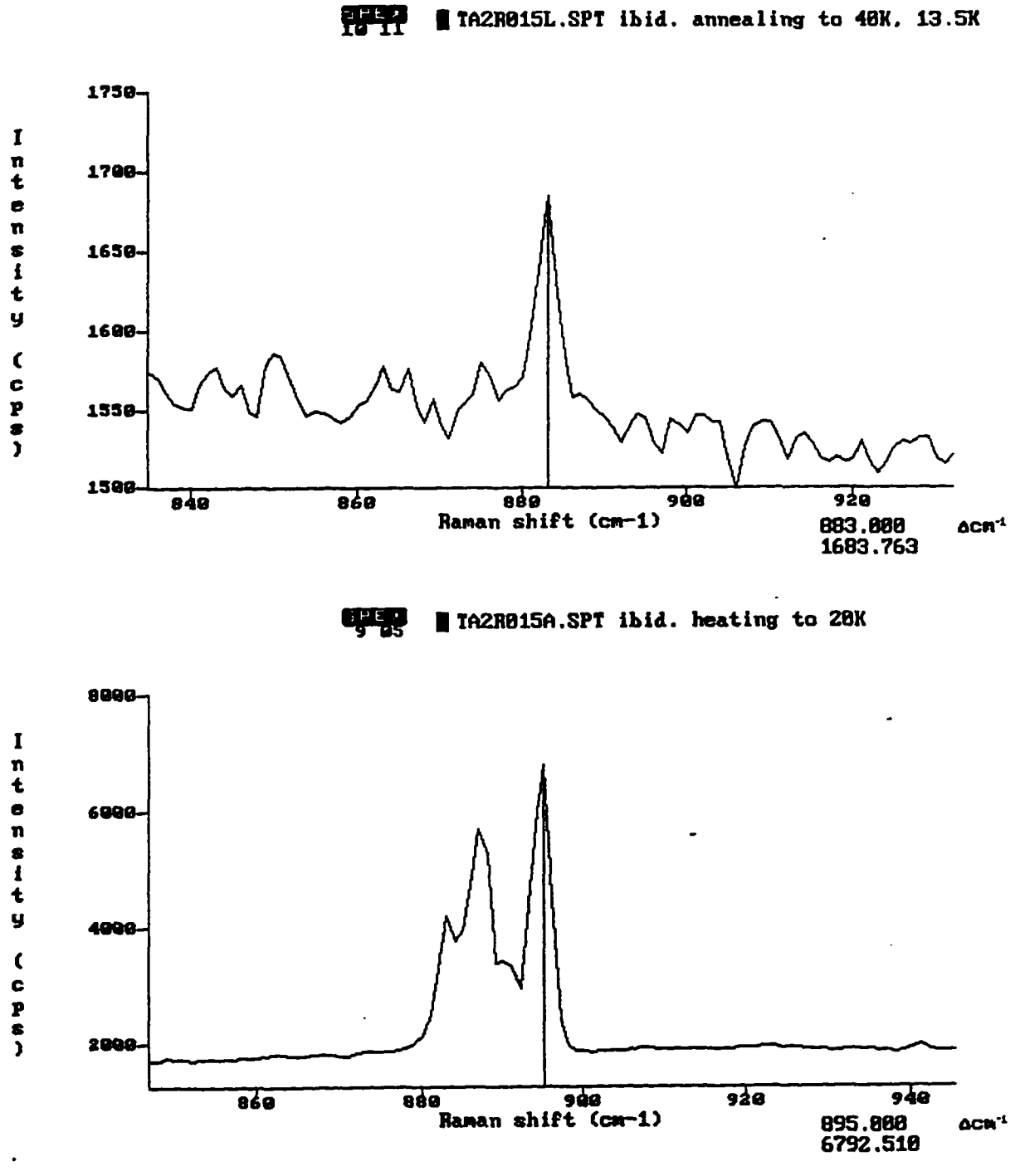

IV.2.Raman Spectra of mass-selected nickel dimers in argon matrices

Huaiming Wang,Hanae Haouari,Robert Craig,John R.Lombardi, and D.M.Lindsay

Department of Chemistry and Center of Analysis of Structures and Interfaces (CASI), The City College of New York(CCNY), New York, New York 10031

A.Introduction

In several recent papers we have reported on the resonance Raman spectra of certain mass-selected transition metal dimers[1-6]. One of the important issues in these studies is gauging the extent of the contribution of d-orbitals to the bonding. A study of the diatomic force constants is often a sensitive measure of this contribution. The series of dimers from Fe_2 through Cu_2 provides a good test case since the atomic configuration d shell is increasingly filled. Leopold and Lineberger[7] have suggested that the contribution of 3d-3d bonding changes abruptly to 4s-4s between Co_2 and Ni_2. This may be attributed to the relatively contracted nature of the 3d orbitals compared to the diffuse nature of the 4s orbitals in Ni. However, we have observed[8] that due to the rather large uncertainty in the dinickel force constant, the possibility that the break occurs instead between Ni_2 and

Cu_2 cannot be discounted. With these considerations in mind, we have obtained the resonance Raman spectrum of a mass-selected sample of Ni_2 in an argon matrix at 14K. The Raman data show $\omega_e = 259.2$ (30) cm^{-1} with $\omega_e x_e = 1.9$ (7) cm^{-1}. We have confirmed our assignment by matching predicted isotopic shifts for each of the ^{58}Ni and ^{60}Ni dimer combinations. The resulting improvement in measured force constant enables us to show clearly that an abrupt change does occur from 3d-3d to 4s-4s between Co_2 and Ni_2.

B.Results and discussion

The mass spectrum of nickel dimers is shown in Figure IV.2.1.where the current of the dimers is obtained. The absorption (SDS) spectrum of an approximately 200nA-h sample, of Ni_2 shows two bands, as displayed in Figure IV.2.2. The 325nm band actually consists of four transitions which occur at 305.5, 316.5, 323.0 and 332.0 nm. Since the dimer fragmentation (25~30%, as noted above) was extraordinarily high (compared with our earlier work) and since atomic nickel in argon absorbs at 303, 317, 321 and 329 nm it is clear that these bands are due to interference from fragmented dimers. The second band is very weak, continuous and centered at approximately 480 nm. This band arises from isolated nickel dimers. This assignment is verified by the observation (see below) of resonance Raman spectra for several excitation wavelengths

in the range 457.9~496.5 nm. The plot of the ratio of the Raman intensity of Ni_2 to excitation power vs.excitation wavelength (excitation profile) shows a maximum Raman intensity at about 480 nm. The near coincidence of the dimer Raman excitation profile and the absorption band confirms the assignment. This dimer absorption feature is in agreement with that reported by De Vore et.al.[10] and Moskovits and Hulse

Raman spectra were recorded at six different visible lines of an argon-ion laser. Figure IV.2.3 shows a typical Raman spectrum for Ni_2 in an argon matrix. The principle features of the spectrum are a vibrational progression (labeled $\upsilon'' = 0 \rightarrow \upsilon'' = 1, 2, 3$) and a non resonant Raman transition from the CaF_2 substrate. The $\upsilon'' = 2$ and 3 components each consist of a triplet. Naturally occurring nickel has three dominant isotopes, ^{58}Ni (67.88%), ^{60}Ni (26.23%) and ^{62}Ni (3.6%) so the three components[11] of each band as shown in Figure IV.2.3 can readily be assigned to $^{58}Ni_2$, $^{58}Ni^{60}Ni$, and a combination of $^{60}Ni_2$ plus $^{58}Ni^{62}Ni$. Isotope shifts for the fundamental band ($\upsilon'' = 1$) were too small to be resolved. We were able to reproduce exactly the structure of each Raman transition (see Table IV.2.1) using the expression [12]

$$\nu_{ij} = 1000\xi\left[\frac{(M_i + M_j)}{0.58916 M_i M_j}\right]^{1/2} \qquad (1)$$

where ξ is a constant determined by setting ω_e =259.2 cm^{-1} for ^{58}Ni and Mi, Mj are isotopic masses. We take this fit as an absolute confirmation of the assignment of this spectrum to the nickel dimer species. No intensity is observed on the anti-Stokes side of the exciting light, precluding the possibility that we are observing a radiatively populated excited state.

In Table IV.2.1 we list the average (one standard deviation in parentheses) of the Stokes shifts found for six different excitation wavelengths between 457.9 nm and 496.5 nm and those calculated using equation (1). Using standard methods[13], the Stokes shift data give ω_e = 259.2 (30) cm^{-1} with $\omega_e x_e$=1.9 (7) cm^{-1} for $^{58}Ni_2$ in argon matrix. The calculated frequencies for each isotope are also listed in Table IV.2.1 Previous to this work, the best dimer frequency reported was 280 ± 20 cm^{-1} obtained from photodetachment studies[14]. Although the Raman and photodetachment results nearly differ by more than their reported uncertainties, the dinickel photodetachment spectra are relatively congested. Accordingly, the two values for ω_e should not be viewed as being in disagreement with each other[15].

Any how Our result is somewhat smaller. However, due to the higher resolution and narrower lines afforded by Raman spectroscopy and the clear confirmation of the isotopic shifts, our results are more accurate.

In our previous paper[8], we have compared the force constants of the "late" first row transition metal dimers and shown that a distinct break occurred between cobalt and copper. Because of the relatively large error in the dinickel force constants we could not preclude a transition following Ni_2 rather than after Co_2[8], at that time. In the light of the improved accuracy of our results, it is worthwhile comparing again experimental force constants for the series $Fe_2 \rightarrow Cu_2$ (using the data: Fe_2 1.48 mdyne/Å[16]; Co_2 1.53(6) mdyne/Å[8]; Ni_2 1.16(2) mdyne/Å (this work); Cu_2 1.33 (1) mdyne/Å[17]). As shown in Figure IV.2.4, there is an abrupt drop in this parameter from Co_2 to Ni_2. These observations rather strikingly support the suggestion of Leopold and Lineberger[7] that "chemical bonding in the homonuclear diatomics changes from 3d-3d to 4s-4s between Co_2 and Ni_2." In other words, it can be concluded that there is no substantial 3d electron contribution to the chemical bonding on Ni_2. This confirms earlier theoretical predictions,[18] employing Hartree-Fock methods with extensive configuration interaction, that chemical bonding in nickel dimer originates primarily from the interactions of the 4s orbitals on each Ni atom. In addition Recent calculations[19] utilizing ligand field theory indicate several low lying states arising from the $3d_A^9 3d_B^9 \sigma_g^2$ configurations. The lowest are the case(c) 0^+_g , 0^-_u and 5_u states at 0, 12 and 58 cm^{-1} respectively.

Figure IV.2.4 also shows the force constant for Ni_2 (1.16 mdyne/Å) is even lower than that of Cu_2. This should not be all that surprising since we might expect the 4s orbital of nickel in $3d^94s^1$ to be larger than that of copper in its $3d^{10}4s^1$ configuration. However, a recent gas phase resonant two-photon ionization study[20] has shown by careful rotational analysis that the ground state (which they establish to be case(c) 0^+_g or 0^-_u) bond length of Ni_2 is somewhat shorter (by 0.0652(8) Å) than that of Cu_2. Badger's rule would then suggest a larger force constant for Ni_2 than for Cu_2 contrary to our observations. Several recent measurements suggest that Badger's rule may be violated in transition metal dimers more often than observed for other molecular species. For example in the A state of rhenium dimer[21], a Franck-Condon analysis of the absorption spectrum indicates a decrease in internuclear distance on excitation from the ground (X) state, while the force constant also decreases. This was attributed to a different dissociation limit for the two states. In a gas phase rotational analysis of niobium dimer, James and coworkers[22] found that both the A and the E states show an increase in both force constants and vibrational frequencies with respect to the ground state, once again violating Badger's rule.

Figure IV.2.1 Mass spectrum of Ni clusters from sputtering target, measured in-situ by recording the current on the Faraday plate as a function of magnetic field on the Wien filter.

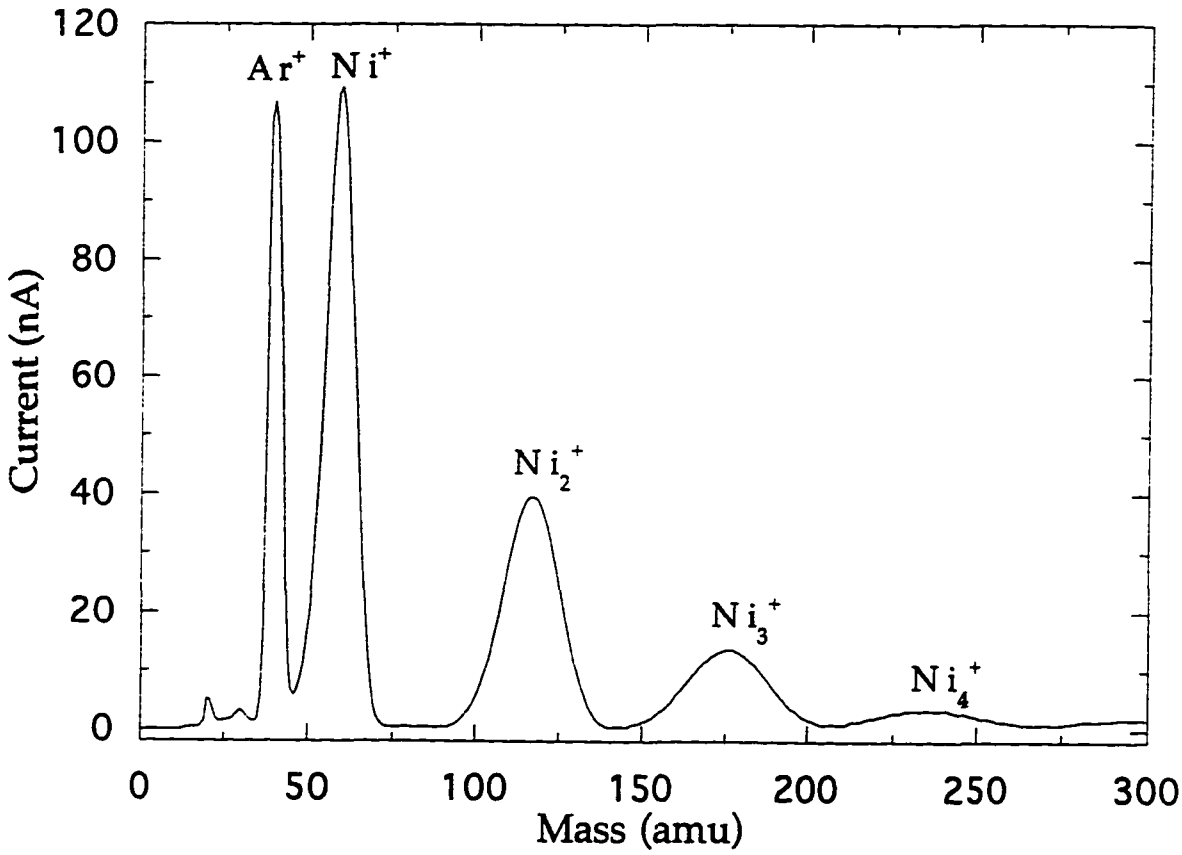

Figure IV.2.2 Absorption (scattering depletion) spectrum of deposited Ni_2 in an argon matrix at 14K. The spectrum was assembled in 2 segments, but has a common ordinate scale. Two regions of absorption occur. That near 325 nm may be assigned to atomic lines. The weak band near 480 nm is assigned to the dimer spectrum. The dotted line (...) represents the background. The insert shows the Raman excitation profile of Ni_2 in an argon matrix.

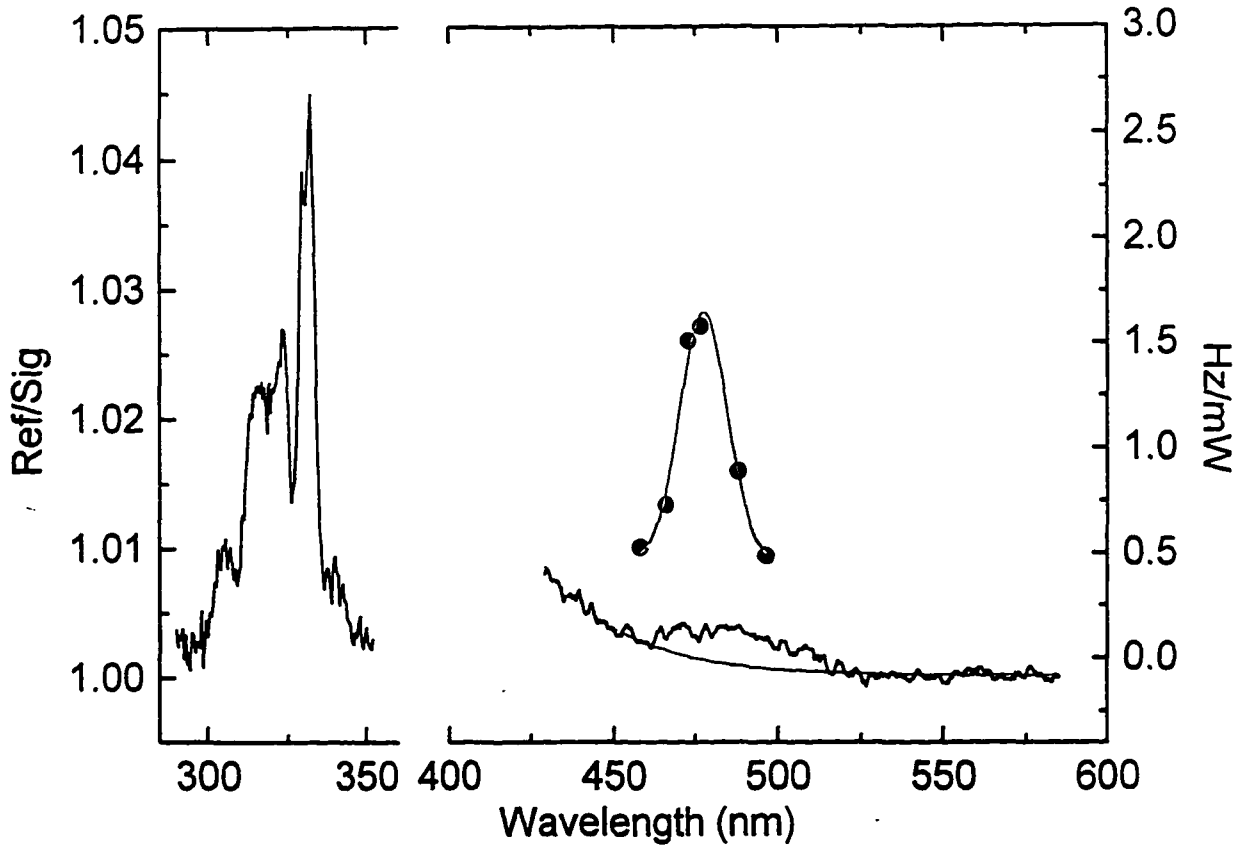

Figure IV.2.3 Raman spectrum of Ni_2 in an argon matrix at 14K with 476.5 nm excitation after subtraction of Rayleigh line. The overtones display a triplet structure which is due to isotopic compositions. The position and intensities of the stick spectra are calculated.

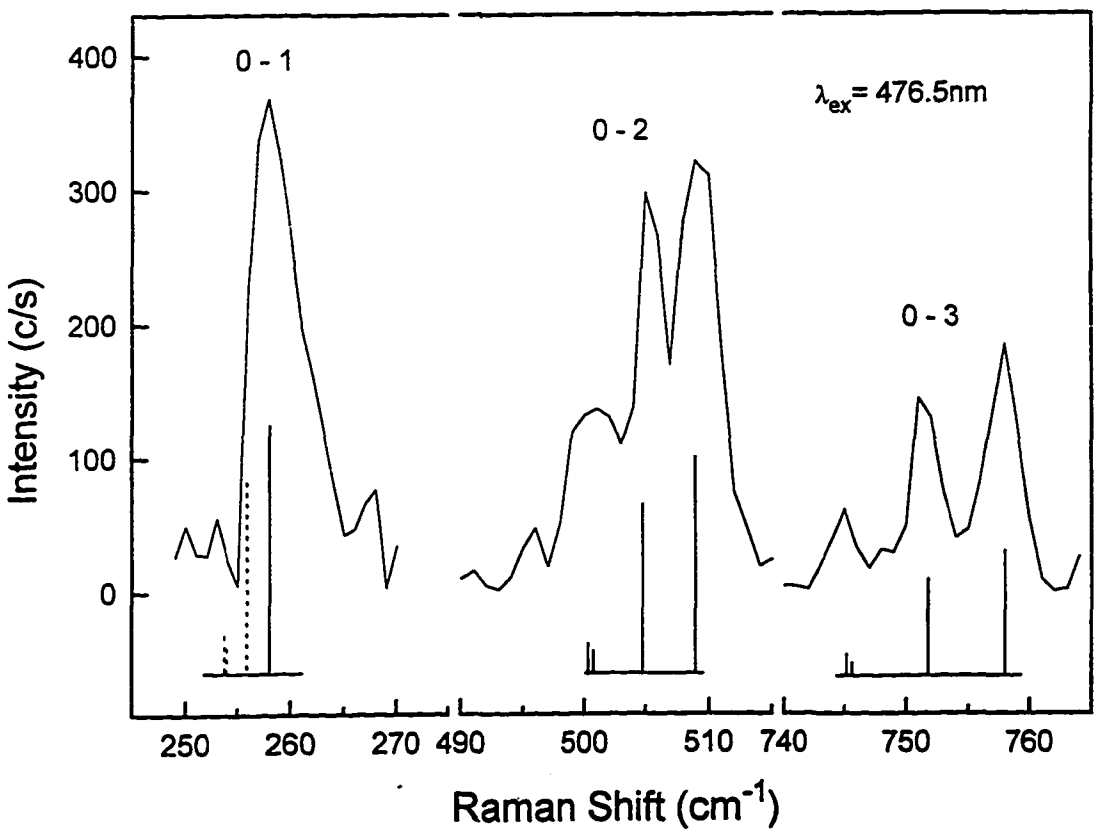

Figure IV.2.4 Experimental force constants (mdyne/Å) vs.atomic number for several first row transition metal dimers. The data (k in mdyne/Å) are: 1.48 for Fe_2 (Ref.16), 1.53(6) for Co_2 (Ref.8),1.16(3) for Ni_2 (this work), and 1.3391(1) for Cu_2(Ref.17).

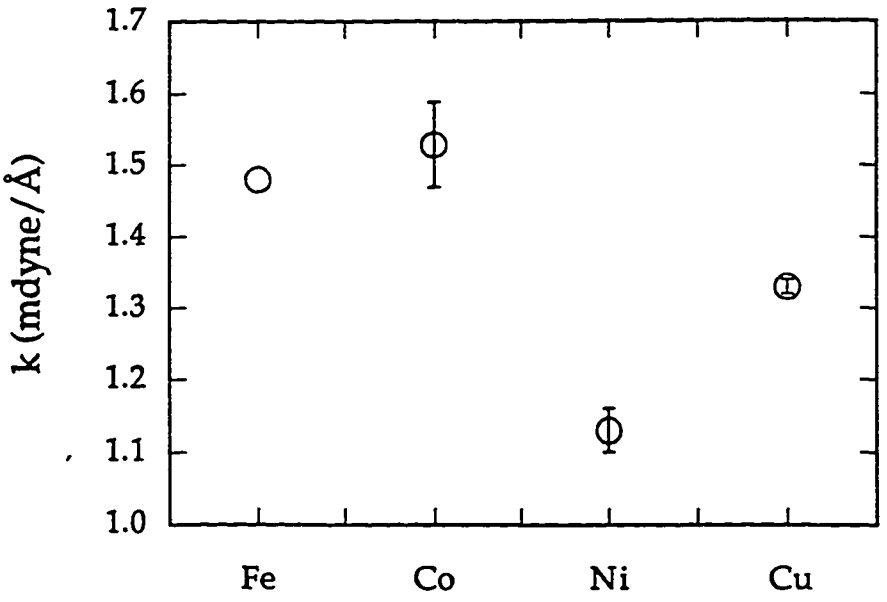

Table IV.2.1 Raman frequency shifts and ground state constants (cm^{-1}) for nickel dimers and their dominant isotopes in an argon matrix. Estimated errors (1 standard deviation) in parentheses.

	$^{58}Ni_2$		$^{58}Ni^{60}Ni$		$^{60}Ni_2$	
ω_e observed	259.2 (30) [a]					
ω_e calculated	259.3 [a]		257.0 [d]		254.8 [d]	
v"	obs. [b]	calc. [c]	obs. [b]	calc. [e]	obs. [b]	calc. [e]
1	256.3 (21)	255.5		253.0		251.1
2	506.5 (15)	507.3	502.5 (15)	503.0	498.9 (20)	498.6
3	755.4 (15)	755.4	749.1 (21)	748.9	743.1 (21)	742.3

a. Using obs. or calc. Stokes shifts and $\Delta G(v"+1/2) = \omega_e - 2\omega_e x_e(v"+1)$. [13]

b. Average Stokes shifts from 6 laser frequencies.

c. Using $\omega_e = 259.2$ (30) cm^{-1} with $\omega_e x_e = 1.9$ (7) cm^{-1}.

d. Using Eqn (1) in text with $\zeta = 1.0714$.

e. Using "ω_e calculated" with $\omega_e x_e = 1.9$ (7) cm^{-1}.

IV.3 Spectroscopy of mass-selected rhodium dimers in argon matrices

Huaiming Wang, Hanae Haouari, Robert Craig, Yifi Liu, John R. Lombardi, and D.M. Lindsay

Department of Chemistry and Center of Analysis of Structures and Interfaces (CASI), The City College of New York (CCNY), New York, New York 10031

A. Introduction

Rhodium metal is quite important as a catalyst in many processes. Despite this fact, relatively little is known experimentally about the properties of small metal clusters[1,2,3] of this material, although there are numerous theoretical calculations on the dimer of rhodium. Shim[4] carried out the first *ab initio* plus CI calculation, while Balasubramanian and Liao[5] conducted a complete active space SCF calculation followed by a multi-reference configuration interaction calculation including spin-orbit interactions. Illas *et. al.*[6] carried out studies utilizing a set of nonempirical relativistic pseudopotentials and a rather large basis set with *f*-orbitals. More recently density functional theory has been applied by Harada and Dexpert[7]. Cocke and Gingerich[8] obtained a thermodynamic value for the dimer dissociation energy (D_e =2.92eV) using third law methods. Of interest here are values for the ground state vibrational frequency (ω_e) and the anharmonicity ($\omega_e x_e$)

from which we can determine a value of the spectroscopic dissociation energy. In the studies mentioned above predicted values of ω_e ranged from 118 cm^{-1} to 267 cm^{-1} while D_e has been reported to be anywhere from 0.25 eV to 2.92 eV. In order to resolve these contradictions, new experimental results are clearly in order.

The resonance Raman spectrum and absorption (scattering depletion) spectrum of Rh_2 in argon matrices have been obtained. Our samples are prepared by neutralizing a mass-selected beam of dimer ions, and therefore there is little or no interference between the spectroscopic transitions of the dimer and those from atoms and trimers. This allows an unambiguous assignment of spectral features. From the absorption spectrum only a single dimer transition (a broad band near 495 nm) could be positively identified. By resonance excitation into this band at eight different Argon ion laser frequencies, we obtained sharp Raman progressions with transitions up to the fourth Stokes line. These data give ω_e=283.9± 1.8 cm^{-1} with $\omega_e x_e$ =1.83 ±0.33 cm^{-1}, which gives a spectroscopic dissociation energy ($D_e = \omega_e^2/4\omega_e x_e$) of 1.4±0.3 eV.

B. Experimental

The CCNY cluster deposition source has been described in detail elsewhere.[9] Briefly, an argon ion beam (typically 15mA at 25keV) sputters a cooled, rhodium target

(Alfa,99.9%). The sputtered products are extracted by electrostatic lenses, mass-selected using a Wien filter, bent by 10° to eliminate neutrals and then guided into the deposition region. Rhodium dimer (or atomic) ions were then co-deposited with argon gas and electrons onto a ~14K substrate, composed of a CaF_2 plate. Ion currents under soft landing conditions could be measured on a Faraday plate in the deposition region and were: Rh^+(70 nA), Rh_2^+(13 nA), and Rh_3^+(12 nA), as shown in Figure IV.3.1. Prior to deposition, the selected ions were simultaneously slowed to 10eV by a surrounding "Faraday cage". Matrices were grown at about 4~6μ/h with an Ar:metal ratio of approximately 10^4:1. By comparing the intensities of known atomic excitation features in a dimer deposition with those obtained from depositions of the atom under similar conditions, the dimer fragmentation is approximately 1%.

Matrix samples were interrogated *in situ* using both absorption and Raman spectroscopy. As previously reported[10,11] the absorption measurements were made by collecting the light at 90° to that incident, a technique we term "Scattering Depletion Spectroscopy" (SDS).

Raman spectra were recorded using eight visible lines of an argon ion laser (Spectra Physics model 2045) between 457.9 nm and 514.5 nm. Scattered light was collected at 90° into a Spex 1877E (0.6m) Triplemate Spectrometer and detected by a liquid nitrogen cooled CCD detector (Spex model "Spectrum One") with DM3000R software.

C. Spectra and analysis

Figure IV.3.2 shows a "Scattering Depletion Spectrum"(SDS) of rhodium dimers in argon matrix at 14K. The spectrum was obtained following the deposition of 50-60nA-h of Rh_2 at an energy of 10eV and was recorded with 0.4 nm resolution using a tungsten lamp. Only one absorption feature is shown with maximum at about 495 nm. Previous studies of rhodium in argon (without mass-selection) had also identified a 495 nm feature, but this was attributed to rhodium trimers. [12]The authors of Ref.(12) also reported optical absorption spectra for atomic rhodium in the range 250-400 nm, and these data are in good agreement with excitation spectra following the deposition of Rh^+ in argon. Annealing the sample to 36K had little effect on the absorption spectrum. By comparing the absorption features of diatomic rhodium in argon with those obtained from the atom in argon[11,12] we can attribute these transitions to rhodium dimer with confidence. This assignment is verified by the observation of resonance Raman spectra for excitation into this band.

Resonance Raman spectra were obtained at eight different Argon ion laser frequencies in the range 457.9-514.5 nm. Up to four Stokes transition could be observed, a typical Raman scan is shown in Figure IV.3.3 Due to the high cost of Rh metal, only one dimer deposition was made,

contrary to our usual practice. However several independent scans of the spectrum were carried out at different points on the sample plate. The average of 8 separate scans produce lines at 281.3(15) cm^{-1}, 556.0 (18)cm^{-1}, 827.4 (22)cm^{-1}, and 1097.0(23) cm^{-1}. We report one standard deviation of each measurement in parentheses. These clearly can be assigned to the v = 0 through v = 3 components of a progression in the single ground state vibrational frequency of rhodium dimer. Analysis of these lines by standard techniques[13] results in a determination of ω_e= 283.9± 1.8 cm^{-1} with $\omega_e x_e$=1.83± 0.33 cm^{-1}. Raman excitation profiles (Stokes intensity divided by laser power) as shown in Figure IV.3.4 closely parallel the 495 nm absorption band, thus further confirming its assignment to the dimer.

D.Discussion

Our results do not shed any light directly on the spin or orbital nature of the ground state of rhodium dimer. However, they do represent the first unambiguous experimental determination of ω_e, $\omega_e x_e$ and, as a result, D_e. It is therefore worthwhile to discuss our data in the light of the widely disparate predictions of the several dimer calculations (summarized in Table IV.3.1) reported to date.

The largest value reported for the dimer dissociation energy (2.92 eV) was determined by Cocke and Gingerich[8], using a third law analysis of high temperature Knudsen

effusion mass spectrometric data. A disadvantage of this method is that it requires knowing ω_e, r_e(the equilibrium internuclear distance) and the electronic partition function for the dimer. Although the value assumed for ω_e(267 cm^{-1}) is close to that reported here(284 cm^{-1}), the remaining parameters are still unknown.

The remainder of the results in Table IV.3.1 represent several quantum mechanical calculations, with varying degrees of sophistication. It is first striking that there is almost total disagreement as to the assignment of the nature of the ground state. Most researchers seem to agree that the ground state is of quintuplet spin degeneracy, but Σ_g^+, Δ_g, and Δ_u are all separately suggested as candidates for the orbital state. This difficulty is due to the open shell nature of the configurations involved, stemming from Rh($4d^8 5s^1$; $^4F_{9/2}$) as well as other spin-orbit components within 0.43 eV of the atomic ground state. In addition, there are low lying excited states ($4d^9$; $^2D_{5/2}$ and $^2D_{3/2}$) at 0.41 and 0.70eV, respectively. Correlation with dissociation to two ^4F atomic states alone predicts 112 low lying molecular states before spin-orbit effects are taken into account. Thus we might anticipate considerable difficulty in determining the properties of the ground state of Rh_2 even with recent advances in computational abilities.

The calculations of Shim[4] were carried out using SCF/CI leading to a $^5\Sigma_g^+$ ground state with the dominant

configuration of $\pi_u^3\delta_g^3\delta_u^3\pi_g^3$. Both ω_e (118 cm^{-1}) and D_e (0.85 eV) are very small by comparison with our results. Given the limited nature of this calculation, it is not expected that very accurate results can be obtained. Somewhat better results were obtained by Harada and Dexpert[7] who utilized density functional theory using an all-electron Gaussian basis set for three different multiplicities, as well as employing a relativistic effective core potential (ECP) with non-local corrections. These calculations make a good case for the quintuplet nature of the ground state. For the quintuplet calculations, a vastly improved ω_e (191 cm^{-1}) is obtained, though this is still considerably lower than the experimental result. This is most likely due to the lack of inclusion of relativistic corrections in the density functional theory. Presumably, effective core potentials were added with the intent of correcting for lack of relativistic terms. However, this modification results in almost no change in the value for vibrational frequency. The density functional value for D_e (2.09 eV) is somewhat larger than the experimental result though the inclusion of the effective core potential reduces the value of this parameter to 1.32 eV. The use of an effective core potential usually tends to lower the dissociation energy, since correlation effects cannot be adequately calculated with elimination of nodal structure in the effective core. Despite the excellent agreement with experiment for D_e for the ECP calculation, the rather poor determination of ω_e,

which should actually be more accurately determined, suggests that the agreement of the calculated value for D_e may be fortuitous.

The best agreement for a value of ω_e between theory and experiment is perhaps provided by the calculations of Balasubramanian and Liao[5]. They carry out a complete active space multireference configuration interaction calculation on 36 electronic states including spin-orbit coupling. They employ relativistic effective core potentials retaining the outer nine electrons on each atom for the active space. A total of 105,000 configurations with single and double excitations were employed. The predicted ground state is $^5\Delta_g$ (4_g), which after spin-orbit effects are included lies 336 cm^{-1} below the first excited (3_g) state. The leading configuration for this calculation is $1\sigma_g^2 2\sigma_g^2 1\sigma_u \delta_g^4 \delta_u^3 \pi_g^2 \pi_u^4$ with an approximate bond order of 3. This differs from that of Shim[4] in that one electron is moved each from the antibonding π_g and σ_u orbitals to the more bonding π_u and δ_g orbitals, resulting in an increased bond order, and presumably increased ω_e, as well as D_e. This CASSCF calculation produces the best theoretical value of ω_e (267 cm^{-1}), very close to the experimental value, and D_e of 2.1 eV., which is somewhat larger than the experimental result. Their value of D_e was obtained by taking the difference between the calculated energy at 8Å separation and that of the equilibrium internuclear distance (2.28 Å). However, Illas *et. al.*[6] are critical of this approach. Using *ab*

initio CI methods, and including only states correlating directly to the atomic grounds states, they determine a ground state of $^5\Delta_u$ in contrast to the g symmetry of Balasubramanian and Liao. They find several low lying electronic states dissociating to the ground state of the isolated atoms which were not included by the latter authors and, further, they note that their (Balasubramanian and Liao) leading configuration does not dissociate to the atomic ground state (^{4}F). Illas *et. al.* suggest that as the internuclear distance increases, the leading configuration of Balasubramanian and Liao will change to one with the correct dissociation products. However, their own values for ω_e (238 cm^{-1}) deviates substantially from that determined here. This may be due to the lack of static correlation. Their atomic integrals were obtained using a monoconfigurational calculation, as opposed to the multireference CASSCF calculation of Balasubramanian and Liao. The value of Illas *et.al.* for D_e (1.5 eV), however, is quite close to the experimental result. Once again, in view of the poor value for ω_e obtained in these calculations, this may also be fortuitous.

It is also possible that the ground state of Rh_2 does indeed dissociate into excited states of the atoms. We have observed this previously for Re_2[14]. In this latter experiment we were aided by an extensive, and sharp absorption spectrum which enabled us to determine dissociation energies for several states. However, the

preference of transition metals for bonding with ns^1 configurations suggests most likely that Rh_2 will dissociate to ^4F ($4d^8 5s^1$) atoms. In any case, if Rh_2 dissociates to excited atoms, the fairly accurate ω_e of Balasubramanian and Liao, despite the limitations, may still represent the best extant theoretical description of the ground state. Our experimental results involve a vibrational frequency and therefore force constant which is greater than those suggested by *all* the quantum theories. This suggests a bond order even greater than 3, and that d orbital contributions are somewhat greater than those invoked in the theories so far. It is clear that further theoretical work is called for.

Table IV.3.1 Comparison of theoretical and thermodynamic results for ground state parameters of Rh_2 with spectroscopic data (this work).

Authors(Ref)	Method	Ground	ω_e^{-1}	D_e(eV))
Shim(4)	SCF/CI	$^5\Sigma_g^+$	118	0.85
Balasubramanian, Liao (5)	MCSCF(CASSCF)	$^5\Delta_g$ (4_g)	267	2.1
Illas et al.(6)	*ab initio*	$^5\Delta_u$	238	1.5
Harada and Dexpert(7)	Gaussian, density functional	singlet	245	0.25
Harada and Dexpert(7)	Gaussian, density functional	triplet	186	1.86
Harada and Dexpert(7)	Gaussian, density funct	quintuplet	191	2.09
Harada and Dexpert(7)	Effective core potential	quintuplet	204	1.32
Cocke, Gingerich(8)	Third law			2.92±0.2
This work			283.9±1.8	1.4±0.3

Figure IV.3.1 Mass spectrum of Rh clusters from sputtering target, measured in-situ by recording the current on the Faraday plate as a function of magnetic field on the Wien filter.

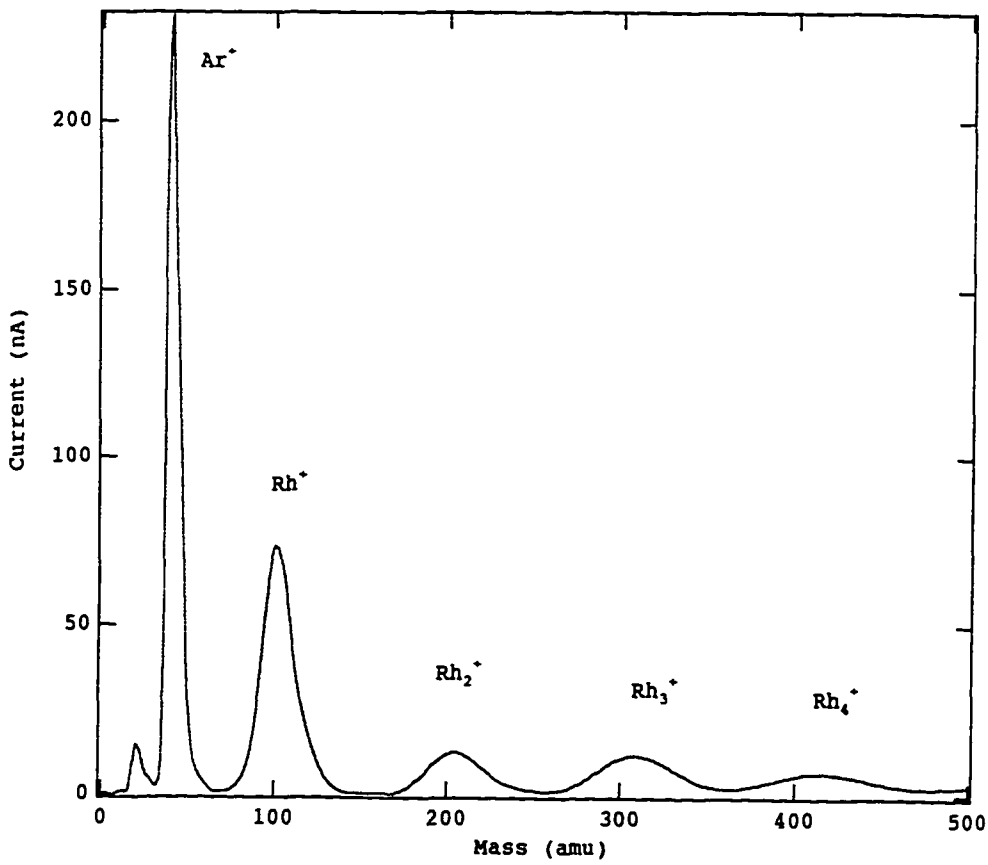

Figure IV.3.2 Absorption(scattering depletion) spectrum of Rh_2 in argon matrix.

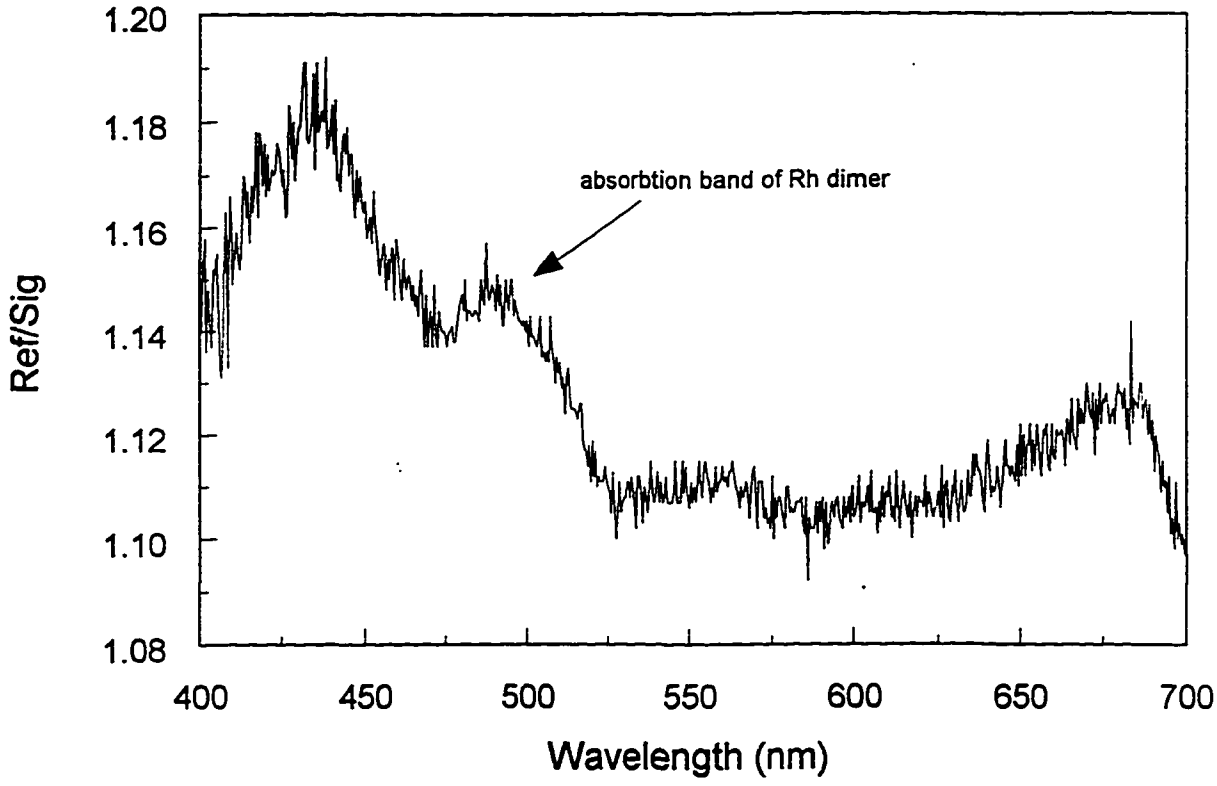

Figure IV.3.3 The resonance Raman spectra of Rh_2 in Ar matrix excited with 488.0 nm radiation.

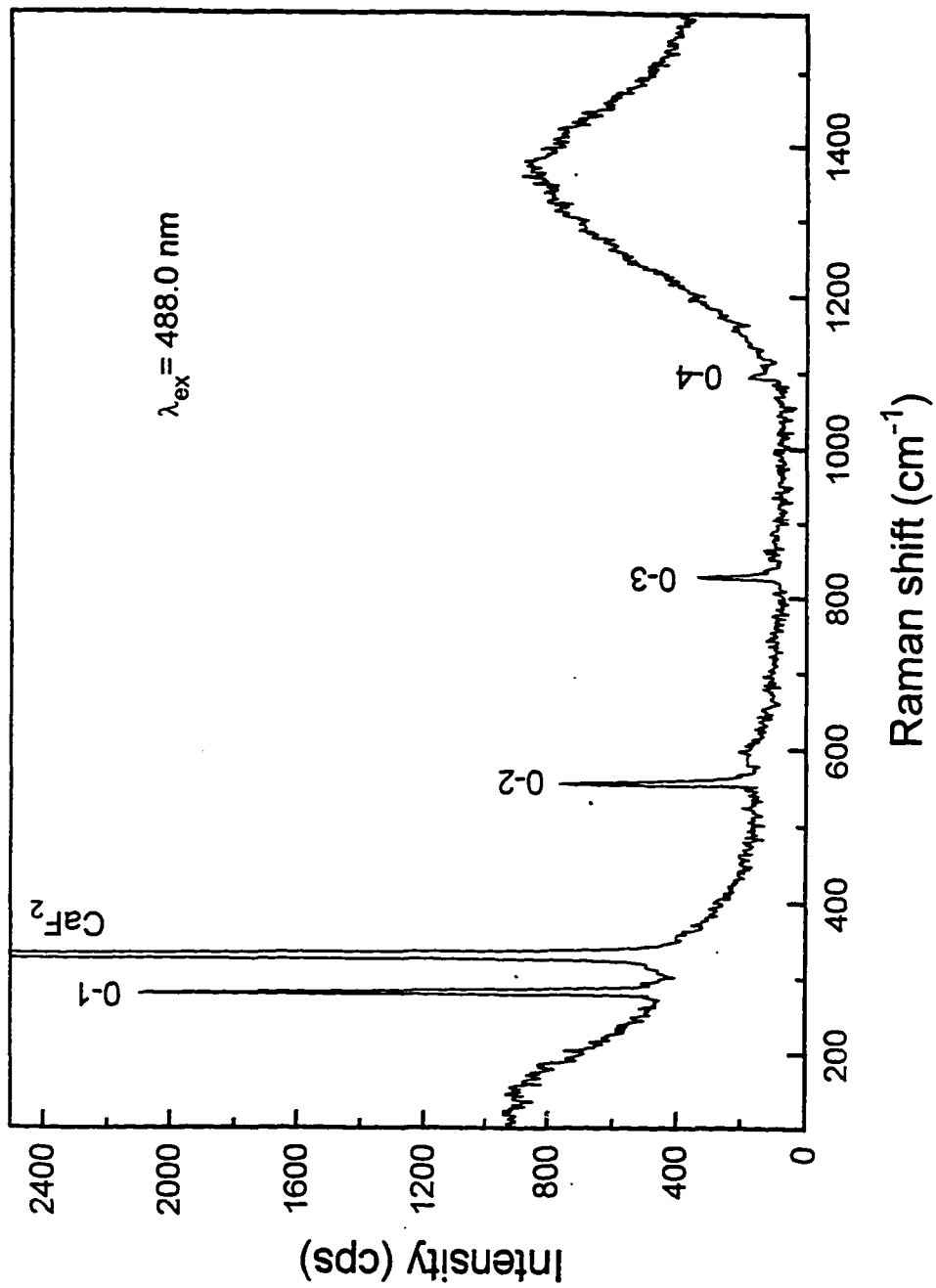

Figure IV.3.4 Raman excitation profiles of Rh_2 on argon matrices

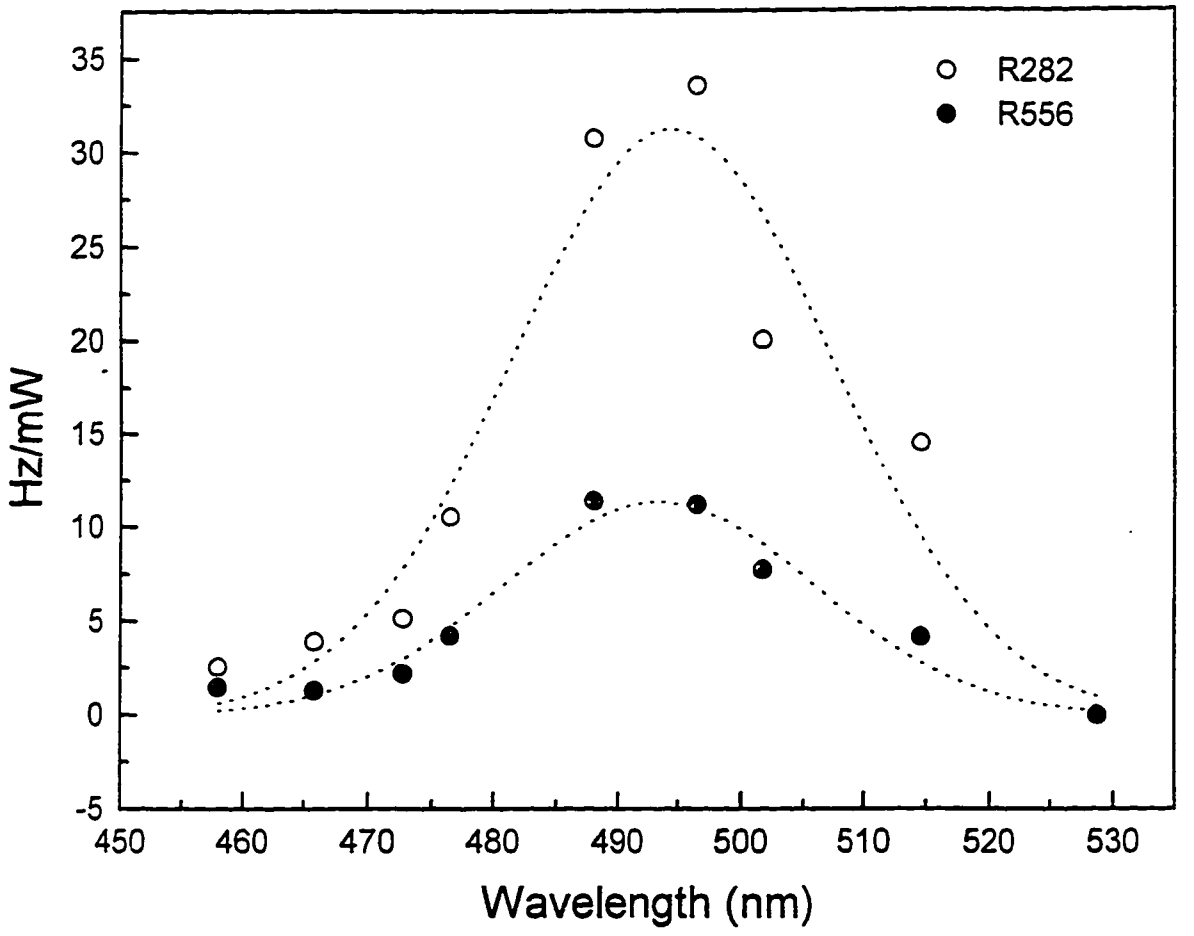

IV.4 Spectroscopy of mass-selected ruthenium dimers in argon matrices

Huaiming Wang, Hanae Haouari, Robert Craig, Yifei Liu, John R. Lombardi, and D.M. Lindsay

Department of Chemistry and Center of Analysis of Structures and Interfaces (CASI), The City College of New York (CCNY), New York, New York 10031

A. Introduction

We have recently reported the results of measurements of the Raman and absorption spectra of several late transition metal dimers. These include studies of Co_2[1], Ni_2[2] and Rh_2[3]. Metals in this region of the periodic table are of interest not only for their catalytic properties but because of the participation of d-orbital electrons in the bonding properties. Ruthenium is also of interest in that several complexes of this metal have been implicated in the cleavage of water and thus efficient conversion of solar energy into chemical energy by photoinduced electron transfer.[4]

Surprisingly little work has been carried out on Ru_2. Miedma and Gingerich[5] estimated D_e from a relationship with the heat of vaporization and surface energy of the pure solid. Several quantum mechanical wave function calculations have been carried out. The earliest was an all-electron ab initio SCF-CI calculation by Cotton and Shim.[6] Das and Balasubramanian[7] used the complete active

space multiconfiguration SCF method, while there are have also been several density functional calculations[8,9,10]. Common to all these calculations is the assignment of the ground state as a $^7\Delta_u$ state. However, the calculated values for ω_e as well as D_e vary considerably among the several reports.

We have obtained resonance Raman spectra and absorption (scattering depletion) spectrum of Ru_2 in argon matrices. Our samples are prepared by neutralizing a mass-selected beam of dimer ion, and therefore there is little or no interference between the spectroscopic transitions of the dimer and those from atom and trimer. This allows unambiguous assignment of spectral features. From the absorption spectrum only a single transition of ruthenium dimer can be identified in the visible region with a broad band observed at 470 nm. By resonance excitation into this band with various lines of a tunable dye laser and Argon ion laser, we obtain a sharp progression of Raman vibrational lines up to $V''=5$. The resulting value for ω_e is 347.1(9) cm^{-1} and for D_e is 2.0 (2) eV.

B. Experimental

The CCNY cluster deposition source has been described in details elsewhere[11]. Briefly, an argon ion beam(typically 15mA at 25KeV) sputters a cooled, ruthenium target (Tosoch DMD inc,99.8%). The sputtered products are

extracted by electrostatic lenses, mass-selected using a Wien filter, bent by 10° to eliminate neutrals and then guided into the deposition region. Ruthenium dimer(or atomic) ions were then co-deposited with argon gas and electrons onto a ~ 14K substrate, composed of CaF_2 plate. Ion currents under soft landing conditions could be measured on a Faraday plate in the deposition region and were:Ru^+(62nA), Ru_2^+(23nA) and Ru_3^+(20nA) as shown in Figure.IV.4.1. Prior to deposition, the selected ions were simultaneously slowed to 10eV by a surrounding "Faraday cage". Matrices were grown at about 4-6μ/h with an Ar:metal ratio of approximately 10^4:1. By comparing the intensities of known atomic excitation features in a dimer deposition with those obtained from depositions of the atom under similar conditions, the dimer fragmentation is estimated to be less than 1%.

Matrix samples were interrogated in situ both absorption and Raman spectroscopy. As previously reported[12] the absorption were made by collecting the light at 90° to that incident, a technique we termed "scattering Depletion Spectroscopy" (SDS).

Raman spectra were recorded using the visible output of an argon ion laser (spectra Physics model 2045) pumped dye laser. Scattered light was collected at 90 into a Spex 1877E 0.6m Triplemate Spectrometer and detected by a liquid nitrogen cooled CCD detector (Spex model" Spectrum one") with DM3000R software.

C. Spectra and analysis

The "scattering depletion"(absorption) spectrum of Ru_2 is shown in Figure IV.4.2. It consists of a single broad transition centered about 470 nm. No other features attributable to Ru_2 are observed.

The resonance Raman spectrum of Ru_2 excited at 458.7 nm is shown in Figure IV.4.3. A line due to the CaF_2 substrate is also in evidence. The spectrum consists of a single progression of almost equally spaced lines each accompanied by a weak side-band to higher frequencies. The lines may be assigned to the 0-n (n=1-5) vibrational transitions. Averaging over eighteen separate spectra taken at various excitation wavelengths(between 458 and 514 nm) we obtain mean line positions of lines at 343.8±2.6cm^{-1}, 681.6±3.2 cm^{-1}, 1017.5±2.6 cm^{-1}, 1350.2±2.5 cm^{-1} and 1678.9±0.8 cm^{-1}. Using standard techniques of analysis[13] we obtain ω_e=347.1 (9) cm^{-1} with $\omega_e x_e$=1.85(15) cm^{-1}.

The natural abundance of the isotopes of Ru involve masses of 96, 98, 99, 100, 101, 102, 104 amu. The most abundant, 102 is only present as 31.6%. The resulting isotope distribution contributes to a slight broadening of the spectral lines, which becomes more pronounced in the higher overtones. Assuming a common force constant (and linewidth) for all the possible dimers, we may simulate the effect on lineshape. In Figure IV.4.4 we illustrate the

result of including 28 isotopes, comparing the result with the observed spectrum for the 0-4 transition. These fits increase our confidence in our analysis, and allow more accuracy in line positions. They further show that the observed side-bands are definitely not due to isotope effects.

In order to eliminate the possibility that the side-bands were due to sites effects, we carried out an annealing experiment, raising the temperature of the sample gradually from 14K to 35K, and lowering it back down again. The sides-bands did not disappear, but the relative intensity of the sharp peaks to the side-bands changed in a reproducible manner. This behavior is characteristic of phonon interactions, where the sharp peak is the zero phonon line and the side-band represents energy exchange with the lattice. As a test of this we measured the integrated intensity of the zero phonon line (I_z) and the total intensity (I_t) as a function of temperature (T). The relationship is[14]

$$\ln(I_z/I_t) = -S[1 + 6.6\ (T/\Theta_D)2]$$

where Θ_D is the Debye temperature, which for Ar is 92K, and S is the Huang-Rhys factor which measures the phonon coupling strength. Excellent fits are obtained for this functional form, with S=0.083, 0.142, and 0.38 for the 0-1, 0-2 and 0-3 transitions, respectively. The coupling is, as

expected quite weak and increases when going to high overtones because the interaction is more felt at this levels. However, this is the first time we have encountered phonon side-bands of any sort in our spectra, presumably due to extremely weak coupling.

D.Discussion

In the experiment we have measured values for ω_e and $\omega_e x_e$ which enables us to determine both the force constant and the dissociation energy of Ru_2. The value for K_e=3.57 mdyn/Å, while using $D_e=\omega_e^2/4\omega_e x_e$ we obtain a value of 2.0eV. In Table IV.4.1 we collect a summary of the various calculations of the harmonic frequency and the dissociation energy for the sake of comparison. The calculations all agree that the ground state is $^7\Delta_u$ arising from a $1\sigma_g^2 1\pi_u^4 1\delta_g^3 2\sigma_g^2 1\delta_u^2 1\pi_g^2 1\sigma_u$ (predominately, in the case of multiconfiguration calculations) configuration, but there the agreement ends. Our measurements neither confirm nor dispute this assignment of the orbital nature of the state.

The only calculation of D_e which comes close to the experiment is that of Das and Balasubramanian[7], whose CASSCF multiconfiguration calculations were also quite good for Rh_2[3]. Their value for ω_e, however is somewhat low. All other calculated values for D_e are quite far from the experimental value, while the only value for ω_e which is higher than the observed value is the density functional

theory of Goursot, Pedocchi, Coq[9]. Using a pseudopotential density functional approach Chen,Krasowski, and Fitzgerald[8] obtain 335 cm^{-1}. This is the closet result. However, a sampling of their calculations for other dimers (such as Ni_2: 380cm^{-1} vs 259 cm^{-1} experimental or Rh_2: 331 cm^{-1} vs. 284 cm^{-1} experimental) raises the possibility that the agreement in the case of Ru_2 might be fortuitous.

As with the late first row[2] transition dimers, it is worthwhile comparing the force constants obtained for the series Ru_2, Rh_2, Pd_2, and Ag_2. These are illustrated along with the first row series in Figure IV.4.5. In the first row series, a small but decided break is evident between Co_2 and Ni_2 which was interpreted as indicating the point at which d-orbital participation in chemical bonding ceases. No such break is observed in the second row series, but a smooth decline in K_e from Ru_2 through Pd_2 followed by a further but smaller decline for Ag_2 may be observed. Thus the participation of the d-electrons in bonding may be seen to decline monotonically and smoothly in this row. This shows that the d-electron participation in the chemical bonding will be more significant for the second and third transition series than for the first. The ground state atomic configurations for these elements are Ru($5s^14d^7$), Rh($5s^14d^8$). Pd($4d^{10}$), Ag($5s^14d^{10}$). Due to favorability of s^1 configurations for dimer bonding, it is likely that for Pd a promotion to $5s^14d^9$ occurs, accounting for the smoothness of the K_e curve. From the magnitude of the force constant,

it is likely that the Ag_2 dimer has a single bond. Since the force constant for Ru_2 is over three times greater than that for Ag_2, by Pauling's rule[15] we might infer a bond order of over three. This is consistent with the configuration $1\sigma_g^2 1\pi_u^4 1\delta_g^3 2\sigma_g^2 1\delta_u^2 1\pi_g^2 1\sigma_u$ which led to the $^7\Delta_u$ state assignment for the ground state. Of all the late transition metal dimers measured so far, Ru_2 has the highest observed force constant.

Figure IV.4.1 Mass spectrum of Ru clusters from sputtering target, measured in-situ by recording the current on the Faraday plate as a function of magnetic field on the Wien filter.

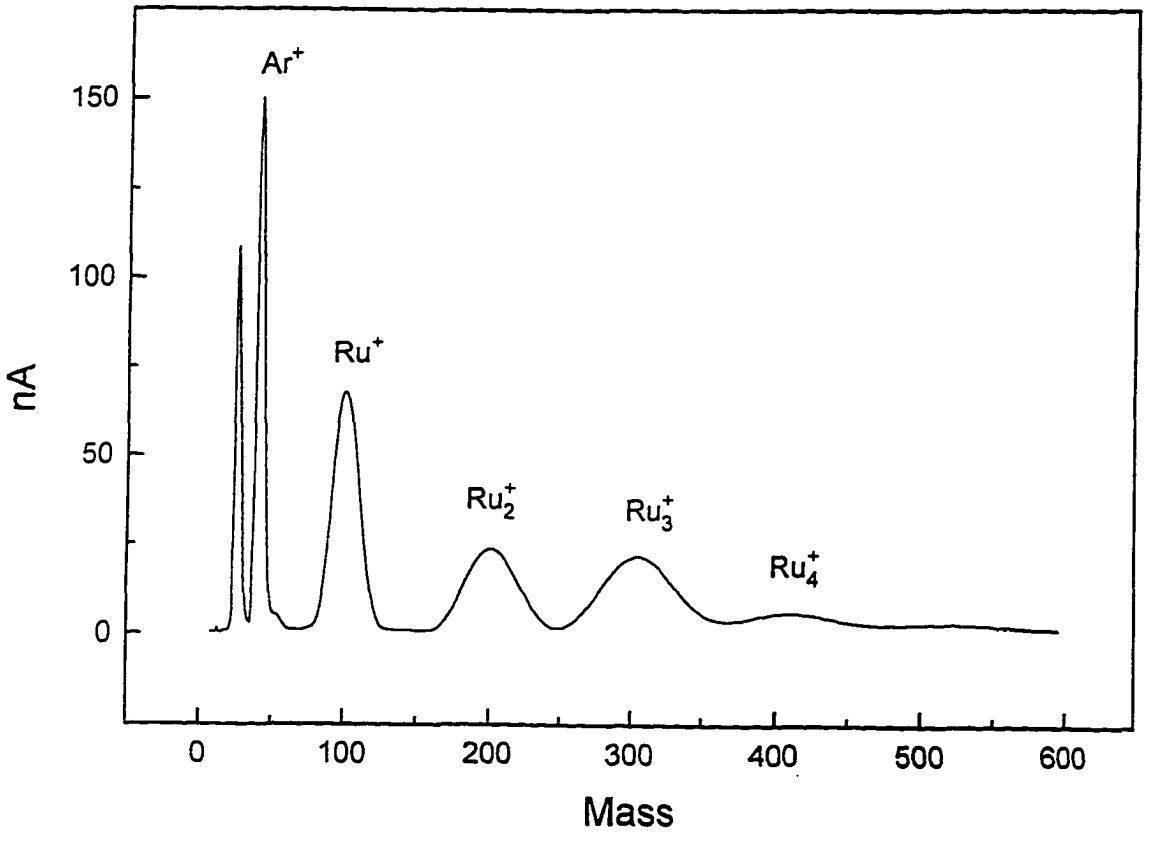

Figure IV.4.2 Absorption(scattering depletion) spectrum of Ru_2 in argon matrix.

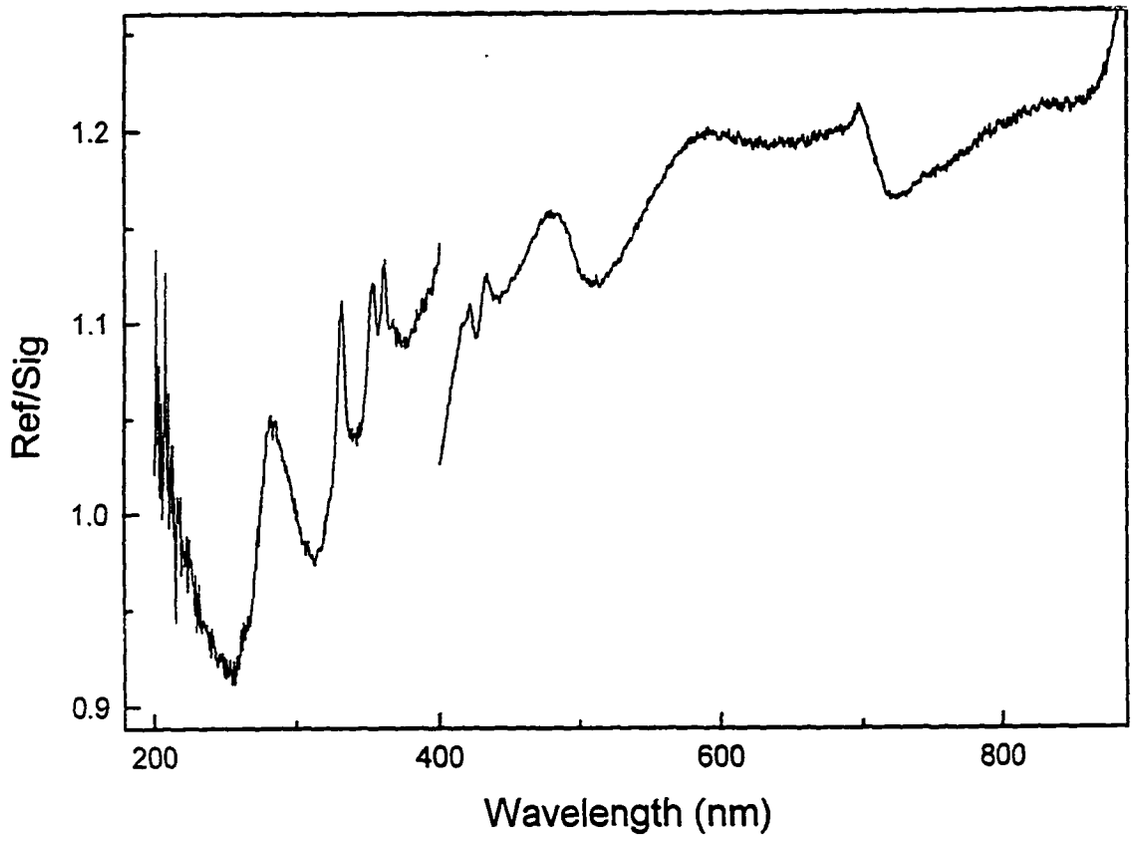

Figure IV.4.3 The resonance Raman spectra of Ru_2 in Ar matrix excited with 458.7 nm radiation.

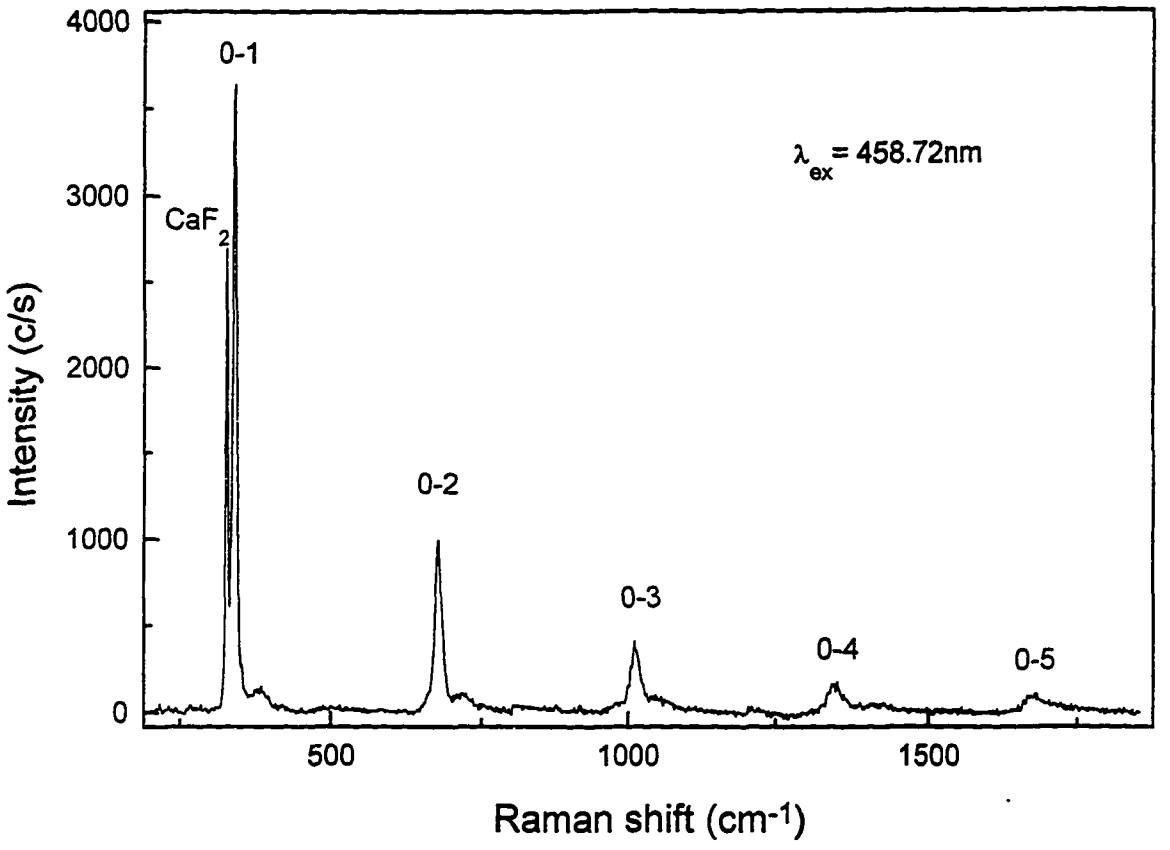

Figure IV.4.4 Simulated effect of twenty eight isotopes of Ru_2 on the shape of the 0-4 overtone, and comparison with the experimentally observed line.

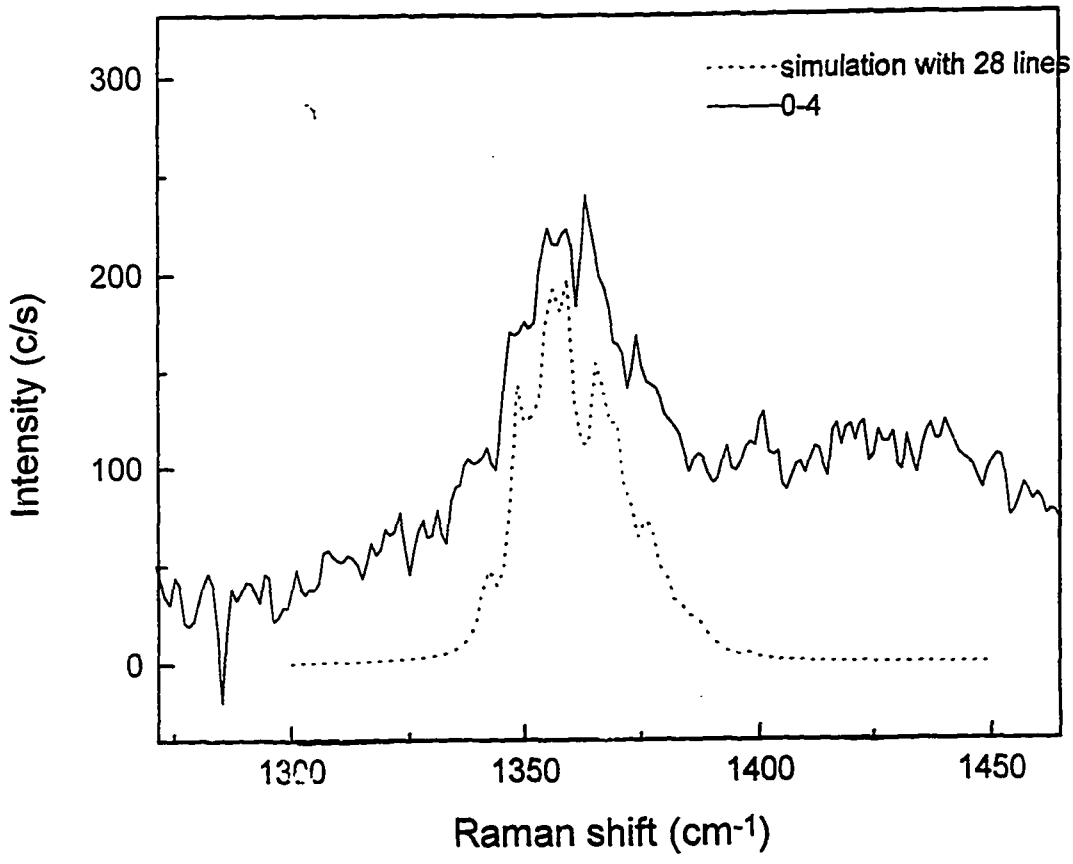

Figure IV.4.5 Experimental force constants (mdyne/Å) vs atomic number for several second row transition metal dimers. The data(k in mdyne/A) are:3.585 (0.018) for Ru_2(this work), 2.443 (0.031) for Rh_2(Ref.3), 1.382(0.13) for Pd_2(Ref.16), 1.196(0.006) for Ag_2(Ref.17). For the 3d curve see Fig.IV.2.4 for the data references.

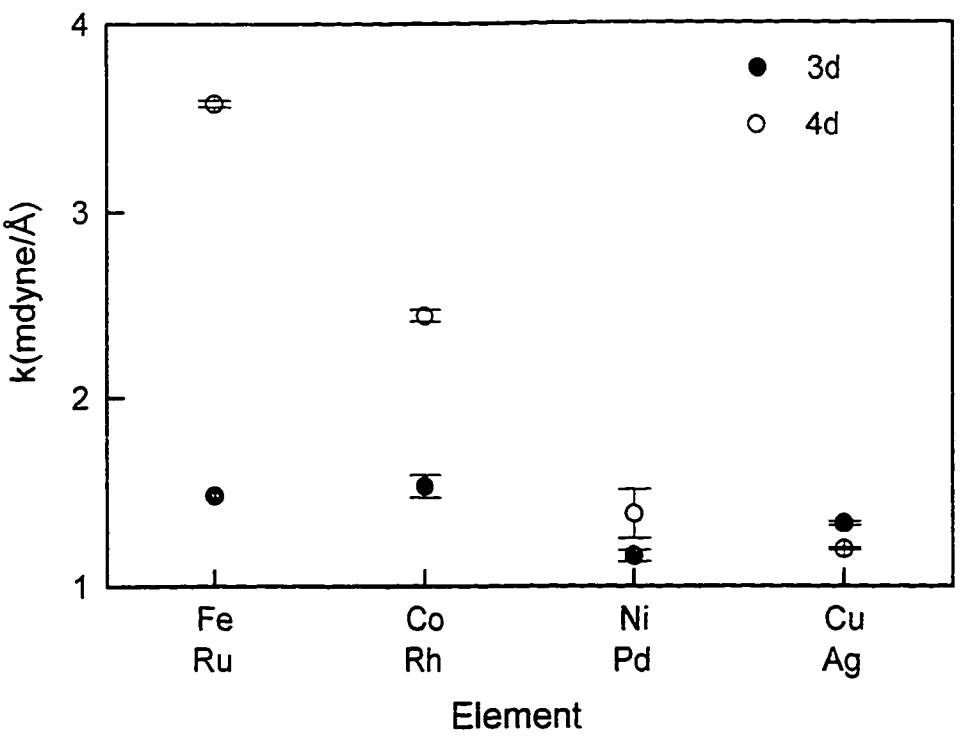

Table IV.4.1 Comparison of theoretical and thermodynamic results for the ground state parameters of Ru_2 with spectroscopic data(this work).

Authors(Ref)	Method	Ground	ω_e^{-1}	D_e(eV)
Cotton and Shim(6)	SCF/CI	$^7\Delta_u$	116	0.6
Das,Balasubramanian (7)	MCSCF(CASSCF)	$^7\Delta_u$	273	2.0
Chen,Krasowski,Fitzgerald(8)	Gaussian, density functional	-	335	-
Goursot,Pedocchi,Coq (9)	Gaussian, density functional	$^7\Delta_u$	380	-
Harada, Dexpert (10)	Gaussian, density functional	heptet	274	2.5
Harada, Dexpert (10)	Effective core potentials	heptet	203	1.1
Miedma and Gingerich (5)	Heat of Vaporization	-		3.3
This work			343.8	2.0

IV.5 Bonding in transition metal dimers

Investigators have always been fascinated by how the bonding of small transition metal clusters is achieved. Hence many investigations have been carried out for many years in this specific area. In fact interest in this field arises because investigators want to understand fully and comprehensively these difficult electronic systems. As we know the d-orbital contributions to bonding can strengthen the bond. However this effect first increases and then lessens as one moves left to right across the periodic table because the radial size of the d orbital decreases significantly relative to the radial size of the s orbital (see Figure IV.5.2 and Figure IV.5.3). Furthermore there is often an energetic price that must be paid to promote the constituent atoms to an electron configuration that adiabatically correlates to ground state molecules.

While there are many experimental data in the gas phase or matrices for the 3d series, little is known either experimentally or from theory about diatomics formed from the 4d and 5d series. The lack of theoretical data is certainly not because there are less practical applications for these metals but instead there are less appropriate methods for incorporating relativistic corrections or correlation effects. Certainly relativistic effects become quite important in the later half of the 4d transition series and remain important throughout the 5d transition

series. Together these factors make the transition metal clusters a particularly difficult challenge for theoretical chemistry.

Table IV.5.1 summarizes all ground state force constants data (in mdyne/A) known for homonuclear transition metal diatomic species. The CCNY results are shown in bold; the remaining data come from other spectroscopic measurements either in low temperature matrices or from the gas phase, more recently in elegant molecular beam experiments. There is a good review article about transition metal atoms and dimers by Dennis R. salahub[2]. In it the author attempted to summarize all the theoretical and experimental work that have been done for all transition metal dimers.

A profound understanding of the bonding properties of small transition metal clusters can best be achieved through a symbiosis of experiments and calculations. However theoretical progress has been impeded by difficulties in treating the weak, multiple d-d bonding of the transition metal elements. Furthermore one has to worry about the problem of correlation and relativity. In general the relativistic corrections will have little effect on the properties of 3d systems, a small but non-negligible influence for the 4d series and dramatic, even qualitative consequences for 5d. Besides the relativistic shifts for the later members of the 3d series are probably larger than

many would have expected. In any case they should not be neglected if very high accuracy is required.

The first and second row transition metals have been thoroughly investigated, for instance we can explain the d orbital contribution to bonding in the series Fe through Cu. As well as the passage from van der Waals bonding in Mn to strong chemical bonding in Re_2. However Very little is known either experimentally or theoretically about the properties of any of the third row transition metals. Thus a relatively strong bond and large force constant is a notable characteristic of many "early" group 3B-7B transition metal dimers. Table IV.5.3 shows transitions elements with their atomic number and electron configuration.

An alternative approach to probing the change in bonding character of the group 7B (Mn, Tc, Re) dimer will be to study the mixed, isoelectronic species, for example CrFe, MoRu, FeMo etc...the principal difficulty that we anticipate here is the feasibility of fabricating suitable sputtering targets and most of all mass separating the many possible combination by a Wien filter, which probably won't be an easy task. In addition the heat of vaporization of the metals should be taken in consideration see.Figure IV.5.1 for the values of all TM groups. As in these circumstance it is better to know in advance the heat of vaporization of each element.

Chemical bond formation is most favorable in those substances where at least one of the interacting atomic moieties has an open s-shell configuration s^1d^m as opposed to s^2d^{m-1}. If s^1d^m is not the ground state bonding can still take place but at the cost of a certain energy.
The dimer bond strength is then largely dependent upon the amount of overlap between the atomic d orbitals, one determinant of which is the relative size of the (n+1)s and nd orbitals.
If this ratio $\langle r_{(n+1)s}\rangle/\langle r_{nd}\rangle$ is small this means that the d orbital metal can form a strong bond. The d orbital overlap is even more favorable for the third row elements but the s^1d^m configuration is energetically relatively remote for many third row elements.

The relatively strong bonding of the " early "(groups 3B-7B Mn, Tc, Re) notably are the group 6B (Cr, Mo, W). Various molecular structure calculations conclude that bond formation in the group 6B dimers is strongly influenced by the overlap of d orbital. It is also interesting to note that the dimer force constant increases from Cr_2 to Mo_2 , but decreases for the third row congener W_2. A similar effect has been noted for other early transition metal dimers and has been interpreted in terms of the atomic s-d promotion energy.
In general, the force constants (and concomitantly bond strengths) for the early transition metal dimers are much larger than those of the later elements. This effect arises

from a combination of the greater d-orbital contraction (smaller overlap) in the heavier elements of a particular period and the natural tendency for more antibonding orbitals to be filled in a dimer composed of atoms whose d orbital are more than half filled.

For those elements with a half-filled or filled d-shell (Mn and group 2B) the bonding is described as van der Waals in nature. An interesting exception is dirhenium which, despite a ground state configuration of $5d^5 6s^2$ for the atom, has the second largest force constant yet reported for any transition metal dimer after Mo_2.

For groups 4B, 5B, 6B the dimer force constant increases in passing from the 3d to 4d metals but then decreases for the third row congener despite the relatively greater diffusiveness (i.e. better overlap) of the atomic 5d orbitals. This phenomenon apparently arises from the large s-d promotion (atom preparation) energies of Hf, Ta, W, which in turn may be traced to the fact that the lanthanide elements immediately precede Hf in the periodic table.

More over The adiabatic strength will accordingly be defined as the measured adiabatic bond strength plus the promotion energy. The bond strengths and promotion energies E_p of all the homonuclear diatomic transition monocations in the 3d transition metal series and neutrals are given in Table[1] IV.5.2.

Diatomic bonding changes from 3d-3d to 4s-4s between Co_2 and Ni_2. The nickel dimer species appear to have no d-

orbital bonding. However no such change occurs in the second row series especially between Pd_2 and Ag_2 as is expected if we follow the trend in the first row series. This could be explained by the fact that the 3d and 4d orbitals contract considerably as the nuclear charge increases. In the extreme limit of d-orbital contraction, the orbitals will be too contracted to overlap significantly, thereby eliminating the possibility of d-electron bonds. The nd contraction is much more severe for the 3d transitions series than for the 4d and 5d transition series indicating that the d-electron participation in the chemical bonding will be more significant for the second and third transition series than for the first.

If $\langle r_{nd} \rangle$ is higher means that d-orbital tends to form stronger bond. The d orbital overlap is even more favorable for third row elements i.e. $\langle r_{6s} \rangle / \langle r_{5d} \rangle$ is smaller than $\langle r_{5s} \rangle / \langle r_{4d} \rangle$. Exception is for Nb->Ta, Mo->W and Zr->Hf because of the s-d promotion energy which means the elements must first promote an s-electron to a d orbital before significant chemical bonding occur. However the promotion energy required to prepare the atoms for bonding reduces the strength of the chemical bonds that are gained.

Periodic trends in the metal dimer bond energies show that d-orbital interactions play major roles in the bonding of the early transition metal diatomics, with the importance of these roles decreasing dramatically later in the series. Though there are some exceptions like the case

of Ni_2 and Cu_2 where the force constant increases when going from Ni_2 to Cu_2 as was explained in Chap IV.2.

We can determine D_e, ω_e, $\omega_e x_e$ through Raman measurements. For "normal" case $\omega_e x_e > 0$

$$\Delta G(v+ 1/2) = G(v+1) - G(v)$$

i.e. Separation of adjacent levels

Plugging in for energy levels of Anharmonic oscillator

$$G(v) = \omega_e (v+1/2) - \omega_e X_e (v+1/2)^2 +$$

$$\Delta G (v +1/2) = \omega_e - 2\omega_e X_e - 2\omega_e X_e v$$

$$= \omega_e - 2\omega_e X_e (1+ v)$$

From the plot $\Delta G(v + 1/2)$ Vs $2(1+ v)$, the intercept is the vibrational frequency ω_e and the slope is the Anharmonic constant $\omega_e X_e$. Knowing ω_e and $\omega_e X_e$ we can calculate the force constant and the dissociation energy by applying the formulas given below.

K : Force constant

$$K \text{ (mdyne/Å)} = 5.8919\ 8\ 10^{-7} * \omega_e (cm^{-1}) \text{^} 2 * mass(amu)/2.$$

D_e : Dissociation energy

$$D_e\ (cm^{-1}) = (\omega_e) \text{^} 2/4 * \omega_e X_e cm^{-1}$$

Figure IV.5.1 Heat of vaporization of transition metal.

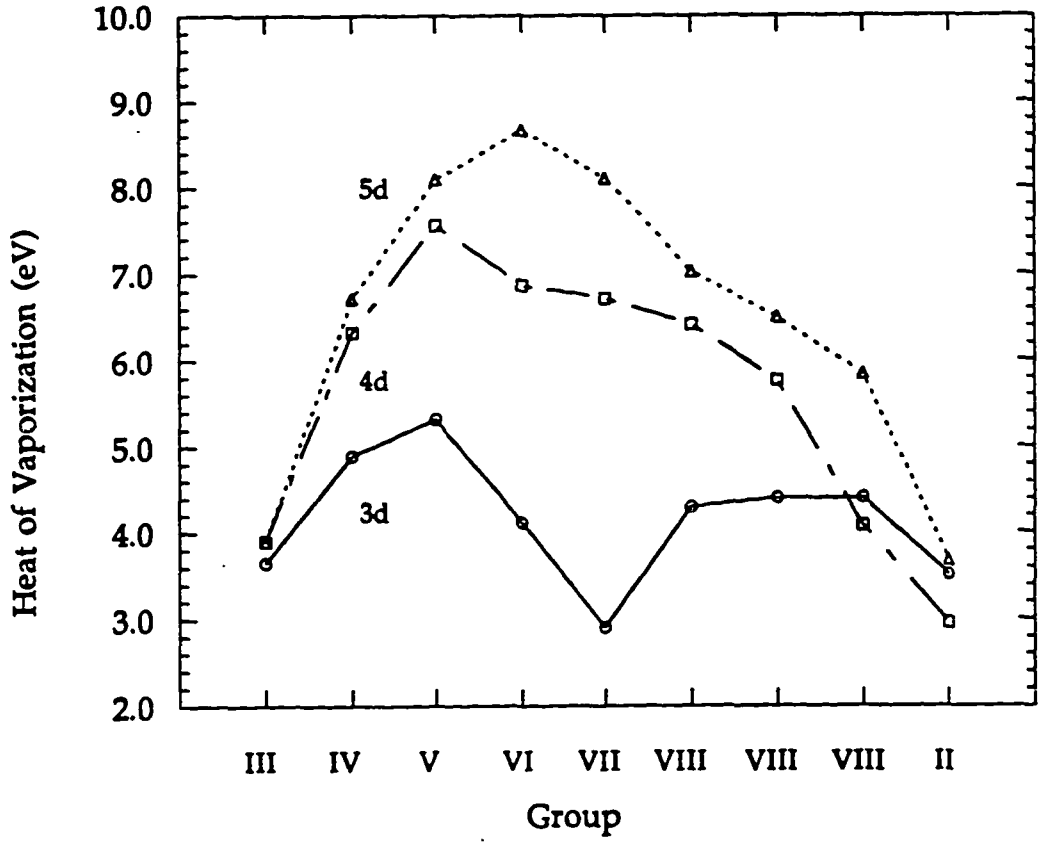

Figure IV.5.2 Force constants of 3d, 4d and 5d transition metal dimers.

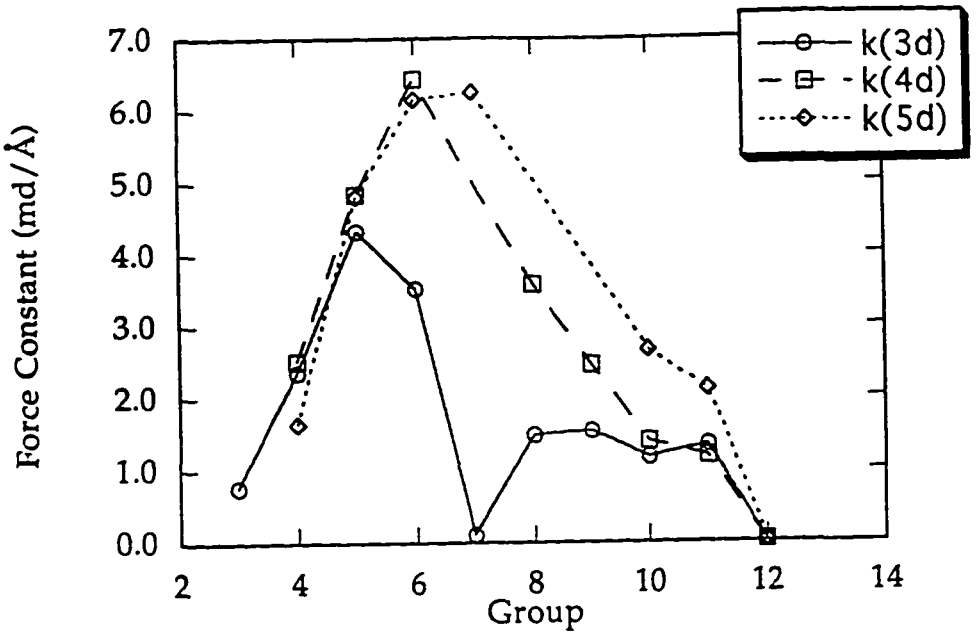

Figure IV.5.3 Force constants in the bulk phase of 3d, 4d and 5d transition metal dimers.

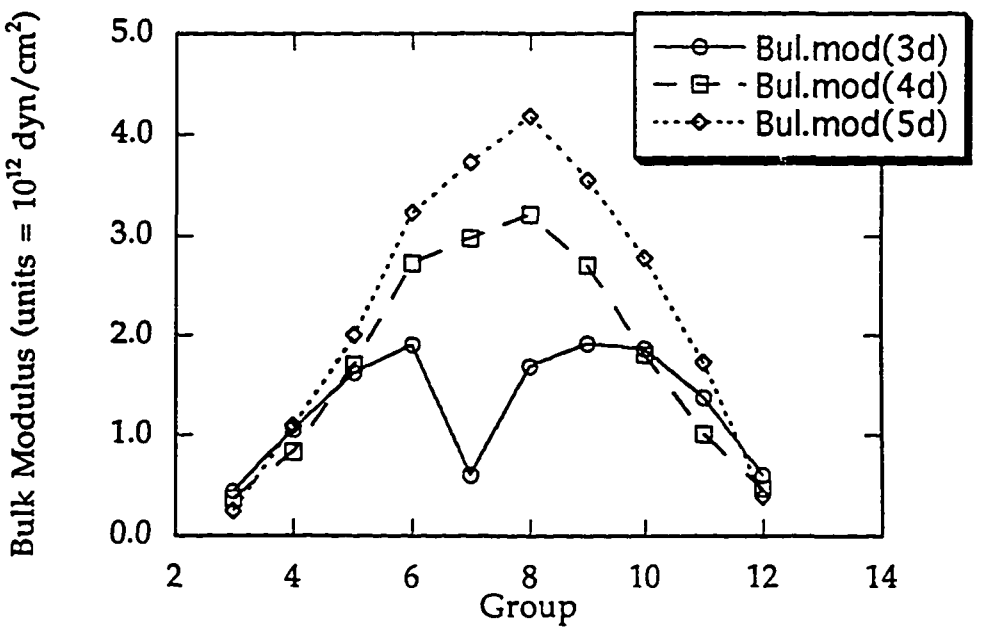

Table IV.5.1 Experimental ground state harmonic frequencies of metallic diatomics (in cm^{-1}) and their corresponding force constants in mdyn $Å^{-1}$.(CCNY results underlined).

Sc_2[a]	Ti_2[b]	V_2[e]	Cr_2[h]	Mn_2[k]	Fe_2[m]	Co_2[o]	Ni_2[q]	Cu_2[t]	Zn_2[w]
283.9	407.90	536.90	479.0	76.4	300.3	294.80	259.2	266.43	25.70
0.75	2.348	4.326	3.515	0.094	1.484	1.509	1.16	1.332	0.013
Y_2	Zr_2[c]	Nb_2[f]	Mo_2[i]	Tc_2	Ru_2[n]	Rh_2[p]	Pd_2[r]	Ag_2[u]	Cd_2[x]
	305.70	420.50	477.10		347.1	283.9	210.00	192.40	23.00
	2.511	4.840	6.433		3.57	2.44	1.382	1.176	0.018
La_2	Hf_2[d]	Ta_2[g]	W_2[j]	Re_2[l]	Os_2	Ir_2	Pt_2[s]	Au_2[v]	Hg_2[y]
	176.2	300.2	336.8	348.4			215.00	190.90	18.50
	1.632	4.804	6.144	6.658			2.657	2.115	0.020

a. Moskovits,M;Dilella,D.P.;Limm,W.J.Chem.Phys.1984,80, 626.Using ω_e=238.9cm^{-1}.

b. Cosse,C;Fouassier,M.;Mejean,T.;Tranquille,M.;Dilella, D.P.;Moskovits,M.J.chem.Phys.1980,73,6076.Using ω_e=407.9cm^{-1}.

c. Hu,Z.;Zhou,Q.;Lombardi,J.R.;Lindsay,D.M.In Physics and Chemistry of finite System:from Clusters to crystals;Jena,P.,Khanna,S.N.,Rao,B.K.,Eds.,Kluwer Academic:Dordrecht, the Netherlands, 1992;p969.Using ω_e=305.7cm^{-1}.

d. Z.Hu,J-G.Dong,J.R.Lombardi, and D.M.Lindsay, J.Chem.Phys.97,9263(1993).Using ω_e=176.2cm^{-1}.

e. Hu,Z.;Shen,B;Zhou,Q;Deosaran,S.;Lombardi,J.R;Lindsay, D.M.;Harbich,W.J.Chem.Phys.1991,95,2206.Using ω_e=536.9cm^{-1}.See also ref b.

f. Hu,Z.;Shen,B;Zhou,Q;Deosaran,S.;Lombardi,J.R;Lindsay, D.M. Proc. SPIE 1992,1599,65.Using ω_e=420.5cm^{-1}.

g. Hu,Z.;Shen,B.;Lombardi,J.R.;Lindsay,D.M.J.Chem.Phys. 1992,96,8757.Using ω_e=300.2cm^{-1}.

h. Casey,S.P.;Villalta,P.W.;Bengali,A.A.;Cheng,C.-L;Dick,J.P.;Fenn,P.T.;Leopold,D.G.J.Amm.Chem.Soc.1991, 11 3,6688.Using ω_e=479cm^{-1}.

i. Efremov,Y.M.;Samoilova,A.N.;Kozhukhovsky,V.B.; Gurvich,L.V.J.Mol.Spectrosc.1978,73,430.Using ω_e=477.1cm^{-1}.

j. Z.Hu,J-G.Dong,J.R.Lombardi, and D.M.Lindsay, J.Chem.Phys.1992,97,8811.Using ω_e=336.8cm^{-1}.

k. Bier,K.D.;Haslett,T.L.;Kirkwood,A.D.;Moskovits,M.J. Chem.Phys.1988,89,6.Using $\omega e=76.4cm^{-1}$.

l. Z.Hu,J-G.Dong,J.R.Lombardi,and D.M.Lindsay.; Harbich,W.J.Chem.Phys.101,95(1994).Using $\omega_e=348.4cm^{-1}$.

m. Haslett,T.L.;Moskovits,M.J.Mol.Spectrosc.1989,135,259. Using $\omega e=299.5cm^{-1}$.

n. H.Wang,H.Haouari,R.Craig,J.R.Lombardi, and D.M.Lindsay. Submitted to J.Chem.Phys. 104,3420(1995). Using $\omega_e=347.1cm^{-1}$.

o. J-G.Dong,Z.Hu, J.R.Lombardi, and D.M.Lindsay. J.Chem.Phys.101,9280(1994).Using $\omega_e=296.8cm^{-1}$.

p. H.Wang,H.Haouari,R.Craig,J.R.Lombardi, and D.M.Lindsay.Submitted to J.Chem.Phys.Using $\omega_e=283.9cm^{-1}$.

q. H.Wang,H.Haouari,R.Craig,J.R.Lombardi, and D.M.Lindsay.J.Chem.Phys.104,3420(1995).Using $\omega_e=259.2cm^{-1}$.

r. Ho,J.;Ervin,K.M.;Polak,M.L.;Gilles,M.K.; Lineberger,W.C.J. Chem.Phys.1991,95,4845.Using $\omega_e=210cm^{-1}$.

s. Ho,J.Ph.D Thesis, University of Colorado, Boudler, 1991.Using $\omega_e=215cm^{-1}$.

t. Rohlfing,E.A.;Valentini,J.J.J.Chem.Phys.1986,84, 6560.Using $\omega_e=266.4cm^{-1}$.

u. Huber,K.P.;Herzberg,G.Constants of diatomic Molecules;Van Nostrand:New York,1979.

v. same as ref s. Using ω_e=190.9cm^{-1}.

w. Czajkowski,M.;Bobkowski,R.;Krause,L.Phys.Rev.1990, A41,277. ω_e=25.7cm^{-1}.

x. Czajkowski,M.;Bobkowski,R.;Krause,L.Phys.Rev.1989, A40,4338. Using ω_e=22.9cm^{-1}.

y. Van Zee, R.D.;Blankespoor, S.C.;Zwier, T.S.J.Chem.Phys.1988,88,4650. Using ω_e=18.5cm^{-1}.

Table IV.5.2 Bond strength and promotion energies of diatomic transition metal ions and neutrals. All values in eV.(Ref.1)

Molecule	Measured D_0° [a]	E_p [a,b]
Ti_2^+	2.435(2)[c]	0.113[d]
Ti_2	1.54(19)[e]	2×0.813[d]
V_2^+	3.140(2)[c]	
V_2	2.753(1)[f]	2×0.262[g]
Cr_2^+	1.30(6)[h]	
Cr_2	1.443(56)[i]	
Mn_2^+	≥1.4[j]	
Mn_2	0.3(3)[k]	
Fe_2^+	2.74(10)[l]	0.232[m]
Fe_2	1.14(1)[n]	2×0.859[m]
Co_2^+	2.765(1)[c]	
Co_2	0.7–1.4[o]	2×0.432[p]
Ni_2^+	2.08(7)[q]	
Ni_2	2.042(2)[r]	2×0.025[s]
Cu_2^+	1.84(8)[t]	
Cu_2	2.03(2)[u]	

[a]Uncertainties in the final digits are given in parentheses.

[b]See the text for definition.

[c]Larry M.Russon, Scott A.Heidecke, Michell K.Birke, J.Conceicao, Michael D.Morse, and P.B.Armentrout, J.Chem.Phys.100,4747(1993).

[d]C.Corliss and J.Sugar, J.Phys.Chem.Ref.Data 8,1(1979).
[e]see ref.c.

[f]E.M.spain and M.D.Morse, J.Phys.Chem.96,2479(1992).

[g]J.Sugar and C.Corliss, J.Phys.Chem. Ref.Data 7,1191(1978).

[h]C-X.Su,D.A.Hales,andP.B.Armentrout,Chem.Phys.Lett,201, 199(1993);C-X.Su,P.B.Armentrout,J.Chem.Phys.99,6506(1993).

[i]K.Hilpert and K.Ruthardt,Ber.Bunsenges.Phys.Chem.91,724 (1987).

[j]M.F.Jarrold,A.J.Illies,and M.T.Bowers, J.Am.Chem.Soc. 107, 7339(1985).

[k]T.L.Haslett,M.Moskovits,and A.L.Weitzman,J.Mol. Spectrosc. 135,259(1989).

[l]S.K.Loh,D.A.Hales,L.Lian, and P.B.Armentrout,J.Chem.Phys. 90,5466(1989).K.Loh,L.Lian,D.A.Hales and P.B.Armentrout, J.Phys.chem.92,4009(1988);L.Lian,C-X.Su,and P.B.Armentrout, J.Chem.Phys.97,4072(1992).

[m]C.Corliss and J.Sugar,J.Phys.Chem.Ref.Data 11,135(1982).

[n] Ionisation energies from E.A.Rohlfing,D.M.Cox,A.Kaldor, and K.H.Johnson,J.Chem.Phys.81,3846(1984).

[o] see text.

[p] C.Corliss and J.Sugar, J.Phys.Chem.Ref. Data 10,197(1981).

[q] L.Lian,C-X.Su,andP.B.Armentrout,Chem.Phys.Lett.180,168 (1991);J.Chem.Phys.96,7542(1985).

[r] J.C.Pinegar,J.D.Langenberg, and M.D.Morse (unpublished).

[s] C.Corliss and J.Sugar,J.Phys.Chem.ref Data 10,197(1981).

[t] A.D.Sappey,J.E.Harrington, and J.C.Weisshaar,J.Chem. Phys. 91,3854(1989).

[u] M.D.Morse, Adv.Metal Semicnd.Clusters 1,83(1993).

Table IV.5.3 Portion of periodic table showing transition elements, their atomic number, symbol, and electron configurations in valence shells

21 Sc $3d4s^2$	22 Ti $3d^24s^2$	23 V $3d^34s^2$	24 Cr $3d^55s$	25 Mn $3d^54s^2$	26 Fe $3d^64s^2$	27 Co $3d^74s^2$	28 Ni $3d^84s^2$	29 Cu $3d^{10}4s$	30 Zn $3d^{10}4s^2$
39 Y $4d5s^2$	40 Zr $4d^25s^2$	41 Nb $4d^45s$	42 Mo $4d^55s$	43 Tc $4d^65s$	44 Ru $4d^75s$	45 Rh $4d^85s$	46 Pd $4d^{10}$	47 Ag $4d^{10}5s$	48 Cd $4d^{10}5s^2$
71 Lu $5d6s^2$	72 Hf $5d^26s^2$	73 Ta $5d^36s^2$	74 W $5d^46s^2$	75 Re $5d^56s^2$	76 Os $5d^66s^2$	77 Ir $5d^9$	78 Pt $5d^96s$	79 Au $5d^{10}6s$	80 Hg $5d^{10}6s^2$

CHAPTER V.TRANSITION METAL TRIMERS.

V.1 Trimers review

An enormous amount of work has been done concerning transition metal clusters (TM) as they are of special interest because of d-d bonding involved. However, detailed electronic and vibrational structure investigations on TM clusters have thus been limited to dimers, a few trimers, and tetramers Ta_4[1], Cu_4^{+2}. This is Because it is quite difficult to obtain accurate results either theoretically or experimentally.

Nonetheless there have been several studies on dimers[3-21]. Theoretical and experimental studies on trimers are quite scarce at least for transition metal clusters. Although Morse and Co-Workers have considered several coinage metals. Their experimental spectroscopic investigations of TM trimers were carried out with supersonic jet expansion methods. The electronic states of jet cooled clusters are then probed by laser-induced fluorescence methods, resonant two-photon ionization, and dissociation methods. In our lab we have recently investigated Zr_3[30] and Nb_3[35] by Resonance Raman spectroscopy in argon matrix. The Zr_3 results are pretty much in agreement as to the nature of the ground state with state of art theoretical calculations done by Balasubramanian. However no theoretical investigation has been done for Nb_3 as yet. Although Balasubramanian[22-29] and

Walch[28-31] have carried out several computations on TM trimers.

In the case of trimers, they can actually have three symmetries which are C_{2v}, D_{3h} and a linear shape. Furthermore excited electronic states of the molecule may have a different symmetry than the ground state. Usually one of the primary concerns we are confronted with when dealing with trimers is to find out the symmetry of each state, at least the lower energy level states. In Table V.1.1, I have summarized some of the studies that have been done regarding TM trimers be it experimental or theoretical. Not only different experimental methods do not agree in their results but also diverse theoretical calculations don't seem to have a general agreement regarding for example the ground state symmetry, the ordering of the low lying electronic states or simply the shape of the molecules. For instance Ag_3 is a linear molecules according to Raman spectra which shows one single Raman line. However the predictions of theoretical calculations on Ag_3 shows that the molecules is slightly bent in its ground state. More over a jet cooled silver trimers studies indicated that the ground state is generally regarded as a Jahn-Teller distorted $^2E'$ state with a nominal D_{3h} symmetry.

ESR[57] studies of metal clusters of group 1B metals indicated that the following trimers Cu_3, Ag_3 and Au_3 are slightly bent with $^2B_2$ electronic ground state in C_{2v}

symmetry with the unpaired electron located mainly on the terminal atoms. The resonance Raman spectrum of matrix-isolated Cu_3 was done by Moskovits. On it the author claims that the Cu_3 is a fluxional Jahn-Teller molecule. And this on the basis of the irregularity of the observed progression and the unusual isotopic structure shown by the vibrational spectral components. The silver trimer has been the subject of UV-VIS and resonance Raman experiments in rare gas matrices, as well as several theoretical calculations. According to these studies the ground state is generally regarded as a Jahn-Teller-distorted $^2E'$ state with nominal D_{3h} symmetry, which becomes a $^2B_2$ minimum energy species in C_{2v} symmetry. Morse[53] using resonant two-photon ionization spectroscopy of jet-cooled Au_3 assigns a progression in a totally symmetric stretching vibration. It is assigned as $\tilde{A}^4E' \leftarrow \tilde{X}^2E'$ transition in the D_{3h} point group, with both $\tilde{X}^2E'$ and $\tilde{A}^4E'$ states undergoing Jahn-Teller distortion. Some theoretical calculations on Pd_3 have been performed, Balasubramanian[56] found at least ten low-lying electronic states of Pd_3 in the absence of spin-orbit coupling when using multiconfiguration self consistent field (MCSCF) followed by multireference singles plus doubles configuration interaction (MRSDCI) calculations. The symmetry of all the these states is an isosceles triangle structure. Since there is no experimental work regarding these molecules one cannot really dispute, confirm or for that matter compare these results with

confidence. Platinum, although it plays a major role in catalysis, is rarely experimentally studied itself. Though Carter[54] performed ab initio generalized valence bond with configuration interaction calculation for low lying electronic states of Pt_3. The ground state exhibits an isosceles triangle geometry with an apex angle less than 60° due to a Jahn-Teller distortion. Muller[55] used scanning tunneling microscopy (STM) of small platinum clusters on highly oriented pyrolytic graphite, and found only two kind of adsorbed Pt trimers either a linear chain or equilateral triangle. Again this repeats disagreement with the previous theoretical results.

It has been possible to calculate the barrier to pseudorotation of transition metal trimers for non fluxional molecules. Then if the barrier is not too high like in the case of Cu_3[40a] which has a C_{2v} symmetry in its ground state the molecule will pass from minimum to minimum, never adopting a D_{3h} symmetry. Rh_3 has been investigated by ESR[49]. The trimer has an equilateral triangle structure (D_{3h} symmetry) which is in agreement with the theoretical calculation carried out by Balasubramanian[50] with the condition that the barrier to pseudorotation of the $^6A_1$ ground state (C_{2v} symmetry) is so small as to allow complete fluxional behavior at 2K. Another example of fluxional trimers is Sc_3[51] which has been isolated in a rare gas matrices at a temperature near 4k. ESR spectra established that the structure of Sc_3 is an

equilibrium triangle with $^2A'_1$ ground state. Furthermore the possibility remains that Sc_3 is a fluxional bent molecule with a very low barrier to pseudorotation. The same studies shows that Y_3 is not an equilateral triangle and is most probably a bent molecule. In fact it is probable that Y3 has an isosceles triangle shape at 4k, however the ESR spectra do not definitely decide between an obtuse or an acute apical angle. What is needed now is more experimental studies to verified and interpret thoroughly this findings. Perhaps resonance Raman studies of these trimers will be an excellent tool to confirm the theoretical work.

In a resonance Raman spectra of a D_{3h} molecules, the highest frequency is the totally symmetric one and therefore the one likely to form the resonance Raman progression. However in a linear triatomic the totally symmetric vibration is the lowest frequency vibration. Using this observation one can be able to determine the correct geometry. This is actually true when both stretching vibrations are observed. Another guide to determine the geometry of the trimers is by taking the ratio of the fundamentals. For example if the ratio is near $\sqrt{2}$ which is the ratio expected in the case of a central force field, then the geometry is an equilateral triangle.

As I said before, in the case of the trimers we are faced with three geometrical configurations which are equilateral triangle, isosceles triangle and linear chain.

Experimental investigations using matrix isolation technique and resonance Raman, ESR, absorption, or spectroscopy in the gas phase like for instance photoelectron spectroscopy or optical absorption/fluorescence spectroscopic can resolve the problem of determining the correct geometry and electronic state symmetry of the trimers, their molecular term symbols, vibrational and rotational constants as well as bond lengths. To determine all these parameters is mainly one of the purpose of the comprehensive studies of TM trimers.

The majority of the TM trimers are Jahn-Teller or Renner-Teller unstable, producing a fluxional or pseudo-rotating molecule even in a matrix environment. Hence the concept of a vibrational state may no longer be applicable and in this case the spectroscopic study of the trimers should be considered in terms of vibronic states. In any event the concept of vibronic interactions enables us to analyze all molecular properties, including molecular transformations, from a common point of view. The theoretical background for this concept lies in the successive account of vibronic mixing of electronic state by nuclear displacements by the break down of Born-oppenheimer approximation. Vibronic effects directly influence the structure and properties of molecules and crystals, and should be taken into account in any investigation of the origin of their properties and the

prediction of new properties. Hence the symmetry of the degenerate states can be determined.

Thus the most intriguing aspect of triatomic spectra is the role of the Jahn-Teller interaction, which has been characterized in quite a few molecules Na_3[36], Cu_3[37-43] , Mn_3[44] Ag_3[47] , Ni_3[48] , Rh_3[49]. For the homonuclear trimers the distortions is from D_{3h} to C_{2v} symmetry, splitting $^2E'$ state in (D_{3h}) into $^2A_1$ and $^2B_2$ states (in C_{2v}). A Jahn-Teller distortion removes the electronic degeneracy present in D_{3h} symmetry, giving rise to an isosceles geometry (point group C_{2v}) with an apical angle either greater than or less than 60° (the"obtuse" and "acute" isomers, respectively). This J-T effect cannot occur in systems with fewer than three atoms, making the homonuclear alkali and coinage metal trimers the simplest examples of systems exhibiting this effect. As such, they are of great interest from both a theoretical and an experimental point of view. Other TM trimers have expressed these effect like Y_3[51]. Though it wasn't possible to prove the presence of J-T effect in Zr_3 and Nb_3 due to the short progression observed in Raman spectra of both trimers. However the effect is not ruled out.

The J-T effect has been regarded as equivalent to or even synonymous with a distorted configuration. In fact a distorted situation amounts to a reduction of the symmetry of the system. However the term 'static distortion' could often be replaced with advantage by 'vibronically

stabilized distortion'[45]. The term static J-T effect is the effect of the vibronic interactions on the potential functions in the degenerate electronic states of non-linear molecules. However when we consider the energy levels that arise when J-T effects are actually present, that is, the dynamic J-T effect[46].

Furthermore The spin-orbit interaction affects the electronic structure of the TM trimers, especially when investigating the heavier third row TM trimers. It may even quench the J-T effect[1]. The general result is that the spin-orbit interaction tends to reduce the effects of J-T instabilities.

Early TM trimers exhibit extensive d-d bonding, while coinage metal trimers with their filled d shells have little d-d interaction. Yet some interesting and controversial questions are raised which is whether the late TM trimers with open d shells will have extensive d-d bonding like the early TM trimers or the bonding will be mostly s-s bonding. Further more is s-d mixing important, does s dominate over d or vice versa or for that matter does p-orbital mixing play a role. Nonetheless it is most probable that d-d interactions will be less dominant in late TMs, since the d orbitals in late TMs are considerably smaller than in early TMs. In fact, in TM dimers It was proven that there is a changeover from d-d bonding to s-s bonding along the series Fe_2->Cu_2. This point will be illustrated in chap IV. However, for an overall view of

transition metal systems theoretical studies especially the 4d and 5d series, one has to confront a number of problems besides correlation, or sometimes as part of it: open-shell systems involving a large number of electrons, magnetism, ligand lability, close-lying states, metal-metal bonds, core or 'semi-core' electrons that occupy the same part of space as the valence shell, fast electrons requiring relativistic corrections to name a few.

To summarize, in the first row of the periodic table, nickel and copper trimers have been the most explored. Regarding the second row, only silver trimers have been thoroughly studied not only in matrices but in the gas phase as well. However in the third row gold trimers have been one of the mostly investigated trimers experimentally and theoretically. Hopefully with our system we will be able to investigate thoroughly all transition metal trimers in the future. In fact two examples, zirconium and niobium will be treated in chapV using the CCNY cluster deposition apparatus.

The ultimate goal for TM trimers studies is to concentrate exclusively on the detailed chemical bonding and electronic architecture of TM trimers clusters.
I have attempted to include in the reference list all the transition metal trimers that have been investigated either experimentally or theoretically in Table V.1.1. My aim was to summarize and review all the work that has been done on TM trimers and give their ground state geometries as well

as their bond angles. Needless to say that the empty boxes should stimulate both experimentalist and theoretician for more extensive work in this area, because many of these transition metal systems are of special practical interest (catalysts, photographic clusters, industrial alloys, metallo-enzymes, etc.).

The symmetry and bond angle of the trimers in bold face were investigated experimentally, however The rest of the information was obtained from theoretical calculations.

Table V.1.1 Ground state symmetry and bond angle of some Transition metal trimers.

Sc_3[1]	Ti_3[2]	V_3[3]	Cr_3[4]	Mn_3[5]	Fe_3[6]	Co_3[7]	Ni_3[8]	Cu_3[9]	Zn_3
D_{3h}	D_{3h}	C_{2v}	C_{2v}	D_{3h}	D_{3h}	D_{3h}	C_{2v}	C_{2v}	
			near 60^0				90^o-100^o		
Y_3[10]	Zr_3[11]	Nb_3[12]	Mo_3	Tc_3	Ru_3	Rh_3[13]	Pd_3[14]	Ag_3[15]	Cd_3
D_{3h}	D_{3h}	D_{3h}				D_{3h}	C_{2v}	D_{3h}	
La_3	Hf_3	Ta_3	W_3	Re_3	Os_3	Ir_3	Pt_3[16]	Au_3[17]	Hg_3
							C_{2v}	D_{3h}	

1. **Properties of Sc_3, Y_3 and $Sc_{13(?)}$ molecules at low temperatures, as determined by ESR.**
T..B .Knight,Jr. and R.W.Woodward,J.Chem.Phy.79,5820 (1983).

On 3d bonding in the transition metal trimers:The electronic structure of equilateral triangle Ca_3, Sc_3, Sc_3^+, and $Ti3^+$.
Stephen P.Walch, and Charles W. Bauschlicher, J.Chem. Phys.83,5735(1985).

Diatomic and triatomic scandium and diatomic manganese A resonance Raman study.
M.Moskovits, D.P.Dilella, and W.Limm, J.Chem.Phys. 80,626(1983).

2. **Structures,binding energies, and charge distributions for two to six atom Ti, Cr, Fe and Ni clusters and their relationship to nucleation and cluster catalysis.**
Alfred B. Anderson J.Chem.Phys.64,4046(1976).

3. **Pulsed field ionization zero kinetic energy photoelectron spectroscopy of small vanadium clusters.Using velocity slip as a mass selector.**
D.D.Yang et al.Chem.Phys.lett.231,177(1994).

Vibrationally resolved negative ion photoelectron spectroscopic studies of bare transition metal trimers.

S.Alex, S.M.E.Green and D.G.Leopold,51st International symposium in Molecular Spectroscopy, Columbus Ohio.

4. **Dichromium and trichromium.**

D.P.Dilella, W.Limm, R.H.Lipson, M.Moskovits, and K.V.Taylor,J.Chem.Phys.77,5263(1982).

5. **The resonance Raman and visible absorbance spectra of matrix isolated Mn_2 and Mn_3 .**

K.D.Bier, T.L.Haslett, A,D.Kirkwood, and M.Moskovits, J.Chem.Phys.89,6(1988).

6. **Photoelectron spectroscopy of size-selected transition metal clusters: Fe_n^-, n=3-24.**

Lai-Sheng Wang, Hang-Song Cheng, Jiawen Fan, J.Chem. Phys.102,9480(1995).

Infrared spectra of Ni_3 and Fe_3 .

E.M.Nour, Alfaro-Franco, K.A.Gingerich, and J.Laane, J.Chem.Phys.86,4779(1987).

Structure and spin in small iron clusters.

P.Ballone and R.O.Jones.Chem.Phys.Lett.233,632(1995).

7. **ESR of Co, Rh, Ir trimers and diatomic ions.**

R.J.Van Zee, Y.M.Hamrick, S.Li and W.Weltner Jr.,Chem. Phys.Lett,195,214(1992).

Photodissociation measurements of bond dissociation energies: Ti_2^+, V_2^+, Co_2^+, and Co_3^+ .

Larry M.Russon, scott A.Heidecke, Michelle K.Birke, J.Conceicao, Michael D.Morse, and P.B.Armentrout. J.Chem.Phys.100,4747(1994).

8. **Infrared spectra of Ni_3 and Fe_3.**

E.M.Nour, Alfaro-Franco, K.A.Gingerich, and J.Laane, J.Chem.Phys.86,4779(1987).

Electron and vibrational structure of transition metal trimers:Phtotoelectron spectra of Ni_3^-, Pd_3^-, and Pt_3^- .

Kent M. Ervin, Joe Ho, and W.C.Lineberger, J.Chem.Phys.89,4514(1988).

Trinickel.

Martin Moskovits and Daniel P.Dilella, J.Chem.Phys.72, 2267(1979).

Computed potential surfaces for six low-lying states of Ni_3 .

Stephen Walch,J.Chem.Phys.86,5082(1987).

The ultraviolet-visible spectra of diatomic, triatomic, and higher nickel clusters .

M.Moskovits and J.E.Hulse, J.Chem.Phys.66,3988(1976).

Geometry,electronic structure, and magnetism of small Ni_n(n=2-6,8,13).

F.A.Reuse and S.N.Khanna.Chem.Phys.Lett.234,77(1995).

The structure of small nickel clusters.I.Ni_3^- Ni_{15} .

E.K.Parks,L.Zhu,J.Ho, and S.J.Riley.J.Chem.Phys. 100,7206(1994).

9. **Laser-Excited fluorescence spectroscopy of the jet cooled copper trimer.**

Eric A.Rohlfing and James J.Valentini, Chem.Phys.Lett. 126,113(1986).

Tricopper. A fluxional molecule .

D.P.Dilella, K.V. Taylor, and M.Moskovits, J.Phys. Chem.87,524(1983).

The geometric and electronic structures of small metal clusters of group IB metals .

J.A.Howard and R.Sutcliffe and B.Mile, Surf.Scien. 156,214(1985).

Electron Spin Resonance Spectrum of matrix isolated Cu_3 .

James A.Howard, Kelth F.Preston, Roger Sutcliffe and Brynmor Mile, J.Phys.Chem.87, 536(1983).

Theoretical studies of diatomic and triatomic systems containing the group IB atoms Cu, Ag, and Au.

Stephen P.Walch, Charles W.Bauschlicher, Jr and Stephen R.langhoffJ.Chem.Phys.85,5900(1986).

Photodissociation of copper clusters,Cu_n^+(n=3-8),in the 370-710 nm wavelength region.

Martin F.Jarrold and Kathleen M.Kreegan, International Journal of Mass Spectrometry and Ion Processes,102 (1990)161.

Geometric phase in two Kramers doublets molecular systems.

H.Koizumi and S.Sugano,J.Chem.Phys.102,4472(1995).

Structural and electronic properties of small copper clusters: a first principles study.
Massobrio,Pasquarello, and Car,Chem.Phys.Lett.238, 215(1995).

Photodissociation spectroscopy of Cu_3, Cu_3Ar, and Cu_3Kr.
Mark B.Knickelbein,J.Chem.Phys.100,4729(1994).

The copper trimer and its argon van der Waals complex:An anomalous shift in the A-X photodissociation spectrum.
Mark B.Knickelbein,J.Chem.Phys.100,2388(1994).

The cavity ring down dye laser spectroscopy of jet-cooled metal clusters;Cu_2 and Cu_3.
A.O'Keefe et.al. Chem.Phys.Lett 172,214(1990).

Electronic and geometric structure of the Cu_n cluster anions(n<10).
H.Akeby et.al.J.Phys.Chem.94,5471(1990).

10. **Electronic states of Y_n (n= 2-4).**
Dingguo Dai and K.Balasubramanian,J.Chem.Phys,98,7098 (1993).

Properties of Sc_3, Y_3 and $Sc_{13(?)}$ molecules at low temperatures, as determined by ESR.
L.B.Knight,Jr. and R.Woodward, R.J.Van Zee and W.weltner,Jr.J.Chem.Phys.79,5820(1983).

11. **Twelve electronic states and potential energy surface of Zr_3 .**

Dingguo Dai,K.Balasubramanian,Chem.Phys.Lett.231,352 (1994).

Resonance Raman spectrum and excitation profile of mass selected zirconium trimers.

Hanae Haouari, Huaiming Wang, Robert Craig, John R. Lombardi, and D.M.Lindsay. J.Chem.Phys.103,9527(1995).

12. **Resonance Raman spectrum of niobium trimer in argon matrices .**

Huaiming Wang, Robert Craig,Hanae Haouari, Yifei Liu, John R. Lombardi, and D.M.Lindsay.J.chem.Phys.Accepted May 96.

13. **Potential energy surfaces of eight low-lying electronic states of Rh_3.**

Kalyan K. Das and K.balasubramanian, J.Chem. Phys.93,625(1990).

ESR of Co, Rh, Ir trimers and diatomic ions .

R.J.Van Zee,Y.M.Hamrick, S.Li and W.Weltner Jr.Chem. Phys.Lett.195,214(1992).

High-spin electronic states of the rhodium trimer(Rh_3).

Dingguo Dai,K.Balasubramanian, Chem.Phys.Lett.195,207 (1992).

14. **Ten low-lying electronic states of Pd_3.**

K.Balasubramanian,J.Chem.Phys.91,307(1989).

Electronic states of Pd_3 .

D.G.Dai, K.K Das and K.Balasubramanian,Chem.Phys.Lett .184,589(1991).

Electronic and vibrational structure of transition metal trimers: Photoelectron spectra of Ni_3^-, Pd_3^-, and Pt_3^-.

Kent M. Ervin, Joe Ho, and W.C.Lineberger,J.Chem. Phys.89,4514(1988).

15. **Cryochemical studies.1.ESR of Ag_3 .**

J.A.Howard and K.F.Preston,A.Chem.Soc,103,6226(1981).

Vibronic spectroscopy and dynamics in the jet-cooled silver trimer.

P.Y.Cheng and M.A.Duncan,Chem.Phys.Lett.152,341(1988).

Vibrational properties of ligand-Free metal clusters: Ag_n (n=3, 4, 5, 6, 7, 12, 13).

Geoffrey A.Ozin and Douglas F.Mcintosh,J.Phys.Chem. 90,5756(1985).

Electronic states and potential energy surfaces of gold and silver trimers.

K.Balasubramanian and M.Z.Liao, Chem.Phys.127, 313(1988).

ESR spectra of Ag_3 ($^2A_1$) in an N_2 matrix.

K.Kernisant, G.A.Thompson, and D.M.Lindsay,J.Chem. Phys.82,4739(1985).

The geometric and electronic structures of small metal clusters of group IB metals.

J.A.Howard and R.Sutcliffe, B.Mile, Surf.scien.156,214 (1985).

Theoretical studies of diatomic and triatomic systems containing the group IB atoms Cu, Ag, and Au.

Stephen P. Walch, Charles W.Bauschlicher, Jr and Stephen R. langhoffJ.Chem.Phys.85,5900(1986).

A theoretical study of the excited states of Ag_3.

Stephen P. Walch, J.Chem.Phys.87,6776(1987).

Matrix Raman spectra of Ag_2 and Ag_3.

W.Schulze, H.U.Becker and R.Minkwitz and K.Manzel, Chem.Phys.Lett.55(1978),59.

Optical emission of Ag molecules in the gas evaporation technique.

Tsugio Okazaki,Yahachi saito, Atsuo Kasuya and Yuichiro Nishina, J.Chem.Phys.104,812(1996).

High resolution photodetachment spectroscopy of jet-cooled metal cluster anions:Au_2^- and Ag_3^-.

Gantefor, Cox, and Kaldor.J.Chem.Phys.93,8395(1990).

Non additive interactions and the relative stability of neutral and anionic silver clusters.

Kaplan,Santamaria, and Novaro.Int.J.Quantum.Chem. 55,237(1995).

Dispersed fluorescence spectroscopic study of the ground electronic state of silver trimer.

Ellis,Robles, and Miller.Chem.Phys.Lett.201,132 (1993).

16. **Electronic structure, binding energies, and interaction potentials of transition metal clusters.**
H.P. Cheng and D.E.Ellis.J.Chem.Phys.94,3735(1990).

Photoemission from Mass-Selected Monodispersed Pt clusters.
W.Eberhardt, P.Fayet, D.M.Cox, Z.Fu, A.Kaldo, R.Sherwood,and D.Sondericker, Phys.Rev.Lett.64,780 (1989).

Electron and vibrational structure of transition metal trimers:Photoelectron spectra of Ni_3^-, Pd_3^-, and Pt_3^-.
Kent M.Ervin, Joe Ho, and W.C.Lineberger,J.Chem.Phys. 89,4514(1988).

Metal-metal bonding in transition-metal clusters with open d Shells: Pt_3.
H.Hua Wang and Emily A.Carter.J.Phys.Chem.96, 1197(1991).

Electronic and geometrical structures of Pt_3 and Pt_4.An ab initio one-electron proposal.
J.Rubio et al.Chem.Phys.Lett.217,283(1994).

17. **The geometric and electronic structures of small metal clusters of group IB metals.**

J.A.Howard and R.Sutcliffe, B.Mile, Surf.scien.156,214 (1985).

Electronic states and potential energy surfaces of gold and silver trimers.

K.Balasubramanian and M.Z.Liao, Chem.Phys.127, 313(1988).

CASSCF/CI calculations of low-lying states and potential energy surfaces of Au_3 .

K.Balasubramanian and M.Z.Liao, J.Chem.Phys.86,5587 (1987).

Resonant two-photon ionization spectroscopy of jet-cooled Au_3.

Bregory A.Bishea and Michael D.Morse,J.Chem.Phys.95, 8779(1991).

Theoretical studies of diatomic and triatomic systems containing the group IB atoms Cu, Ag, and Au.

Stephen P.Walch, Charles W.Bauschlicher,Jr and Stephen R.langhoffJ.Chem.Phys.85,5900(1986).

Photoelectron spectroscopy of metal cluster anions:Cu_n^-, Ag_n^-, and Au_n^-.

Ho, Ervin, and Lineberger.J.Chem.Phys.193,6987(1990).

The ionization potential of Ag_n and Au_3 and binding energies of Ag_n, Au_n, Ag_n^+, and Au_n^+(n=1-4).

K.Balasubramanian and P.Y.Feng.Chem.Phys.Lett.159,452 (1989).

V.1.1 Badger's rule

There are different ways to calculate the vibrational frequencies and the force constants of trimers. Ozin and McIntosh have suggested a scheme to predict the force constants of higher clusters from that of dimers. They suggest that the reduction in force constant should be proportional to the increased number of bonds each atom is involved with.

One of the simplest and earliest methods to correlate force constant and bond length was proposed by R.M.Badger. This correlation is often referred to as "Badger's rule".[52-53]. Actually it is an empirical formula that has been proposed to describe the variation of harmonic bond stretching force constants with bond length and with chemical properties of the bonded atoms, and this often gives satisfactory results for polyatomic as well as diatomic molecules.

$$k_e (r_e - d_{ij})^3 = C$$

k_e force constant in mdyn /Å

r_e internuclear distance in Å

d_{ij} is an empirical "distance of nearest approach" in Å that depends on the row i and j in which the atoms of the diatomic reside in the periodic table .

Below is a table giving different geometries for trimers with their corresponding normal modes and formula to determine their frequencies and force constants.

V.1.2 Some useful formulas

Geometry	Symmetry	Normal Modes	Spectra	Frequencies
Linear[1] $D_{\infty h}$	Σ_g^+	sym st	R	$\lambda_1 = 4\pi^2\nu^2 = (k_{11}+k_{12})/m$
	Π_u	bend	IR	$\lambda_2 = 6\ (k_{bend})/m^2$
Bent[2]	C_{2v}	a_1 sym st	IR, R	$\lambda_1 = 3\,(k/m)$
		b_1 asym st	IR, R	$\lambda_2 = 2\cos^2(\phi/2)\,(k/m)$
		a_2 bend	IR, R	$\lambda_3 = (3-2\cos^2(\phi/2))\,(k/m)$ (best in limit $\phi = 2\alpha = 60^0$)
		symm/asym (±) st (switch for $\phi > 90^0$)		$\lambda_\pm = (2 \pm \cos(\phi))\,(k/m)$ (*best in limit* $\phi = 180^0$)
Equilateral Triangle[1,3]	D_{3h}	a'_1 sym st	R	$\lambda_1 = 3\,(k/m)$

Notes:

1) Herzberg IR&R p. 160 ($m_x = m_y = m$) $a_{11} = a_{33} =$

More accurately for c_{2v} case, let $\kappa_{1,3} = k_{1,3}/m$

then $\lambda_3 = (3 - 2\cos^2(\phi/2))\,\kappa_1$

$\lambda_1 + \lambda_2 = 2\kappa_3 + (1 + 2\cos^2(\phi/2))\,\kappa_1$

$\lambda_1 \lambda_2 = 6\cos^2(\phi/2)\,\kappa_1 \kappa_3$

Letting $s = \lambda_1 + \lambda_2 - 1/3\ \lambda_3$ then

$\kappa_3 = s/4 \pm 1/2\ \sqrt{\ s^2/4 - 8/9\ \lambda_1 \lambda_2}$

$\kappa_1 = (\lambda_1 + \lambda_2 + \lambda_3 - 2\kappa_3)/4$

$\cos^2(\phi/2) = \lambda_1 \lambda_2 / 6(\kappa_1 \kappa_3)$

2) Moscovits & DeLella J.Chem.Phys.**72**,2267(1980)

$k_{13} = 0 \qquad r = \lambda_+/\lambda_- \qquad \cos\phi = 2(r-1)/(r+1)$

More accurately if $k_{13} \neq 0$ let $\mu = 1/m$ (atom 2 is central atom)

$\kappa = \mu k$

$\lambda^2 - \lambda\,[\,k(\mu_1 + 2\mu_2 + \mu_3) + 2\mu_2 k_{13}\cos(\phi)] + (k^2 - k_{13}^2)$

$[(\mu_1+\mu_2)(\mu_2+\mu_3)-\mu_2^2\cos^2(\phi)] = 0$

or if $\mu_1 = \mu_2 = \mu_3$

$\lambda^2 - \lambda\,[\,4\kappa_1 + 2\kappa_3\cos(\phi)] + (\kappa_1^2 - \kappa_3^2)\,[4 - \cos^2(\phi)] = 0$

3) $\lambda_1/\lambda_2 = 2$

4) CONVERSION FACTORS:

note that κ and λ have units of $(cm^{-1})^2$ In order to convert to force constant k(mdyne/A) =m(amu)κ use the factor 1 = 5.8919×10^{-7} $(mdyne/A\text{-}amu\text{-}cm^{-2})$.

5) For small deviations from a D_{3h} symmetry $\phi = 60° + \delta$

$$\nu_3 - \nu_2 = 2/3(\cos 30)\,\delta\,(3xk/2m)^{1/2}$$

$$1/2\,(\nu_3 + \nu_2) = (3xk/2m)^{1/2}$$

k force constant, m mass in amu.

ν vibrational frequency.

V.2 Resonance Raman spectrum and excitation profile of mass-selected zirconium trimers

Hanae Haouari, Huaiming Wang, Robert Craig, John R. Lombardi, and D.M. Lindsay

Department of Chemistry and Center of Analysis of Structures and Interfaces (CASI), The City College of New York (CCNY), New York, New York 10031

A. Introduction

Transition metal clusters present a particularly difficult challenge to our understanding of molecular structure due to strong electron correlation and the existence of many low lying electronic states. The heavier transition metal clusters have the additional problem of large relativistic effects, which can severely alter chemical bonding. Geometries and force constants can vary wildly among these low lying states. Thus, at various levels of sophistication in theory, predictions as to the correct energy level ordering can vary. Several articles, both experimental and theoretical, have recently appeared concerning the structure and bonding in zirconium clusters. Theoretical predictions of the dimer ground state[1,2] indicate either a $^1\Sigma_g^+$ or $^1\Delta_g$ state, a result which is confirmed by experiment[3]. The remaining theoretical articles involve the trimer[4] and tetramer[5] A recent

resonance two photon ionization technique done by Ulf Sassenberg[15] has found that the ground state of Zr_2 is $^3\Delta$.

In this article we present results of a Raman spectroscopic study of zirconium trimers in an argon matrix. Our samples are prepared by neutralizing a mass-selected beam of trimer ions, and therefore suffer from little interference from atomic or dimer spectral features. Recent improvements in our experimental apparatus enable us to obtain more sensitive Raman spectra, as well as high quality Raman excitation profiles. Since our samples are optically quite thin, absorption spectra are hard to obtain, and Raman excitation profiles often provide higher sensitivity. Although no visible absorption spectra of Zr_3 could be obtained, we have identified two optical transitions by scanning the visible region of Raman excitation. The Raman spectrum itself indicates that in the ground state, zirconium trimer is an equilateral (D_{3h}) geometry. Both the totally symmetric a'_1 and degenerate e' vibrations are observed.

B. Experimental

The cluster deposition source located at The City College of New York has been presented in previous publications[6-11] An intense (typically 10 mA at 25 keV) argon ion beam for a "CORDIS" ion source (Rokion Ionenstrahl-Technologie, Darmstadt, Germany) sputters zirconium cluster ions from a water cooled, zirconium

target (Rembar, 99.9%) maintained at about 350 V. Secondary ions were extracted with a modified Colutron model 200-B lens system and then mass selected using a Wien filter (Colutron 600-B). The cluster ion beam was then bent by 10° to prevent neutrals from reaching the deposition region, which consists of a cooled (approximately 14 K) CaF_2 substrate surrounded by a "Faraday cage." The polished substrate is mounted to a closed cycle cryostat (APD Displex, 204SL/DMX-6) and temperature is measured with a Si diode in conjunction with a Scientific Instruments model 5500 temperature controller. Zirconium cluster ions were codeposited with Ar gas (99.9998% Ar, Matheson) from a coaxial injector ring and low energy electrons (for neutralization) from a tungsten filament. Matrices were grown at 4 μ/h with an argon:metal dilution ratio of 8000:1, to ensure that clusters remain isolated both from each other and any impurity species. Ion currents are measured by using a Faraday plate situated perpendicular to the CaF_2 substrate. The difference in voltage (V_{dep}) between the target and Faraday cage determines the metal cluster deposition energy (eV_{dep}), which was held at approximately 10 eV in the experiments described here. Under these "soft-landing" conditions, measured ion currents were 81 nA for Zr^+, 76 nA for Zr_2^+, 15 nA for Zr_3^+, and 7 nA for Zr_4^+; as shown in Figure V.2.1. Fragmentation may be estimated by comparing the intensities of atomic excitation features in the trimer deposition with

those obtained from depositions of the atom under similar conditions. By this measure, we may estimate the fragmentation of zirconium trimers to atoms ($Zr_3 \rightarrow 3Zr$) to be less than 3 %

Matrix samples were interrogated *in situ* using both absorption and Raman spectroscopy. For the absorption spectra, we employed a broad band (deuterium or tungsten) light source dispersed by a 1/4 m monochromator (calibrated with Hg lamp), and then focused onto the matrix sample. Absorption spectra were recorded by observing the light scattered at right angles to the matrix surface. This technique (which we term "scattering depletion spectroscopy"{SDS}) has been shown to be equivalent to the absorption spectrum, but with slightly improved sensitivity for our apparatus.

Raman spectra were recorded using an argon ion laser (Spectra Physics model 2045) pumping a dye laser (Coherent CR 599, with rhodamine 6G or rhodamine 110 as dyes). Typical fluences were 25-50 mW focused down to an estimated 50 μ spot size. The exciting laser line was generally predispersed with a grating in order to minimize fluorescence from the dye. Light scattered at 90° was collected in a SPEX Triplemate Spectrometer and detected with a SPEX model "Spectrum One" CCD detector, and DM1000 series software. Raman excitation profiles were obtained by measuring the intensity of an observed Raman line, subtracting out background, and plotting, for each

excitation wavelength, the ratio of intensity to that of the CaF_2 Raman line observed in all our spectra at 330cm^{-1}.

C. Results

Despite repeated attempts in several deposited samples, no trace of an absorption or SDS spectrum could be observed. It is our conclusion that due to our optically thin samples, any visible transitions are too weak to be observed under these experimental conditions. Such a circumstance presents some difficulty in obtaining resonance Raman spectra since it is not clear exactly where to begin. However, after searching at several excitation wavelengths, we were able to observe Raman spectra. A typical spectrum are shown in Figure V.2.2 and Figure V.2.3 in which the excitation wavelength is chosen to be 608.2 nm and 611.5 nm respectively. Three Raman lines may be ascribed to Zr_3 , the remaining line at 330 cm^{-1} is due to the substrate CaF_2. Similar spectra were observed at numerous excitation wavelengths, over which we have averaged the observed lines (when sufficiently intense). The averages, along with standard deviations (in parentheses) are 176.7 (1.3) cm^{-1} (ν_2), 258.0 (1.2) cm^{-1} (ν_1), and 516.1 (0.8) cm^{-1} ($2\nu_1$).

The (very weak) high frequency line is almost exactly twice that of the most intense line and we take it to be the first overtone. The ratio of the frequencies of the two lowest lines (ν_1/ν_2) is 1.46, which is very close to $\sqrt{2}$.

This is indicative of a symmetrical equilateral geometry (D_{3h})[12]. In such a case we expect two normal frequencies: one for a totally symmetric stretch of symmetry a'_1 (ν_1) and a doubly degenerate bend of symmetry e' (ν_2).

The Raman excitation profiles of the two lines in the region 450-650 nm are shown in Figure V.2.4 along with least squares fits of Gaussian bands. The profile of the ν_1 (a'_1) line shows two broad maxima, one near 491 nm and the other near 614 nm. The ν_2 (e') profile, while somewhat noisier due to its lower intensity, shows a broad region of intensity near 614 nm, and is otherwise too weak to be reliably observed elsewhere.

D. Discussion

The Raman spectrum of the zirconium trimer indicates clearly that the structure is most likely that of an equilateral triangle. Only two fundamentals are observed, and their ratio is almost exactly that expected for a D_{3h} geometry. The experimental bond force constant obtained from this analysis is 1.19 mdyne/Å. This may be compared with that of the dimer[3], which is 2.51 mdyne/Å. Ozin and MacIntosh[13] have suggested a scheme by which to predict the force constants of higher clusters from that of the dimer. They suggest that the reduction in force constant should be proportional to the increased number of bonds each atom is involved with. For an equilateral trimer this factor is

1/2, so that they would predict a trimer force constant of 1.26 mdyne/A, quite close to our measured value.

Additional information as to the nature of the ground and excited states may be obtained from an analysis of the Raman excitation profiles. These show evidence of two excited electronic states. The lack of a long progression in either vibration indicates that there is little change in geometry between ground and excited states. Note that the e' vibration shows intensity only in the 614 nm region, while the 491 nm band is present only in the a'_1 vibrational profile. In D_{3h} symmetry we expect either singly or doubly degenerate electronic states. In the absence of vibronic coupling, resonance Raman spectra should only be observed for totally symmetric ground state vibrations. The Jahn-Teller theorem indicates that a doubly degenerate electronic state must necessarily couple with a vibration of the same symmetry. We may conclude, therefore, that the 491 nm band lacks any measurable vibronic coupling, in either state, and must represent a transition between non-degenerate electronic states. The ground state is thus non-degenerate. On the contrary, since we observe intensity in the e' vibration in the 614 nm region one of the two electronic states involved in this transition must be vibronically coupled. Since the ground state must be non-degenerate, the excited state must arise from a doubly degenerate electronic state. Figure V.2.5 shows the shape

of the symmetrized displacements in case of triangular X_3 molecules.

At this point it is worthwhile to examine theoretical predictions as to the electronic states available to the molecule. To our knowledge, only one paper has been published on the zirconium trimer by Dai and Balasubramanian

In all, they examine the properties of 12 electronic states of Zr_3 by two methods. In the first, they utilize the complete active space multiconfiguration self-consistent field (CAS-MCSCF) and follow with multireference single and double configuration interaction (MRSDCI) calculations. Although both levels of calculations disagree as to the ordering of the states, the MRSDCI calculation is considered the more accurate treatment, and we will only discuss those results. The lowest lying states predicted by these calculations come from the following configurations:

Configuration	**State (D_{3h})**
$(1a'_1)^2(2a'_1)^2(1e')^4(1a''_1)^2(1a''_2)^2$	$^1A'_1$
$(1a'_1)^2(2a'_1)^2(1e')^4(1a''_2)^2(1a''_1)^1(2e')^1$	$^3E''$, $^1E''$
$(1a'_1)^2(2a'_1)^2(1a''_2)^2(1a''_1)^1(1e'')^3(2e')^2$	$^5E''$

Dai and Balasubramanian predict the ground state to be the $^1A'_1$, and while the next states are predicted to be split by Jahn-Teller interactions, their minima lie within

0.73 eV of the predicted ground state. Further they predict the ground state to be slightly distorted to C_{2v} geometry with an apex angle of 71.1°. In Figure V.2.6 is shown in general, the three possible types of Jahn-teller effects. In the limit of D_{3h} geometry our experimental results are in agreement with the theoretical results as to the nature of the ground state. If this assignment is indeed correct, considering D_{3h} selection rules, we may further assign the 614 nm band to be $^1A'_1 - {}^1E'$ (x,y polarized) while the 491 nm band must be $^1A'_1 - {}^1A''_2$ (z polarized). The short progressions observed justify the maintenance of D_{3h} notation in the excited states as well. Although these assignments must be viewed as tentative, it is hoped that they will provide a stimulus to further theoretical and experimental work on this molecule.

ACKNOWLEDGMENTS

We wish to thank Ms. Emily Chu for assistance in analyzing the results. This work was supported by the National Science Foundation under Cooperative Agreement No. RII-9353488 and Grant No. CHE-9412804 and by the City University of New York PSC-BHE Faculty Research Award Program.

Figure V.2.1 Mass Spectrum of Zr clusters from sputtering target, measured *in situ* by recording the current on the Faraday plate as a function of magnetic field on the Wien filter.

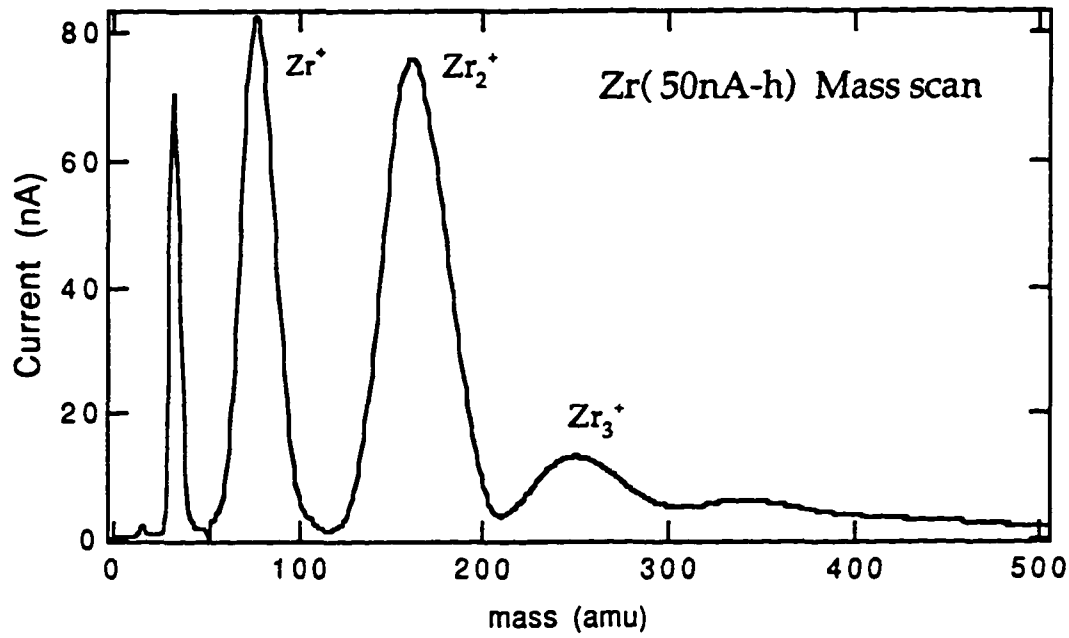

Figure V.2.2 The resonance Raman spectrum of Zr_3 at 14K in Ar matrix. In addition to the line at 330 cm^{-1} due to the CaF_2 substrate, three spectral lines are observed as indicated.

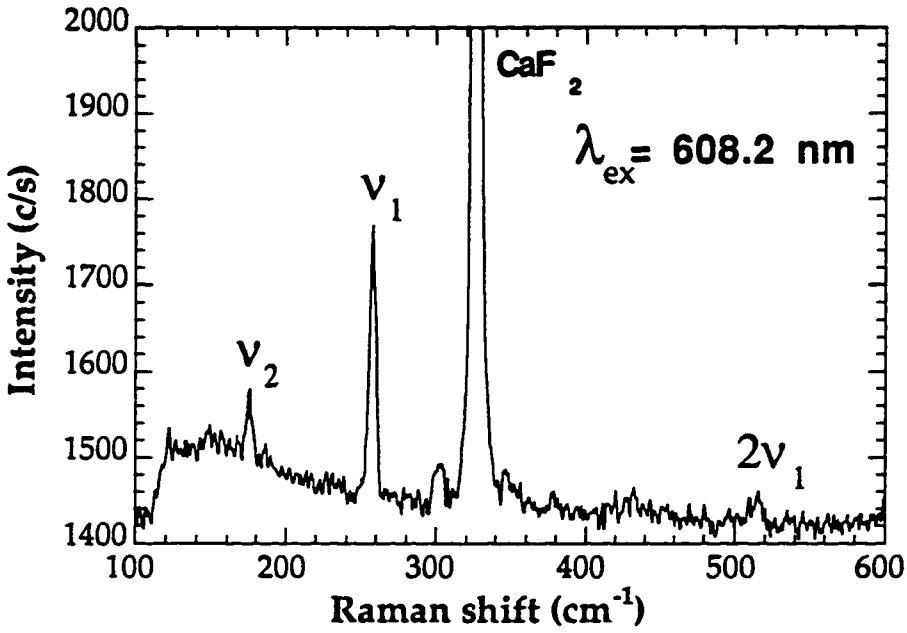

Figure V.2.3 The resonance Raman spectrum of Zr_3 at 14K in Ar matrix. In addition to the line at 330 cm^{-1} due to the CaF_2 substrate, three spectral lines are observed as indicated.

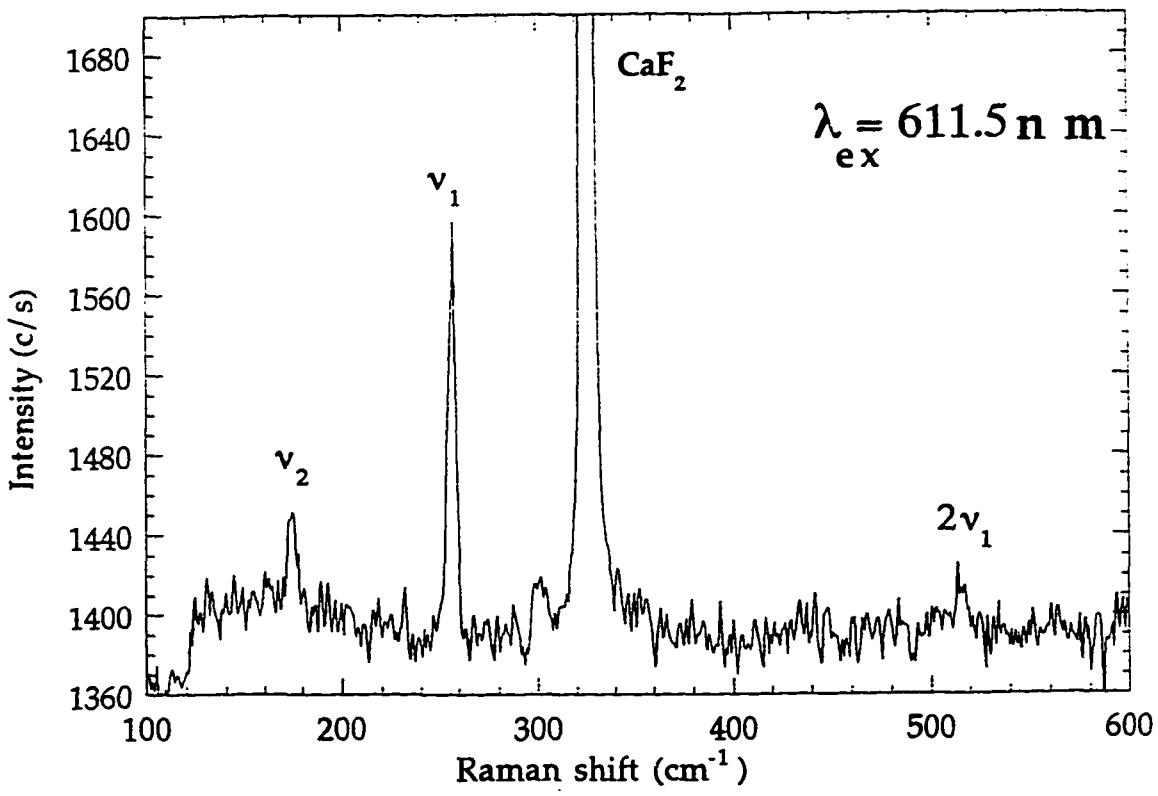

Figure V.2.4 Raman excitation profiles for the ν_1 (a'_1) [filled circles] and the ν_2(e') [open circles] lines of Zr_3. In the former we observe two broad intense regions, near 491 and 614 nm, while for the latter, intensity is observed only near 614 nm. The solid curves show least squares Gaussian fits to the observed points.

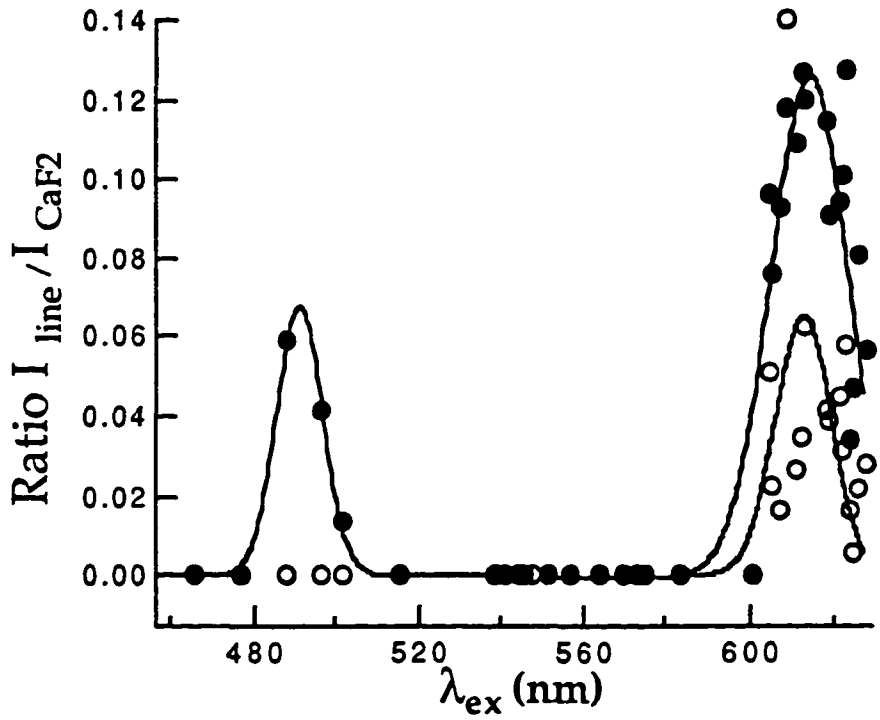

Figure V.2.5 Shape of symmetrized (normal) displacements in case of triangular X_3 molecules. (Ref.14)

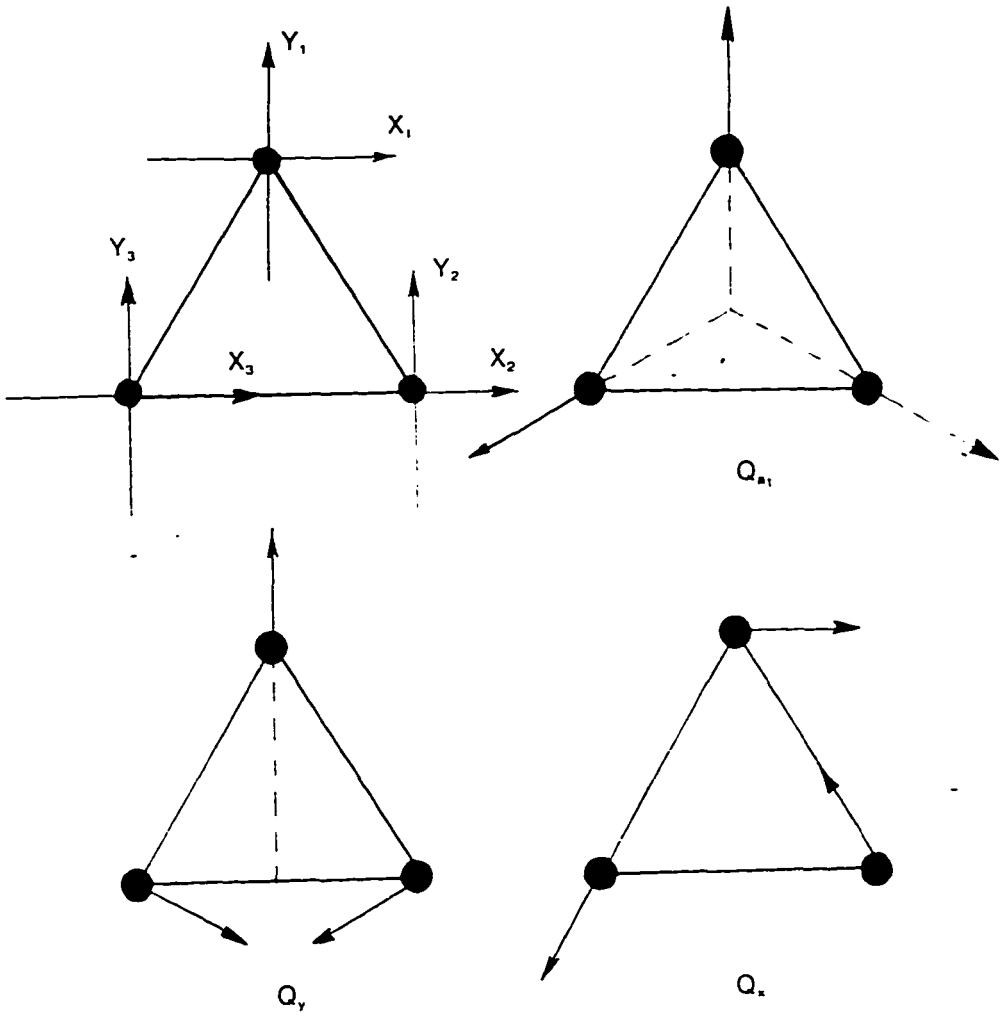

Figure V.2.6 Schematic illustration of the three main types of specific adiabatic potential behavior due to vibronic interactions: (a) electronic degeneracy-The Jahn-Teller; (b) electronic pseudodegeneracy-the pseudo-Jahn-Teller effect; (c) electronic rearrangement effect.(Ref.14).

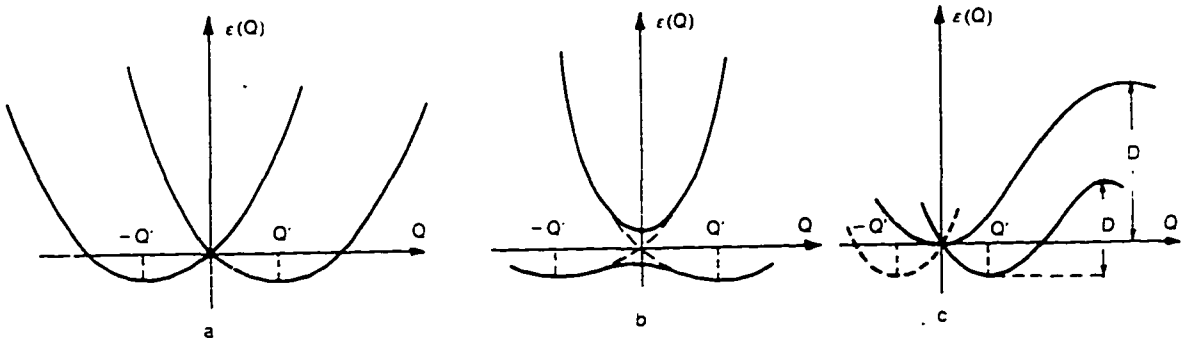

V.3 Resonance Raman spectra and excitation profiles of mass-selected niobium trimers

Hualming Wang, Robert Craig, Hanae Haouari, Yifei Liu
John R.Lombardi, and D.M.Lindsay
Department of Chemistry and Center of Analysis of Structures and Interfaces (CASI), The City College of New York(CCNY), New York, New York 10031

A. Introduction

Transition elements contain partially filled d or f shells. This property makes transition metal clusters quite difficult to study because of the many low lying electronic states. While dimers of several transition metals have been thoroughly studied theoretically as well as experimentally, trimers and larger clusters of transition metals are still under study. Nevertheless the largest challenge is still to be able to determine a correct geometrical structure. Structural information on transition metal clusters has been mostly obtained from electron spin resonance and resonance Raman studies of matrix isolated clusters[1-6], but also through gas phase spectroscopy[7-9] using for instance resonant two photon ionization spectroscopy. Diatomic metal molecules have been studied extensively by the means of various experimental measurements and state of art theoretical calculations[19-20]. A detailed understanding of

the chemical bonding and properties of small transition metal clusters is extremely important because of the impact they have on catalysis and materials science in particular. We now know force constants for the ground states of homonuclear transition metal diatomic species in a large portion of the periodic table[14]. Comparatively speaking, the studies of the properties of trimers and higher clusters are quite limited and still require more experimental and theoretical attention. In the case of niobium, several articles have addressed the bonding energies or ionization potentials (IPs) of larger species, but little detailed information, especially regarding the structure and bonding of triniobium has emerged to date. Assuming that the $^6A_1$ state is the ground state of Nb_3 in C_{2v} geometry, Sellers[21] obtained ionization potentials[22-23] and some geometric parameters.

In this paper we report on the observation of resonance Raman spectra and absorption (scattering depletion) spectrum of Nb_3 in argon matrices. Our samples are prepared simply by neutralizing a mass-selected beam of trimer ions. Since our sample was quite concentrated (100nA-h), a visible absorption spectra of Nb_3 could be obtained from which three transition features were observed of the niobium trimer. Resonance Raman spectra indicate that the ground state of the Nb_3 is nearly an equilateral geometry (D_{3h}). with an angle slightly higher than 60°. Both

fundamentals the totally symmetric a_1' and doubly degenerate e' vibrations are observed.

B. Experiment

The cluster deposition source located at the City College of New York has been presented in previous publications[10-16]. An intense (typically 15 mA at 25 KeV) argon ion beam for a "CORDIS" ion source (Rokion Ionenstahl-Technologie, Darmastadt, Germany) sputters niobium cluster ions from a water cooled, niobium target (Goodfellow, 99.9%) maintained at about 350 V. Secondary ions were extracted with a modified colutron model 200-B lens system and then mass selected using a Wien filter (colutron 600-B). The cluster ion beam was then bent by 10° to prevent neutrals from reaching the deposition region, which consists of a cooled (approximately 14K) aluminum substrate surrounded by a "Faraday cage". We have chosen an aluminum substrate instead of CaF_2 or silver plate, in order to avoid interference from the CaF_2 Raman transition (at 330 cm^{-1})[24] and so obtain a better spectrum. The polished substrate is mounted on a closed cycle cryostat (APD Displex, 204SL/DMX-6) and temperature is measured with a Si diode in conjunction with a Scientific Instruments model 5500 temperature controller. The aluminum substrate was held at the same potential as the Faraday cage. Niobium cluster ions were co-deposited with Ar gas (99.9998% Ar, Matheson) from a coaxial injector ring and low energy

electrons (for neutralization) from a tungsten filament. Matrices were grown at 4-6μ/h with an argon:metal dilution ratio of 10^4:1 to ensure that clusters remain isolated both from each other and any impurity species. Ion currents are measured by using a Faraday plate situated perpendicular to the Al substrate. The difference in voltage (V_{dep}) between the target and Faraday cage determines the metal cluster deposition energy (eV_{dep}). Under these "soft-landing" conditions, measured ion currents were: Nb^+ (60nA), Nb_2^+ (120nA), Nb_3^+ (30nA), and Nb_4^+ (15nA) (see Figure V.3.1). Prior to deposition, the selected ions were simultaneously slowed to 10eV by a surrounding "Faraday cage". Fragmentation may be estimated by comparing the intensities of atomic excitation features in the trimer deposition with those obtained from depositions of the atom under similar conditions. By this measure, the trimer fragmentation is estimated to be less than 0.5 % (D_o = 5.0 eV)[19].

Matrix samples were interrogated in-situ using both absorption and Raman spectroscopy, and (in the case of atomic niobium) excitation spectroscopy. As previously reported,[12,16] the absorption measurements were made by collecting the light at 90° to that incident, a technique we term "Scattering Depletion Spectroscopy" (SDS).

Raman spectra were recorded using both the visible lines of an argon ion laser (Spectra Physics model 2045) and a dye laser (Coherent, model CR599) with R110 and R6G

dyes, pumped by "green-blue" lines of the Ar^+ laser. Scattered light was collected at 90°. into a Spex 1877E 0.6m Triplemate Spectrometer and detected by a liquid nitrogen cooled CCD detector (Spex model " Spectrum One") with DM3000R software.

C.Spectra and analysis

Several samples have been deposited on CaF_2, silver and Aluminum substrates. The only successful results were from the latter substrate. But nevertheless resonance Raman spectra were obtained from the deposition on CaF_2 with a lower intensity ion current compare to the Al substrate. The Ag substrate was tested for SERS (Surface Enhanced Raman Scattering). Unfortunately there was no sign of enhancement due to the silver substrate. From the SDS (Scattering Depletion Spectroscopy) spectra and a very thick sample we can make interesting conclusions as far as visible transitions are concerned. Strong trimer absorptions were observed following a 100nA-hours deposition of niobium trimer on argon at an energy of 10eV and was recorded with 0.4nm resolution using a tungsten lamp. Three absorption features are shown with maxima at about 492 nm(20,300cm^{-1};A), 532 nm(18,800cm^{-1};B) and 587nm (17,000cm^{-1};C). No detectable absorption band is observed beyond this region except one broad absorption band centered at 360 nm(27,800cm^{-1}) which may be seen in an SDS spectrum (not shown) taken with a deuterium lamp. Annealing

the sample to 36K had little effect on the absorption spectrum. By comparing the absorption features of triatomic niobium in argon with those obtained from the atomic and dimer niobium in argon[12], we can attribute these transitions to niobium trimer with confidence. Further this assignment is verified by the observation of resonance Raman spectra for excitation into this bands. A thorough analysis is difficult due to the relative lack of features. However, analysis of Raman excitation profile will give us some clue as to their origin. A typical resonance Raman spectra of Nb_3 isolated in argon matrices is shown in Figure V.3.3 where spectrum (a) is obtained excited with 514.5 nm Ar^+ laser radiation; and spectrum (b) with 588.8 nm dye laser radiation respectively. The resonance Raman spectra were observed through the region 458.5-614.0 nm, but not upon excitation at 360 nm band or further to that. The average Stokes shifts (one standard deviation in parentheses) found for 60 different excitation wavelengths are listed in Table V.3.1 The progression observed by excitation into the band A were somewhat more extensive than those observed in the other bands (B and C), but otherwise no significant difference between the spectra were obtained. All the observed lines can be explained by assuming two fundamentals frequencies. The high frequency (ν_1) shows a progression ($v''=0 \rightarrow v''>0$) starting at 334.9(28) cm^{-1} and displays three overtones at 669.7(33), 1,003.8 (28) and 1,340.6(62) cm^{-1}. The low frequency (ν_2) occurs at 227.4

(29) cm^{-1} and has no overtone. The other bands observed in the spectra involve combinations of these two fundamentals. Which are 561.1(2.8) cm^{-1} ($\nu_1+\nu_2$) and 895.9 (4.5) cm^{-1} ($2\nu_1+\nu_2$).

The plot of Raman intensity (scaled by the laser power) vs. laser wavelength is superimposed in Figure V.3.2. Three transitions were observed in the absorption spectrum, one centered at 495 nm and not quite resolved, the second transition maximum at 530 nm, the third transition centered at 595 nm. The excitation profile of the 227.4cm^{-1} (e') line shows one maximum near 520 nm, while The 334.9cm^{-1} (a'_1) profile shows one lower intensity maximum near 520 nm and a higher intensity maximum near 540 nm.

The Raman excitation profile of ν_1 bears a strong resemblance to the triniobium absorption spectrum (Figure V.3.2), but the peaks seem more closely spaced than in the absorption spectrum. This pattern may be a result of interference effects observed in Raman excitation profiles[17]. It was suggested by Spiro[17] that interference from different electronic states may affect vibrational Raman scattering. Also he proposed that destructive interferences affect the excitation profiles.

Both the ν_2 profile and first overtone of ν_1 profile show an intense peak near the band A and a weak tail in the red region. Note that both ν_1 and ν_2 vibrations are observed with the same intensity near the peak A, while the ν_1 vibration dominates the profile at the peak B. Neither display much intensity near the peak C.

D. Discussion

The resonance Raman spectrum of niobium trimer in argon matrix shows two fundamentals at 334.9 and 227.4cm^{-1}. Further analysis of the line shape using least squares fitting of gaussian function indicates that the widths of the 227.4cm^{-1} line (Δv=8.2cm^{-1}) and other combination lines are almost twice that of the 334.9cm^{-1} line (Δv=4.5cm^{-1}). Since the natural abundance of niobium is a single isotope (M=93) and we observe no effect on the line shape during annealing the sample to 36K, we might expect that the fundamental at 227.4cm^{-1} really consists of two unresolved lines, which are so close that they overlap to cause an apparent broadening. Furthermore, notice the ratio of the frequencies (ν_1 / ν_2) is 1.47 very close to $\sqrt{2}$:1 as would be expected for a symmetrical equilateral geometry (D_{3h}).[25] Both observations suggest that the Nb_3 molecule is almost D_{3h} in shape with a possible slight distortion. In this case we assign the high frequency mode as the totally symmetric stretch $a'_1(\nu_1)$ and the low frequency to the doubly degenerate bend $e'(\nu_2)$. The totally symmetric frequency 334.9 cm^{-1} has three overtones, which indicate somewhat of a change in internuclear distance from the ground state along the (a'_1) direction because of this short progression. However the (e') vibrational frequency displays no overtones. A metal-force constant and a

stretch-stretch interaction constant calculated by the Wilson FG method[26] assuming D_{3h} geometry give 1.95 and 0.05 mdyne/Å respectively. By doing a normal mode calculation, it is possible to properly fit the observed frequencies and the force constants. In order to have an accurate comparison with the experimental results, it is necessary to introduce off-diagonal (stretch-stretch interaction) elements into the force constant matrix on the order of 10 % of the diagonal constants. The calculated bond force constant is 2.42 mdyne/Å, obtained from dimers force constant, which is not in agreement with the value obtained by the Wilson FG method.

A Comprehensive analysis of the Raman excitation profile combined with that of SDS could give information about the ground and excited state symmetry. The features in the excitation profile are due to changes in normal mode composition between ground and excited state, which arise from changes in force constants and geometry in the excited state or anharmocity in the normal modes. Sellers[21] has suggested a ground state of Nb_3 as the $^6A_1$ state in C_{2v} geometry because that state dissociates into fragments in their correct ground spin states. At the relativistic effective core potential-configuration interaction, single and double excitations (RECP-CISD) level, he obtains an ionization potential of 4.33eV which is somewhat smaller than the experimental results (IPs=5.6–5.8 eV)[22-23]. The optimum geometry has an angle of 41.5°, far from our

observation. The maximum experimental deviation of the apical angle from 60° (assuming the observed line widths are caused by slight deviations from D_{3h} geometry) is 1.7°. Dai and Balasubramanian have recently reported the electronic structure of Zr trimer[18]. Since Nb has only one more electron than Zr, if we assume the orbital ordering is the same as Zr_3[17] and a D_{3h} geometry. Then the configuration of the ground state is $(1a_1')^2$ $(2a_1')^2$ $(1e')^4$ $(1a_2'')^2$ $(1a_1'')^2$ $(2e')^3$, containing a hole in the second e' orbital and indicating a likely $^2E'$ ground state. This state is susceptible to Jahn-Teller distortion in the D_{3h} geometry. Two vibrations were observed a totally symmetric a'_1 and a doubly degenerate e', however we saw no evidence for Jahn-Teller interactions in the e' vibration, due to short progression in e' vibration. In any case we expect the Jahn-Teller coupling to be smaller because it will probably be quenched by the strong spin-orbit coupling. The broader bandwidth in the e' vibration stems from a possible small splitting.

The absorption spectrum shows three electronic transitions. If the vibronic symmetry of the ground state is $^{ev}E'$, the vibronic selection rules are $^{ev}E' \rightarrow {}^{ev}A''_2$ (x, y polarized) and $^{ev}E' \rightarrow {}^{ev}E''$ (z polarized). Since the fundamental in the e' vibration is observed in the A band (492 nm), this indicates substantial vibronic coupling in one of the states involved in the transition. In this band we also observe a long progression in a'_1 vibration which

indicates that the excited state probably has a large difference in internuclear distance from ground state and therefore is of somewhat different orbital character. In the 532 nm region the intensity of the e' vibration is substantially reduced with a shorter progression in the a'_1 vibration. In this case we infer that the excited and ground state will have similar character and geometry. As to the 587 nm band, it is difficult to assess its character because neither a'_1 nor e' displays much intensity in this region.

Figure V.3.1 Mass spectrum of niobium clusters from sputtering target, measured in-situ by recording the current on the Faraday plate as a function of magnetic field on the Wien filter.

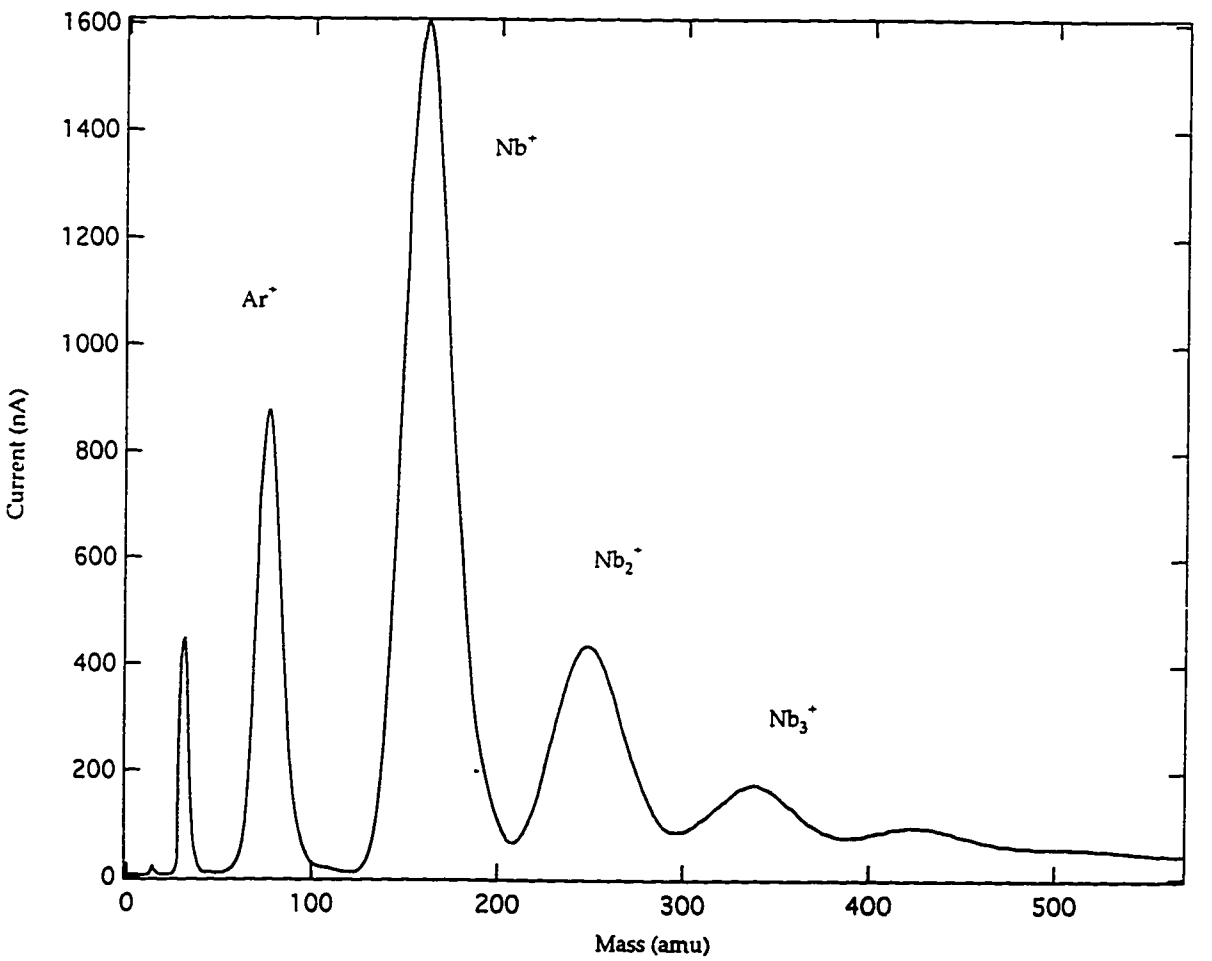

Figure V.3.2 Absorption(Scattering Depletion) spectra (left hand scale) of Nb_3 in argon matrix. Superimposed is the excitation profiles for the two fundamentals and overtone (right hand scale) for triatomic niobium in solid argon.

□: e' 227cm^{-1} (ν_2')

o : a_1'335cm^{-1} (ν_1')

Δ : 2a_1'670cm^{-1} (2ν_1')

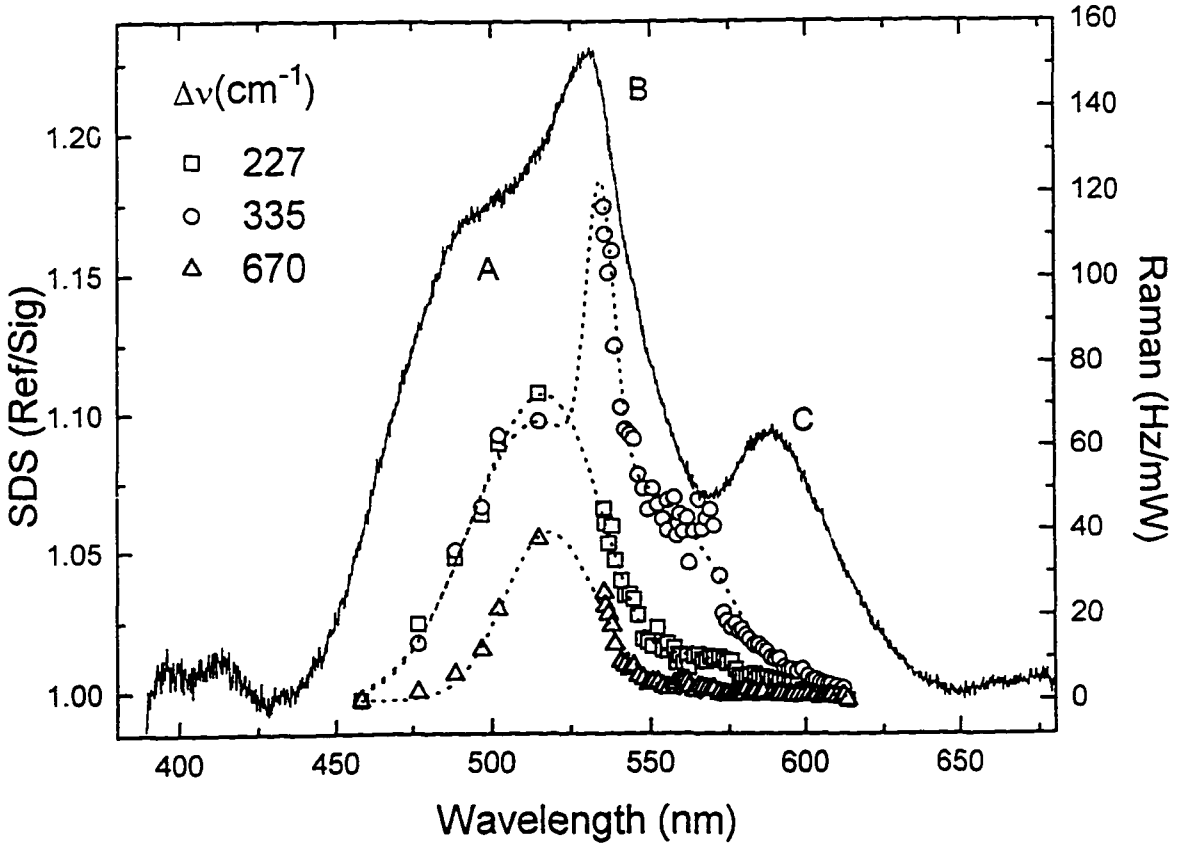

Figure V.3.3 The resonance Raman spectra of Nb_3 in argon matrix excited with (a) 514.5 nm; and (b) 588.8 nm radiation. The intensity in the latter was multiplied by a factor of five as compared to the former.

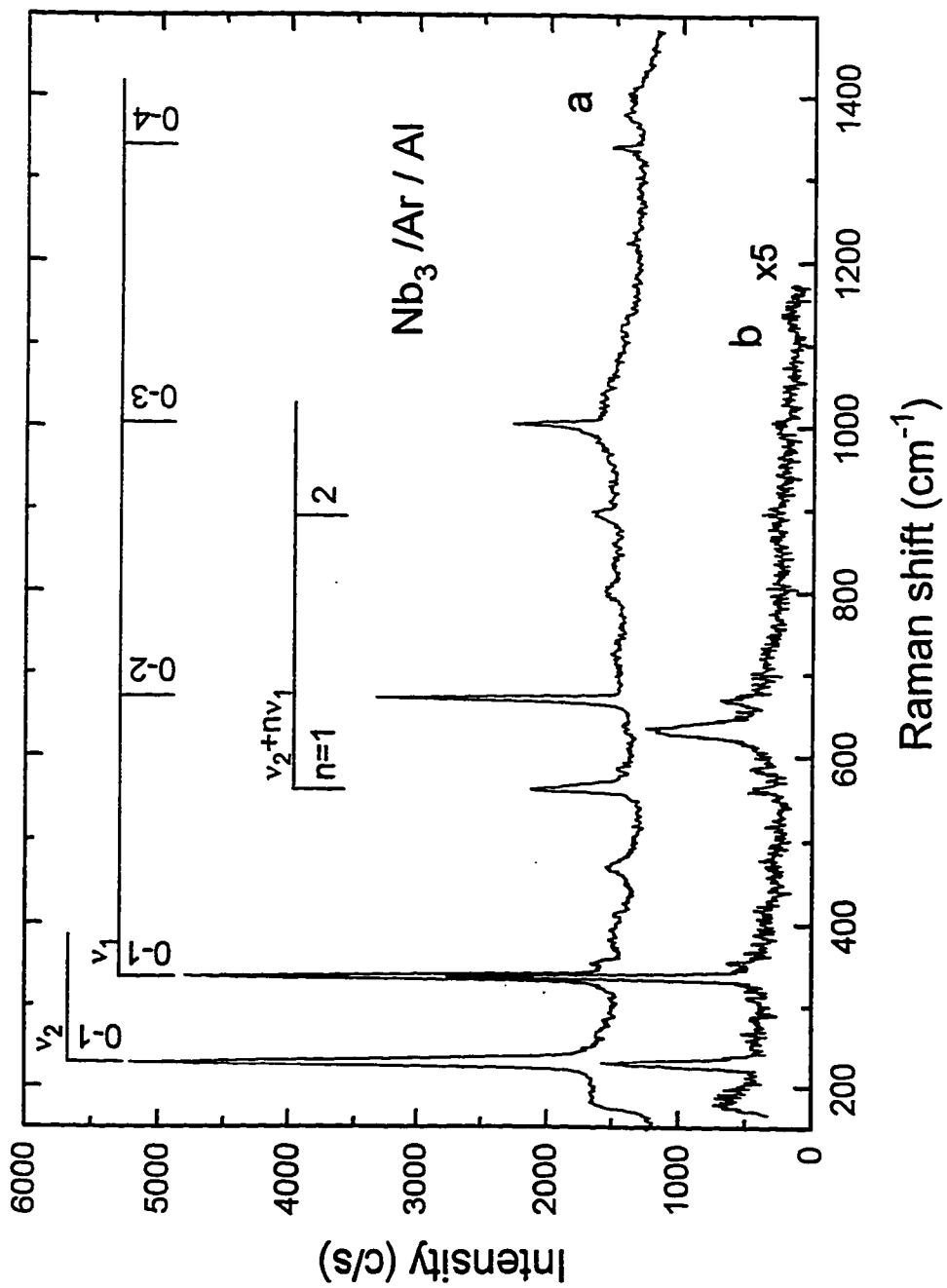

Table V.3.1 **Observed resonance Raman transition (in cm^{-1}) and assignments for the niobium trimer in argon matrix.**

band	$\nu_1(a'_1)$	$\nu_2(e')$
227.4(29)		1
334.9(28)	1	
561.1(28)	1	1
669.7(33)	2	
895.9(45)	2	1
1003.8(28)	3	
1340.6(62)	4	

CHAPTER VI. TRANSITION METAL TETRAMER

VI.1 Absorption and RAMAN spectroscopy of mass-selected tantalum tetramers in argon matrices

Huaiming Wang, Robert Craig, Hanae Haouari, Jian-Guo Dong, Zhendong Hu, Alberto Vivoni, John R. Lombardi, and D.M. Lindsay

Department of Chemistry and Center of Analysis of Structures and Interfaces (CASI), The City College of New York (CCNY), New York, New York 10031

A. Introduction

We have recently investigated the absorption and Raman spectra of a series of mass selected transition metal dimers[1-5] including that of Ta.[6] This series of papers has enabled us to fill in a large portion of the periodic table with dimer force constants[4], some of which are high. In this paper we turn our attention to one of the larger clusters, namely the tetramer of Ta. In addition to questions on the geometry of such clusters, it will also be of interest to determine the effect of bonding to multiple atoms on the magnitude of the stretching force constants.

One of the earliest tetramers to be investigated by Raman spectroscopy was that of phosphorus (P_4)[7]. This was later supplemented by an infrared spectrum[8], as well as

electron diffraction[9], and X-ray diffraction[10]. The diffraction studies, coupled with Raman data indicate that the structure of phosphorus tetramer is tetrahedral. Although no similar experimental results exist for Bi_4, by scaling the dimer force constants from phosphorus vibrational frequencies[11] have been predicted. However earlier reports of a tetramer spectrum[12] have recently been shown to arise from the trimer instead[13]. Silver tetramer have been presumed to be tetrahedral, although no Raman spectra have yet been reported. The tetramer of Si has been studied with surface enhanced Raman Spectroscopy (SERS)[15], and found instead to have a planar rhombus structure. An electron spin resonance study of matrix isolated Cr (Ref.16) indicates either a trigonally distorted tetrahedral Cr_4 or square-based pyramid Cr_5.

It is with these results in mind that we turn to the tetramer of Ta which is the subject of this work. We have been able to deposit a sufficient quantity of Ta_4 to observe several broad optical transitions in which we have excited resonance Raman spectra. These spectra are surprisingly rich, involving three vibrational fundamentals. One of the progressions has a frequency alternation which suggests a weak Jahn-Teller coupling. This result implies that the ground electronic state is degenerate, reducing the likely structural possibilities to either square planar or tetrahedral. The former may be eliminated since the expected fundamental frequencies

should be nearly equal, while for the latter we expect frequency ratios ($2:\sqrt{2}:1$) almost exactly as observed. Our conclusion is that the tetramer of Ta falls into the category of molecules which are tetrahedral in geometry at least in the ground state. We also present evidence of considerable distortions from tetrahedral geometry in the two observed excited states.

B. Experimental

The cluster deposition source located at The City College of New York has been described in previous publications[1-6]. An intense (typically 10 mA at 25 keV) argon ion beam for a "CORDIS" ion source (Rokion Ionenstrahl-Technologie, Darmstadt, Germany) sputters tantalum cluster ions from a water cooled, tantalum target (Rembar, 99.9%) maintained at about 350 V. Secondary ions were extracted with a modified Colutron model 200-B lens system and then mass selected using a Wien filter (Colutron 600-B). The cluster ion beam was then bent by 10° to prevent neutrals from reaching the deposition region, which consists of a cooled (approximately 14 K) CaF_2 substrate surrounded by a "Faraday cage." The polished substrate is mounted to a closed cycle cryostat (APD Displex, 204SL/DMX-6) and temperatures are measured with a Si diode in conjunction with a Scientific Instruments model 5500 temperature controller. Tantalum cluster ions were co-

deposited with Ar gas from a coaxial injector ring (99.9998% Ar, Matheson) and low energy electrons (for neutralization) from a tungsten filament. Matrices were grown at 4μ/h with an argon:metal dilution ratio of 8000:1, to ensure that clusters remain isolated both from each other and any impurity species. Ion currents are measured by using a Faraday plate situated perpendicular to the CaF_2 substrate. The difference in voltage (V_{dep}) between the target and Faraday cage determines the metal cluster deposition energy (eV_{dep}), which was held at approximately 10 eV in the experiments described here. Under these "soft-landing" conditions, measured ion currents were 23 nA for Ta^+, 35 nA for Ta_2^+, 13 nA for Ta_3^+, and 23 nA for Ta_4^+; as shown in Figure VI.1. Fragmentation may be estimated by comparing the intensities of atomic excitation features in a dimer, trimer or tetramer deposition with those obtained from depositions of the atom under similar conditions. By this measure, we may estimate the fragmentation of tantalum tetramers to be less than 0.5 %. The fragmentation of tantalum dimer[6] was also less than 0.5%.

Matrix samples were interrogated *in situ* using both absorption and Raman spectroscopy, and (in the case of atomic tantalum) excitation spectroscopy. For both the absorption and excitation spectra, we employed a broad band (deuterium or tungsten) light source dispersed by a 1/4 m monochromator (calibrated with Hg lamp), and then focused

onto the matrix sample. Absorption (and atomic excitation) spectra were recorded by observing the light scattered at right angles to the matrix surface. This technique (which we term "scattering depletion spectroscopy"{SDS}) has been shown to be equivalent to the absorption spectrum, but with slightly improved sensitivity for our apparatus

Raman and fluorescence spectra were recorded using an argon ion laser (Spectra Physics model 2045) pumping either a dye laser (Coherent CR 599, with rhodamine 6G or DCM as dyes) or a titanium sapphire (TiS) laser (Lexel model 479). Typical fluences were 25-50 mW focused down to an estimated 50 μ spot size. The exciting laser line was actually predispersed with a grating in order to minimize fluorescence from the dye or TiS crystal. Light scattered at 90° was collected in a SPEX Triplemate Spectrometer and detected with a SPEX model "Spectrum One" CCD detector, and DM1000 series software.

C. Analysis

The optical absorption (SDS) spectrum of Ta tetramer is shown in Figure.VI.2 Only two broad transitions were observed, one (marked A) centered at 768 nm, and shaded slightly to the blue, and a second (B) more symmetrical peak at 532 nm. The red transition displays weak structures with features at 13,020 cm^{-1}, 13,260 cm^{-1} and 13,500 cm^{-1}. The spacing of approximately 240 cm^{-1} most likely

corresponds to a vibration in the excited state. Due to the relative lack of features, it is difficult to say much as to the nature of these bands. However an analysis of the Raman resonances will give us some clues as to their origin.

Resonance Raman spectra have been obtained by exciting with a dye or TiS laser into both of the bands shown in Figure VI.2. The progressions observed by excitation into the blue band (B) were somewhat more extensive than those observed in the red band(A), but otherwise no significant differences between the spectra were obtained. We have varied the excitation wavelength extensively throughout both regions, and consequently the Raman shifts reported herein represent averages over approximately fifty separate measurements, and with several different deposited samples. Typical Raman spectra are shown in Figure VI.3 and Figure VI.4 where the excitation wavelength is 538.4 nm and 760.1 nm respectively. Also Figure VI.8 shows superimposed Raman signals at three different excitation wavelengths. Tantalum excitation profile (see Figure VI.7) was plotted so that it might help us to interpret or give us some clue as to the origin of the vibrational transitions observed in the absorption spectra. The Raman shifts observed are listed in Table VI.1 All the observed lines can be explained by assuming three fundamental frequencies. The highest frequency (ν_1) progression starts at 270.2(2) cm^{-1}. The intermediate fundamental (ν_2) occurs at 185.1(1) cm^{-1} and

this has only one overtone at 372.5(2) cm^{-1}. Note at this stage that the ratio of frequencies (ν_1/ν_2) is 1.46, very close to $\sqrt{2}$:1, as would be expected for a tetrahedral geometry[17]. Further evidence for this interpretation will be given below, in which we obtain a value for ν_3 to be 130.6(2) cm^{-1}. The ratio of (ν_2/ν_3) then is 1.42, once again close to $\sqrt{2}$:1 as expected for a tetrahedral molecule. Normal mode calculations for all other reasonable tetramer geometries indicate considerable deviations from these ratios. Normal mode calculation regarding tantalum tetramers are shown in Table VI.3.a, b and c from which we note that the percentage error between the calculated frequencies and observed ones are small. The normal mode vibrations of tetrahedral molecules are illustrated in Figure VI.9. If the geometry is indeed tetrahedral we may assign ν_1 to the totally symmetric a_1 vibration (in T_d), ν_2 to the triply degenerate t vibration and ν_3 to the doubly degenerate e vibration.

The third and lowest progression starts at 134.5(2) cm^{-1} for which a rather long progression up to ν = 8 is observed for excitation in the blue absorption. All the other bands observed in the spectrum involve combinations of the two highest progressions with this lowest progression. The lowest progression actually displays an alternation of frequency separations between 135 cm^{-1} and 126 cm^{-1} with a corresponding alternation in intensities see Figure VI.5. This is characteristic of a weak Jahn-Teller interaction,

which would again indicate a high degree of symmetry for the molecule. Since this alternation occurs in an e vibration, we must first consider whether the coupling is with an E or T electronic state. For T⊗e coupling, no splittings are expected. All levels are merely shifted by a constant amount[18]. Thus it is most likely that the ground state is of E electronic symmetry. For a weak E⊗e Jahn-Teller coupling we expect the vibronic energy levels to be governed by the formula[17]:

$$E_{nlj} = \omega_e \{ n + 1 + 2 \lambda (l^2 - j^2 - 3/4)\}$$

where n is the principal vibrational quantum number (n=0,1,2,3,...) while l is the vibrational angular momentum (l = n, n-2,...,-n+2,-n), and j is the total vibronic angular momentum (j = l ± 1/2). For a particular n the (2n+1)-fold degeneracy is split into n+1 levels, one for each value of l. A two-fold degeneracy remains since the energy is independent of the sign of j. The parameter λ is the Jahn-Teller coupling parameter. Since j is a good quantum number we expect the selection rules Δj= 0 to hold. The vibrational angular momentum quantum number l is not strictly a good quantum number, but in the case of weak coupling we expect Δl=0 to be the most intense transitions with Δl=±1 to be somewhat weaker. This explains the intensity alternation observed. For the lowest state (n,l,j) = (0,0,1/2) we expect transitions to states with

j=1/2, and alternating values of l = 0 (for n even) and 1 (for n odd). The transitions are shown in Figure VI.6 and Figure VI.10. Thus the expected Raman frequencies for transitions to states (n,0 or 1,1/2) are

$$\omega_{nlj} = \omega_e \{ n + \lambda (1 - (-1)^n \}$$

Analysis of the frequencies observed gives a best fit for ω_e = 130.6(2) cm^{-1} and λ =0.017(2). The relatively small value for the latter parameter, which is the dimensioneless vibronic constant, justifies the weak coupling assumption. It also indicates that any geometrical distortion from tetrahedral geometry will be slight.

Thus the resonance Raman spectra of the Ta tetramer indicates that the ground state is of a tetrahedral geometry with an electronic E symmetry. There is weak Jahn-Teller coupling with the e vibration. Our spectra give no information as to the possible spin degeneracy. In fact, for the third row transition elements, we should expect such strong spin-orbit coupling to entirely quench any Jahn-Teller effect. Our value of the Jahn-Teller effect coupling parameter is, of course, extremely small, indicating that spin-orbit quenching is not complete in this case, or that the spin degeneracy is singlet.

As for the nature of the two excited electronic states observed, first it should be noted that electronic transitions from an E state are allowed only to vibronic T

states. Thus a possible interpretation of the 240 cm^{-1} progression observed in the red band is that it is of T vibronic symmetry. This could arise from a T electronic state coupled with an a_1 vibration, slightly less than the 270 cm^{-1} spacing of the a_1 vibration in the ground state. However, this interpretation does not explain why Raman transitions are seen to vibrations of all three symmetries in the ground state. It is usually stated[17] that for resonance Raman spectroscopy, transitions to totally symmetric vibrations are expected to dominate. In fact this statement should be modified since it holds only when vibronic coupling is weak in both states involved. When, for instance, the ground state is vibronically non-totally symmetric, we should say instead that resonance Raman transitions are allowed to those states for which there is *no overall change* in vibronic symmetry. Thus in the present case we would expect (in the absence of severe excited state distortions) to see only e vibrations, since the ground state is vibronically E. Furthermore, if there is strong vibronic mixing in the excited state, so that for example the symmetry is lowered, then transitions are allowed to those totally symmetric states (or states having the same symmetry as the ground state) using the irreducible representations of the point group of the state of lower symmetry. The net result would be transitions to several if not all ground state symmetry species. Here we observe vibrations of all symmetries with intensities

roughly of the same order of magnitude. Thus if the progression in the red band were indeed from the totally symmetric a_1 vibration, we would not see Raman transitions to all tetrahedral normal modes. Rather it is more likely that the excited state involved is severely Jahn-Teller distorted. This distortion may stem from strong coupling of a T electronic state with both the t (and possibly e) vibrations. This coupling results for example in Txt = A_1+E+T vibronic states. States with symmetry of A_1 and T resolve to totally symmetric vibrations in species of lower symmetry. For strong coupling in the excited states, we then would expect resonance Raman transitions to a_1 and t ground state vibrations as well as the e vibrations noted above.

D. Discussion

We have shown that the tetramer of Ta falls in the category of tetrahedral molecules, along with P_4. With the latter molecule, the ratios of observed ground state fundamentals deviates considerably from the ratios $2:\sqrt{2}:1$ expected[17] in the case of a central force field. However, electron and X-ray scattering data indicate these molecules are indeed tetrahedral, so that the assumption of central forces must be called into question. In order to properly fit the observed frequencies it is necessary to introduce off diagonal elements into the force constant matrix on the

order of 10% of the diagonal constants. These represent bond-bond interactions. The tantalum spectra comes a lot closer to the ratios predicted by a central force model. However even in this case an accurate fit to the observed frequencies also requires addition of an off-diagonal stretch-stretch interaction constant to the force constant matrix. In Table VI.3.a, b and c is shown the calculated frequencies from normal mode calculations.

The rather large magnitude of the tantalum dimer force constant (4.80 mdyne/Å) indicates a large contribution of d-orbital character to the chemical bond. This is consistent with other third row transition dimers which have been observed. However, for the tetramer we expect due to the fact that each atom is bonded to three others, the bond-bond stretching force constant will be considerably decreased. In Table VI.2 we compare the dimer and tetramer force constants for several tetramers for which experimental data exists.

Note in all cases the reduction factor is 2 to 3. These may be compared to the scheme proposed by Ozin and MacIntosh[14]. They propose that the reduction in force constant should be proportional to the increased number of bonds each atom is involved with. For tetrahedral geometries they expect a reduction of 1/3 on going from dimers to tetramers. This slightly underestimates the tetramer force constant in all three cases. For the planar rhombus of Si there are two types of bonds, on the edge and across the short diagonal.

A good fit to the experimentally observed frequencies is obtained with both being nearly equal. The predicted constant for the diagonal bond is slightly lower while that for the edge bonds is slightly higher. In fact the predictions are all remarkably close, and we certainly consider this scheme to provide an excellent predictor of spectra. The slightly higher force constants observed could possibly be caused by slight decreases in bond lengths, and/or consequent increases in d-orbital participation in bonding on going from dimer to tetramer. In any case the results presented here should provide as sensitive test of theoretical investigations of third row transition metal wave functions.

ACKNOWLEDGMENTS

We wish to thank Dr. Krishnan Raghavachari for a helpful discussion of the Si_4 spectrum. This work was supported by the National Science Foundation under Cooperative Agreement No. RII-9353488 and Grant No. CHE-9412804 and by the City University of New York PSC-BHE Faculty Research Award Program.

Table VI.1. Observed resonance Raman transitions (in cm^{-1}) and assignments for the tetramer of tantalum.

Band	$\nu_3(e)$	$\nu_2(t)$	$\nu_1(a_1)$
134.5(2)	1		
185.1(1)		1	
260.1(1)	2		
270.2(2)			1
372.5(2)		2	
395.5(1)	3		
447.4(1)	2	1	
521.6(1)	4		
530.9(1)	2		1
581.8(1)	3	1	
656.9(1)	5		
709.0(2)	4	1	
783.6(1)	6		
791.5(1)	4		1
918.2(1)	7		
970.8(1)	6	1	
1045.0(1)	8		
1052.4(1)	6		1
1232.4(1)	8	1	

Table VI.2 Comparison of force constants (mdyne/Å) for dimers and tetramers of several species. P and Ta tetramers are tetrahedral, while Si is a planar rhombus. These are compared with those predicted by utilization of the force field of Ozin and MacIntosh[13].

Element	Dimer force constant	Tetramer force constants	
		Observed	Predicted(Ref.13)
P	5.56	2.07	1.85
Ta	4.80	1.89	1.60
Si(planar)	4.65	1.65	1.86(edge)
		1.65	1.55(diagonal)

Figure VI.1 Mass spectrum of Ta clusters from sputtering target, measured in-situ by recording the current on the Faraday plate as a function of magnetic field on the Wien filter.

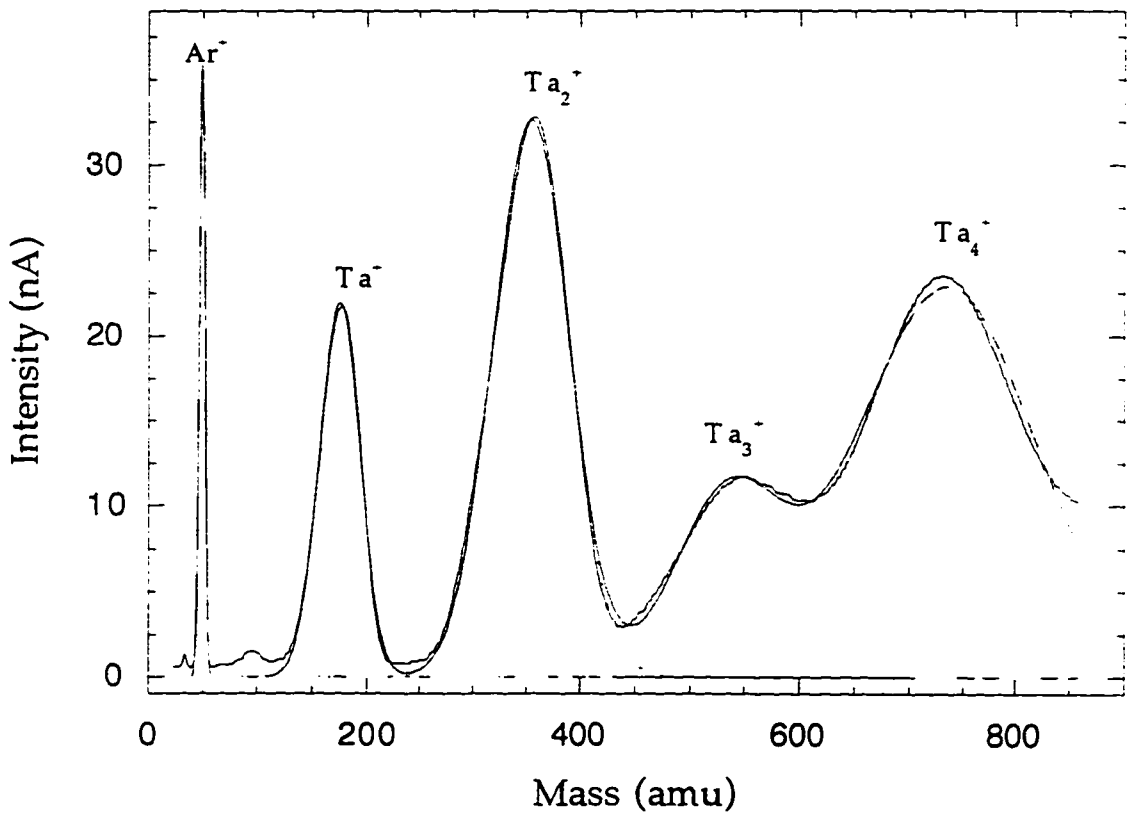

Figure VI.2 Absorption (SDS) spectrum of tantalum tetramer in Ar matrix at 14K.

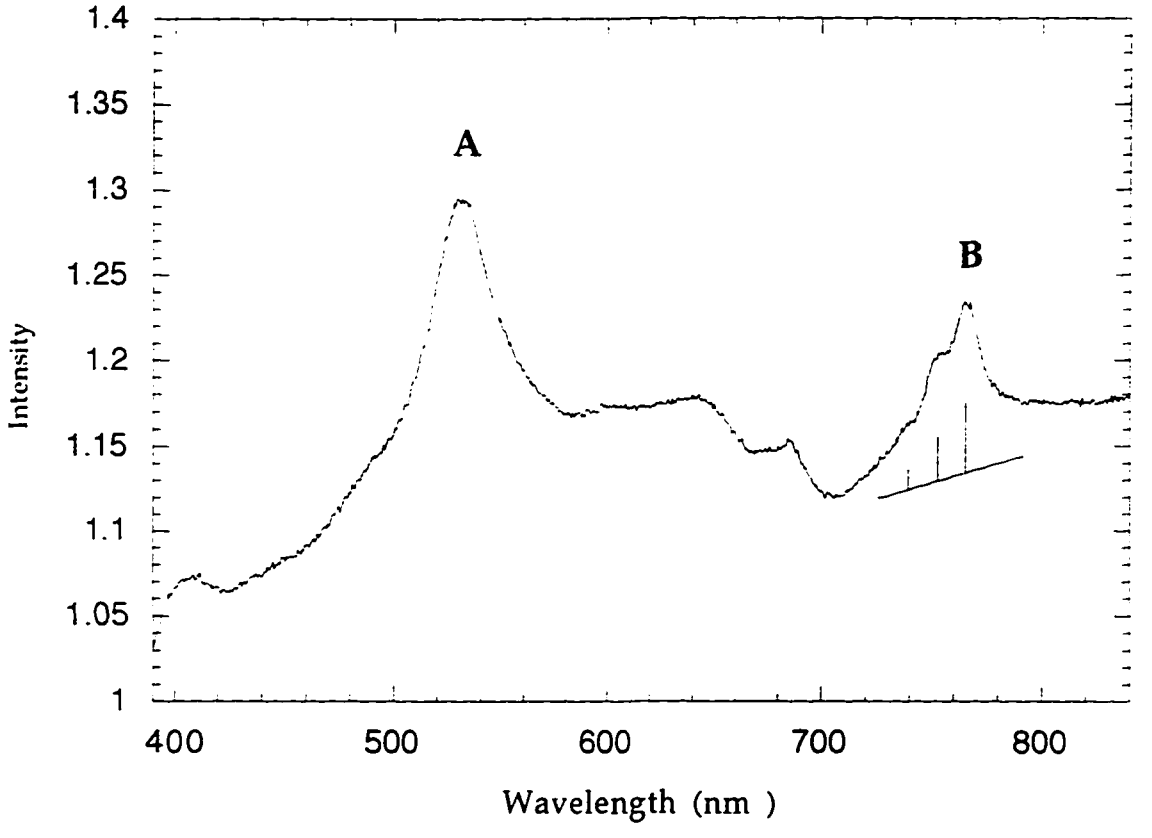

Figure VI.3 Resonance Raman spectrum of tantalum tetramer exciting at 538.4 nm .

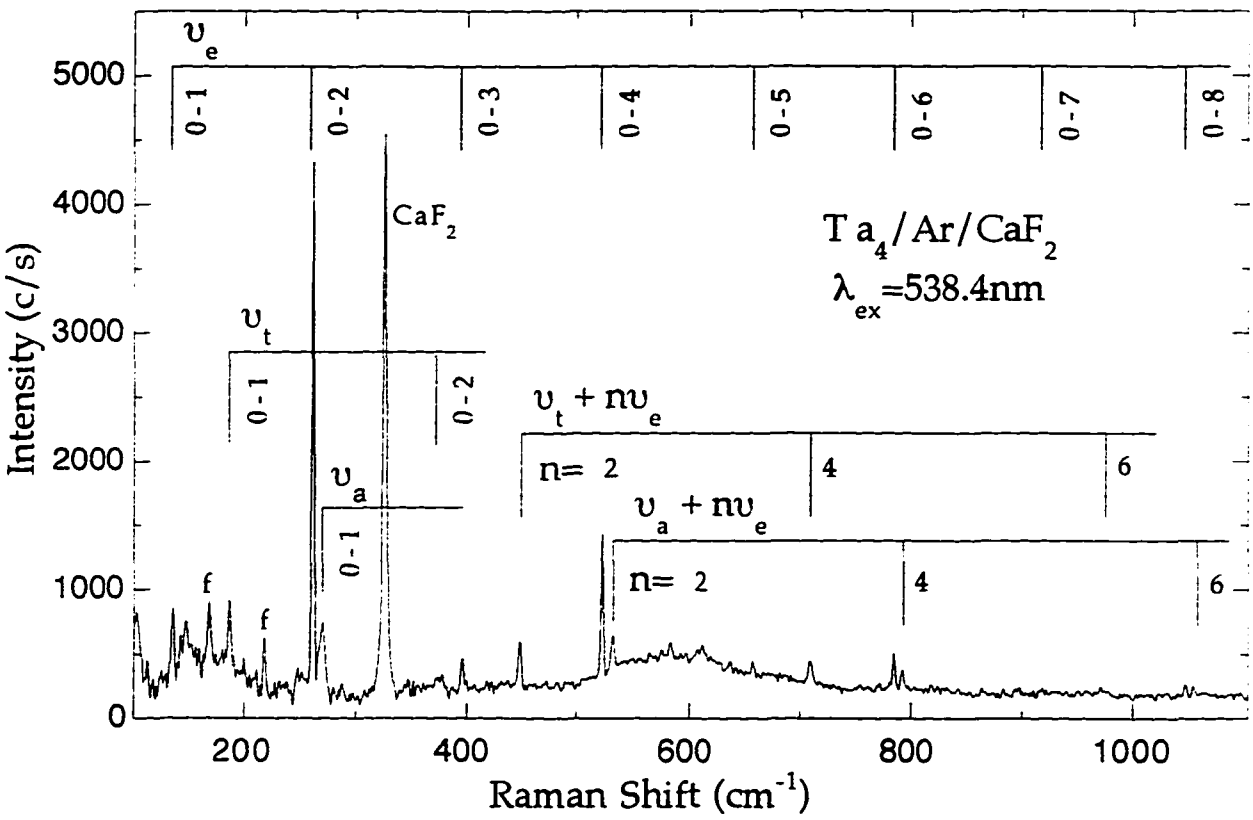

Figure VI.4 Resonance Raman spectrum of tantalum tetramer exciting at 760.1 nm

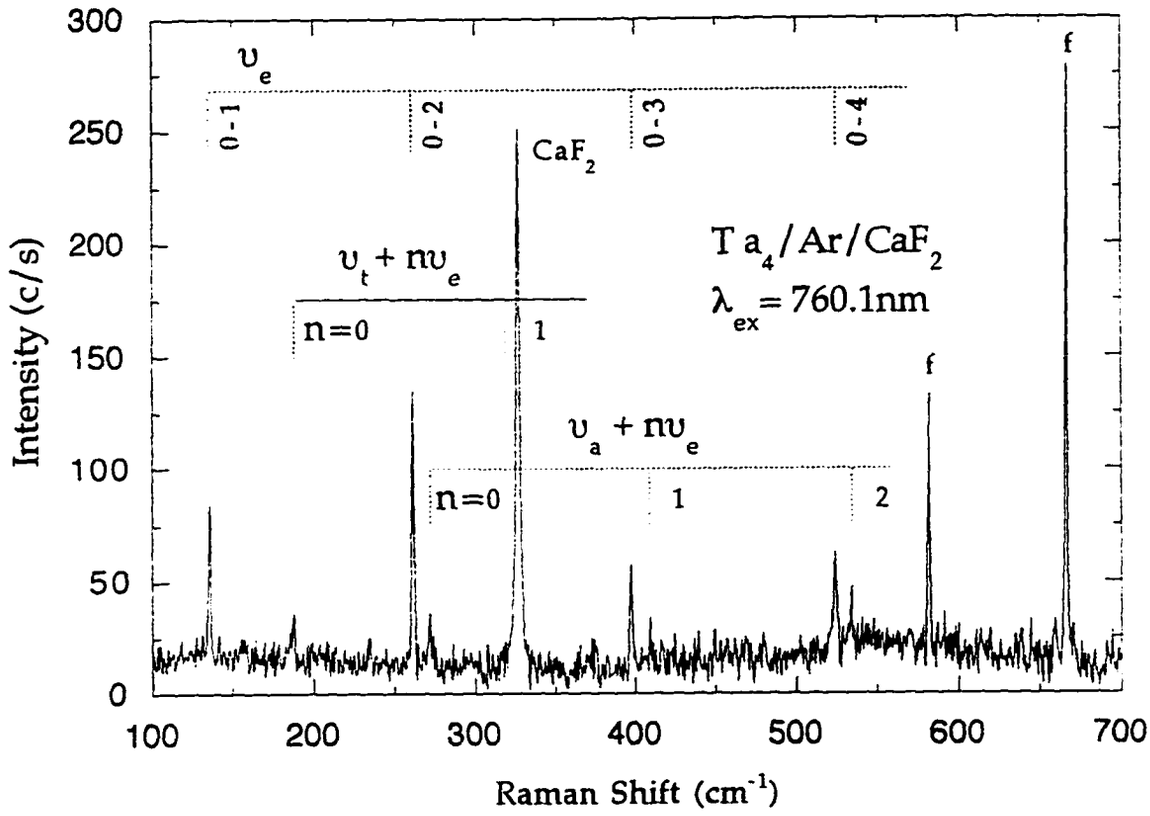

Figure VI.5 Alternating Raman shift in Ta4 (165 nA-h, λ_{ex}=538.44 nm, E symmetry).

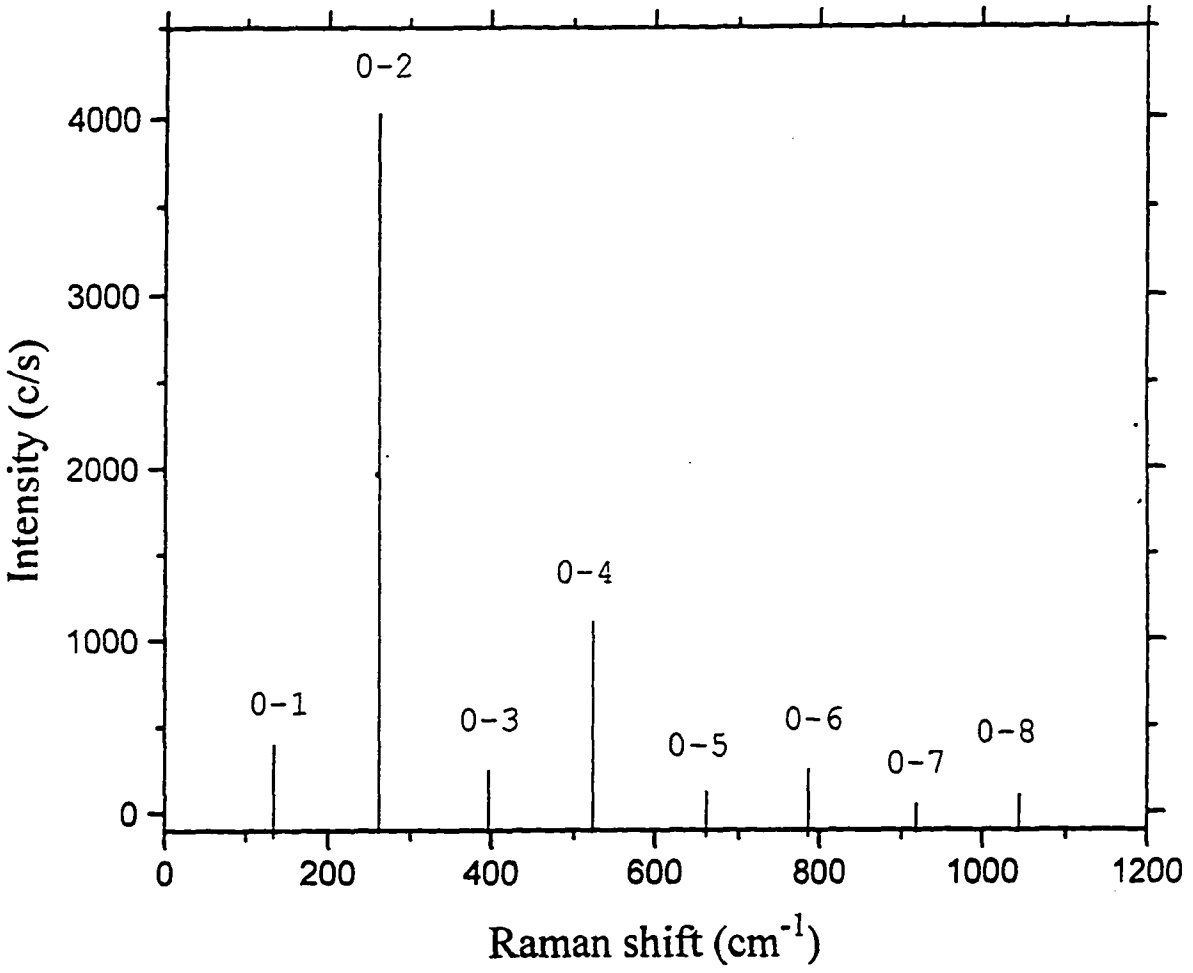

Figure VI.6 Vibronic transitions of Ta_4. Showing E⊗e coupling and Jahn-Teller splitting.

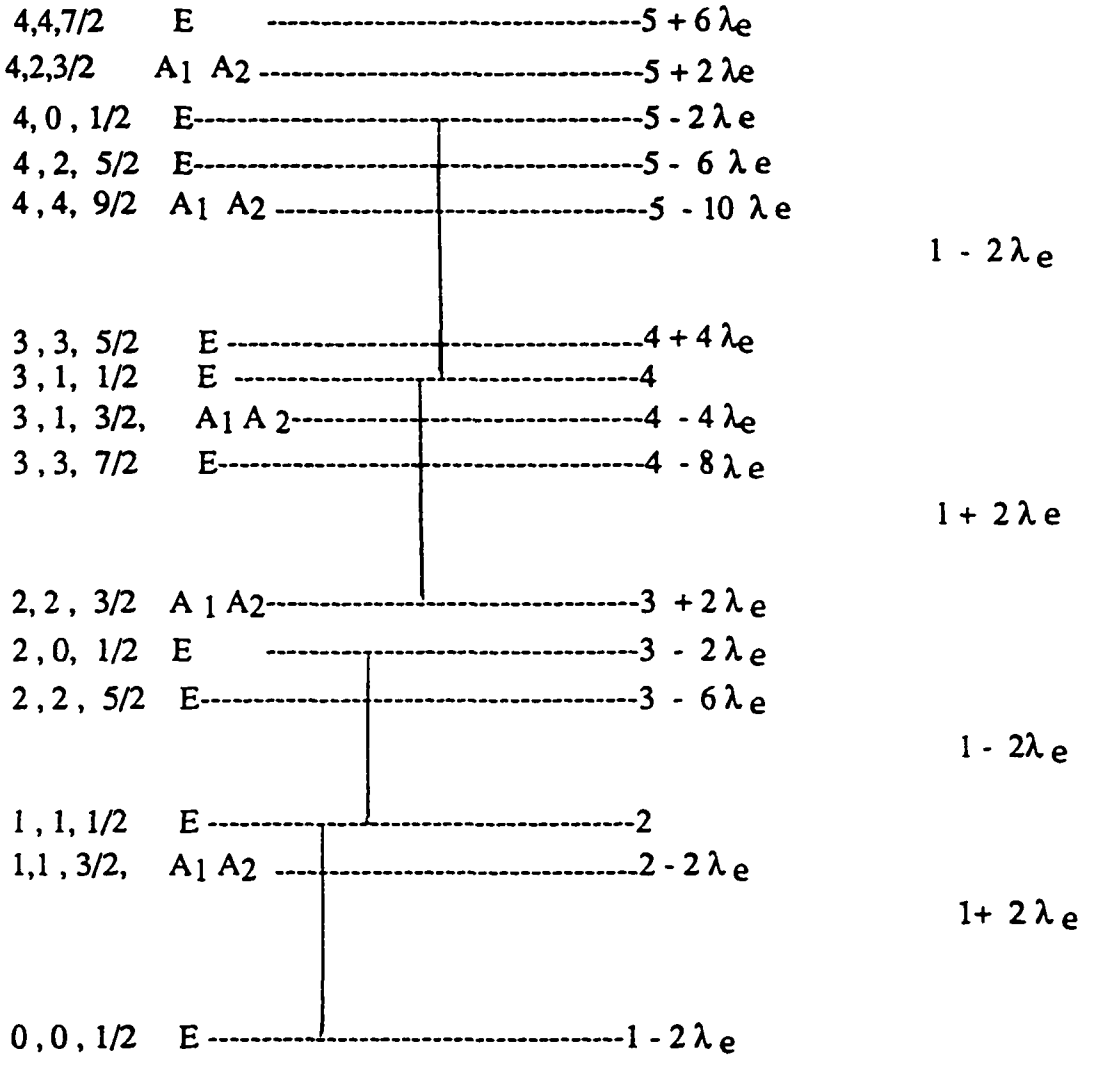

λ_e : splitting coefficient

ω_e = 130.63375 cm^{-1}, Transition to j= 1/2 states.

Hence if $\omega_e \lambda_e = 1/4 * 10\ cm^{-1} = 2.5\ cm^{-1}$, $\lambda_e = 0.017$

Figure VI.7 Ta_4 **Raman excitation profile** (λ_{ex} **=738-780 nm).**

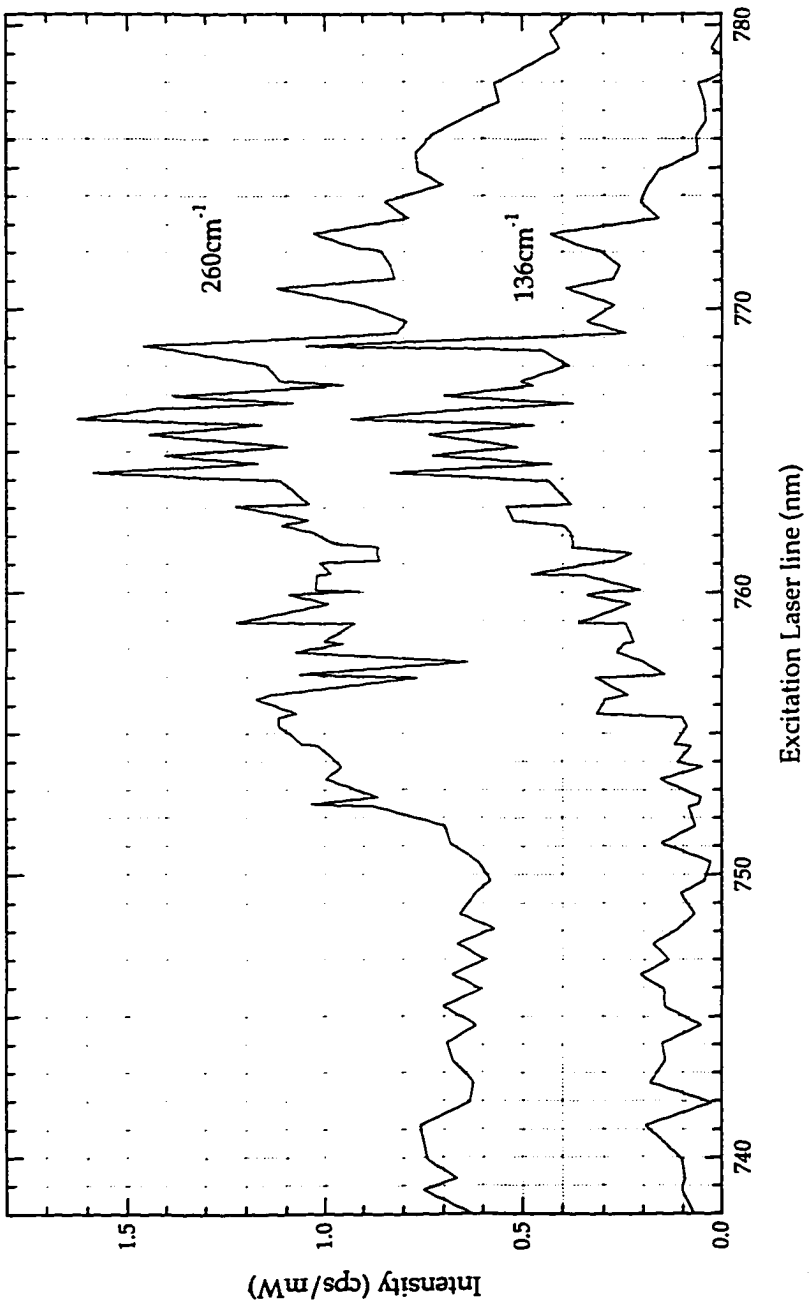

Figure VI.8 Superimposed Raman signales of Ta_4 (108nA-h). A(λ_{ex}= 541.22 nm); B(λ_{ex}= 539.60nm); C(λ_{ex}=538.32 nm).

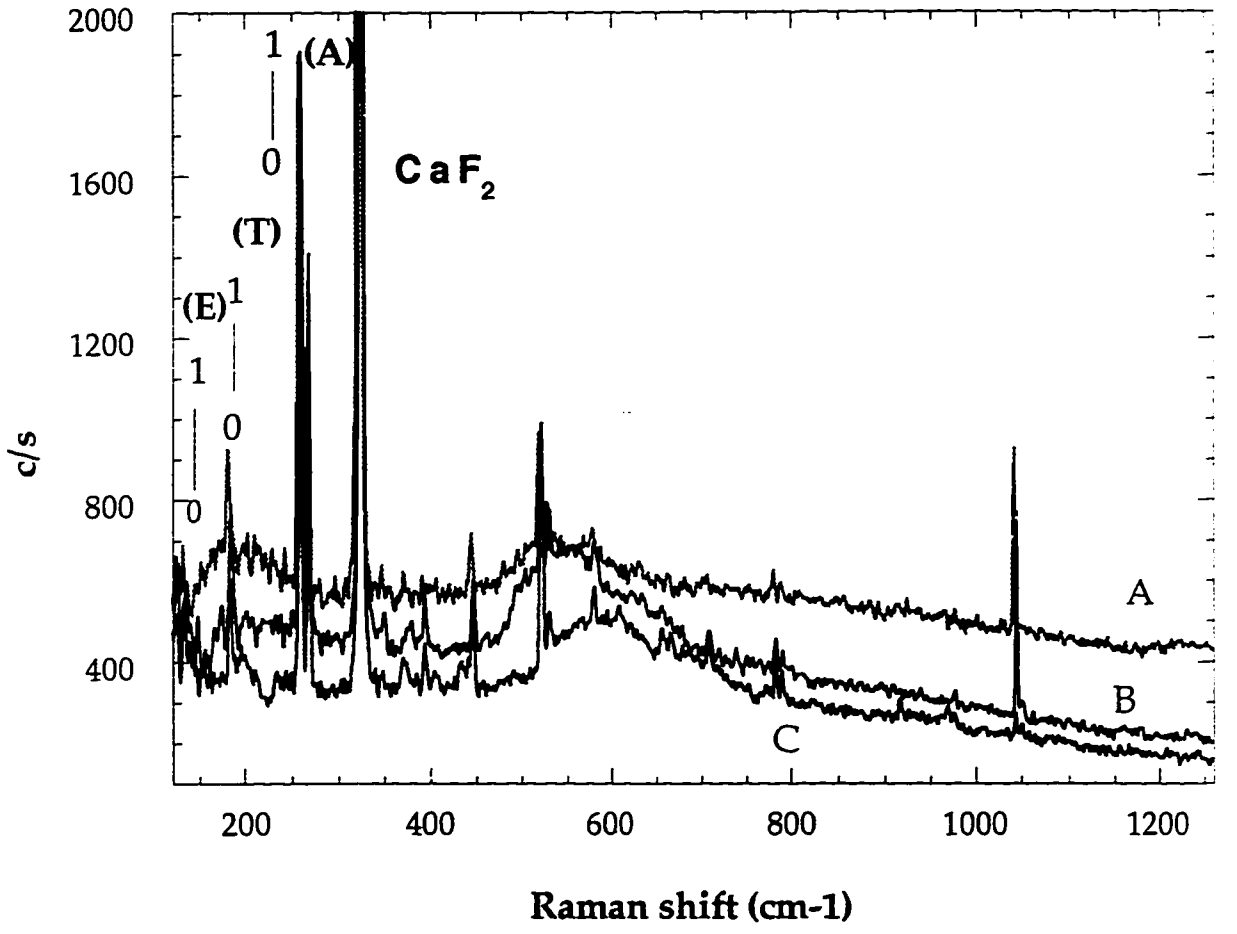

Figure VI.9 Normal vibration of a tetrahedral XY_3 molecules. The three two-fold axes(dot-dashed lines) are chosen as x, y and z axes.(Ref.17).

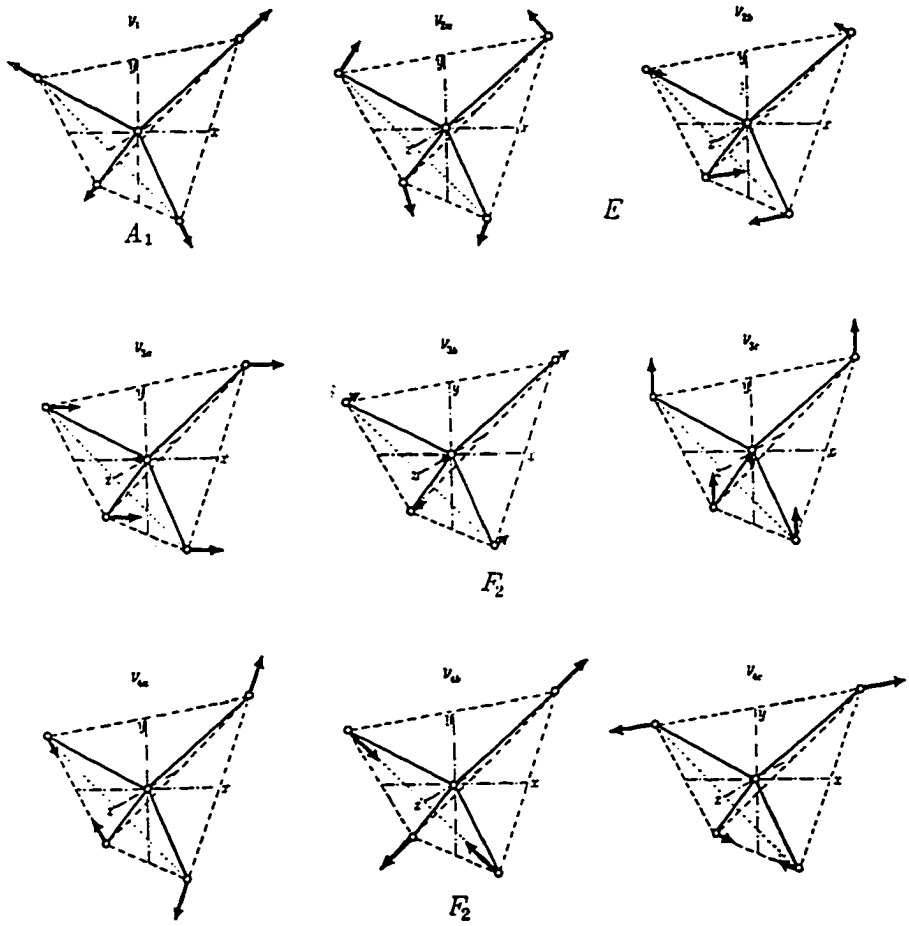

Figure VI.10 Detailed illustration of the cross-section of the adiabatic potential for the linear E-e problem in the case of weak vibronic coupling ($\lambda = 0.017$) with indication of the quantum numbers n,l,m positions of vibrational levels without vibronic coupling are shown by dashed lines.(Ref.18).(m=j)

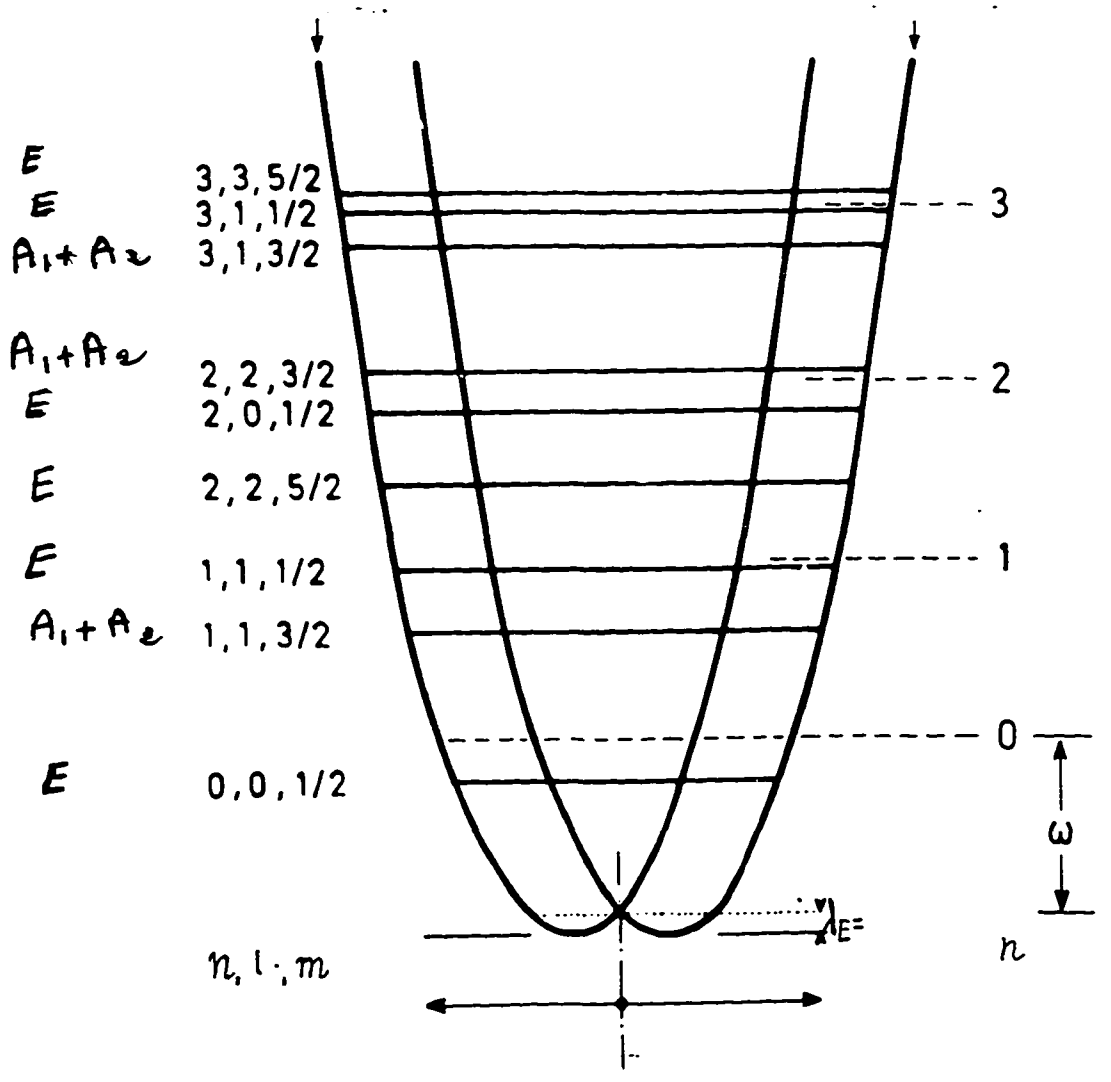

Table VI.3.a Normal mode calculations (Observed and calculated frequencies).

1	1.0000	K(1-2)
2	1.0000	K(1-3)
3	1.0000	K(1-4)
4	1.0000	K(2-3)
5	1.0000	K(2-4)
6	1.0000	K(3-4)

	Observed frequency (cm^{-1})	Calculated frequnecy (cm^{-1})	Diffrence (cm^{-1})	% error	EV
1	269	260.6	9.2	3.398	2.000
2	185.0	184.3	0.7	0.381	1.414
3	185	184.3	0.7	0.381	1.414
4	185	184.3	0.7	0.382	1.414
5	130.6	130.3	0.3	0.217	1.000
6	130.6	130.3	0.3	0.218	1.000

Average error= 2.0cm^{-1} or 0.83 percent

Table VI.3.b Normal mode calculations (potential energy distribution).

Observed frequency=269.8cm^{-1} Calculated frequency=260.6cm^{-1}

Assignment: a (totally symmetric mode)

16.67 Force constant # 1 K(1-2)

16.67 Force constant # 2 K(1-3)

16.67 Force constant # 3 K(1-4)

16.67 Force constant # 4 K(2-3)

16.67 Force constant # 5 K(2-4)

16.67 Force constant # 6 K(3-4)

Observed frequency=185.0cm^{-1} Calculated frequency=184.3cm^{-1}

Assignment: t(triple degenerate mode)

25.00 Force constant # 2 K(1-3)

25.00 Force constant # 3 K(1-4)

25.00 Force constant # 4 K(2-3)

25.00 Force constant # 5 K(2-4)

Observed frequency=185.0cm^{-1} Calculated frequency=184.3cm^{-1}

Assignment: t(triple degenerate mode)

50.00 Force constant # 1 K(1-2)

50.00 Force constant # 6 K(3-4)

Observed frequency=185.0cm^{-1} Calculated frequency=184.3cm^{-1}

Assignment: t(triple degenerate mode)

25.00 Force constant # 2 K(1-3)

25.00 Force constant # 3 K(1-4)

25.00 Force constant # 4 K(2-3)

25.00 Force constant # 5 K(2-4)

Table VI.3.c Normal mode calculations (potential energy distribution).

Observed frequency=130.6cm^{-1} Calculated frequency=130.3cm^{-1}

Assignment e(double degenerate mode)

25.00	Force constant #	2	K(1-3)
25.00	Force constant #	3	K(1-4)
25.00	Force constant #	4	K(2-3)
25.00	Force constant #	5	K(2-4)

Observed frequency=130.6cm^{-1} Calculated frequency=130.3cm^{-1}

Assignment e(double degenerate mode)

33.33	Force constant #	1	K(1-2)
8.33	Force constant #	2	K(1-3)
8.33	Force constant #	3	K(1-4)
8.33	Force constant #	4	K(2-3)
8.33	Force constant #	5	K(2-4)
33.33	Force constant #	6	K(3-4)

BIBLIOGRAPHY

CHAPTER I. INTRODUCTION

1.1 Spectroscopy of metal clusters

1. Thirteenth International School , Erice, Sicily (1987)See: Elemental and Molecular Clusters, ed. by G.Benedek et al. (Springer-Verlag, New York, 1988).

2. Fifth International Meeting on small Particles and Metal clusters, Konstanz, Germany, 1990. See: Zeits.Phys. **D19**, (1991); Sixth International Meeting on small particles and Metal clusters, Chicago, Illinois, 1992. See: Zeits.Phys.**D26**,(1993).

3. International Symposium on the Physics and Chemistry of small Clusters, NATO Advanced Workshop, Richmond, Virginia (1991).See: Physics and Chemistry of finite Systems :From Clusters to Crystals, edited by P.Jena and S.N.Khanna and B.K.Rao (Kluwer, Dordrecht, 1992).

4. Symposium on Clusters and Clusters Assembled Materials, Materials Research Society Meeting, Boston (1990). see: MRS Symposium Series **206**,(1991).

5. First International Conference on Nuclear and Atomic Clusters Turku, Finland (1991); Second International Conference on Nuclear and Atomic Clusters, Santoroni, Greece (1993).

6. Transition Metal Molecules, W.Weltner and R.J.Van Zee,Ann. Rev. Phys.Chem.**35**,291(1984).

7. Clusters of transition-Metal Atoms, M.D.Morse, Chem. rev.**86**,1049(1986).

8. Metal clusters, Edited by M. Moskovits (Wiley, New York,1986).

9. Spectroscopy and Dynamics, edited by M.A. Duncan, Advances in metal and semiconductor Clusters (JAI press,Greenwich CT,1992).

10. L.A.Heimbrook, M.Rasanen, and V.E.Bondybey,J.Phys. Chem.**91**,2468(1986).

11. V.E.Bondybey and J.H.English, J.Chem.Phys.**76**,2165 (1982).

12. T.G.Dietz,M.A.Duncan,D.E.Powers,and R.E.Smalley, J.Chem.Phys.**74**,6511(1981).

13. R.E.Smalley,Laser Chem.**12**,167(1983);D.E.Powers,S.G. Hansen,M.E.Geusic,D.L.Michalopoulos, and R.E.Smalley, J.Chem.Phys.**78**,2866(1982).

14. W.C.Wiley and I.H.McLaren,the Review of Scientific Instruments **26**,1150(1955).

15. Z.Fu, G.W.Lemire, Y.M.Hamrick, S.Taylor, J-C. Shui and M.Morse, J.Chem.phys.**88**,3524(1988).

16. K.LaiHing, P.Y.Cheng and M.A.Duncan, Z,Phys.**D13**, 161 (1989). Tsugio Okazaki, Yahachi Saito, Atsuo Kasuya and Yuichiro Nishina,J.chem.Phys.**104**,812 (1995).

17. C.Cossé,M.Fouassier,T.Mejean,M.Tranquille,D.P.Dilella, and M.Moskovits, J.Chem.Phys.**73**,6076(1980);

M.Moskovits and D.P.Dillela,ibid.**73**,4917(1980); W.E.Klotzbücher and G.A.Ozin,Inorg.Chem.**19**,2484 (1980).

18. W.E.Klotzbücher and G.A.Ozin,J.Am.Chem.Soc.**100**,2262 (1978);M.Moskovits and J.E.Hulse,J.Chem.Phys.**67**, 4271(1977);W.Schulze,H.U.Becker,and H.Abe,Chem. Phys.35,**177**(1978).

19. Optical Properties of molecules in Matrices, Mixed Crystals and Glasses (American Elsevier, New York,1971).

20. A. M . Bass and H.P. Broida, Formation and Trapping of Free Radicals (Academic, New York, 1960).

21. Angew,Chem.Int.Ed. Eng.**22**, 674(1983).

22. Z.Hu, B.Shen, Q.Zhou, S.Deosaran, J.R.Lombardi, D.M.Lindsay, and W.Harbich, J.Chem.Phys.**95**, 2206(1991).

23. Z.Hu, B.Shen, Q.Zhou, S.Deosaran, J.R.Lombardi, and D.M. Lindsay, Proc.SPIE 1599, **65**(1992).

24. Z.Hu, Q.Zhou, J.R.Lombardi, and D. M. Lindsay, in Physics and Chemistry of Finite Systems: From Clusters to Crystals, edited by P.Jena, S.N. Khanna, and B.K Rao (Kluwer Academic, Dordrecht, 1992), p. 969.

25. Z.Hu, J-G.Dong,J.R.Lombardi, and D.M.Lindsay, J.Phys.Chem.**97**,9263(1993).

26. Z.hu, J-G.Dong,J.R.Lombardi, and D.M.Lindsay , J.Chem.phys,**97**,8811(1992).

27. Z.Hu, B.shen, J.R.Lombardi and D.M.Lindsay,J.Chem. Phys.**96**,8757(1992).

28. J-G.Dong, Z.Hu , R.Craig, J.R.Lombardi and D.M.Lindsay,J.Chem.Phys.**101**,9280 (1994).

29. Z.Hu, J-G.Dong,J.R.Lombardi and D.M. Lindsay,J.Chem. Phys.**101**,95(1994).

30. D.M.Lindsay, F,Meyer, and W.Harbich, Z.Phys.D-Atoms, Molecules and Clusters **12**,15(1989).

31. W.Harbich, S.Fedrigo, J.Buttet, and D.M.lindsay , Z.Phys. D-Atoms, Molecules and Clusters **19**,157 (1991).

32. D.A.Garland and D.M.Lindsay, J.Chem.Phys.**80**,4761 (1984).

33. D.A.Garland, and D.M.Lindsay,J.Chem.Phys.**78**,2813 (1983).

34. D.M.Lindsay, D.Garland, F.Tischler, and G.A.Thompson, Am.Chem.Soc.Sym.ser. **179**, Chapter 7, 69(1982).

35. G.A.Thompson, F.Tischler, D.Garland and D.M.Lindsay, Sur.Sci.**106**,408(1981).

36. M.D.Morse, J.B. Hopkins, P.R.R Langridge-Smith, R,E. Smalley:J.chem.Phys.**79**,5316(1983);E.A Rohlfing, J.J.Valentini:Chem.Phys.Lett.**126**, 113(1986); W.H Crumley:J.S.Hayden, J.L.Gole,J.Chem.phys.**84**,5250 (1986).

37. J.R.Woodward, S.H.Cobb and J.L. Gole:J.Chem.Phys.**92**, 1404(1988).

38. P.Y.Cheng, M.A.Duncan:Chem.Phys.Let.**152**,341(1988).

39. M.F.Jarrold, K.M.Kreegan:Chem.Phys.Lett.**166**,116 (1990).

40. K.Balasubramanian,K.K.Das:J.chem.Phys.**94**,2923 (1991).

41. M.Moskovits and J.E.Hulse:J.Chem.Phys.**66**,3988(1977) ;M.Moskovits, J.E.Hulse, J.Chem.Phys.**67**,4271(1977); W.EKlotzbücher and G.A.Ozin, J.Amer.Chem.Soc.**100**,2262 (1978); S.A.Mitchell, G.A.Ozin: J.Amer.Chem. Soc.**100**,6776(1978);G.A.Ozin,H.Huber,Inorg.Chem.**17**, 155 (1978); G.A.Ozin, A.Hanlan:Inorg.Chem.**18**,1781 (1979);W.Schulze, H.U.Becker, H.abe:Chem.Phys. **35**,177(1978); W.E.Klozbucher,G.A.Ozin :Inorg.Chem.**18**, 2101(1979);W.E.Klotzbucher, G.A.Ozin:Inorg.Chem.**19**, 3776(1980);S.A.Mitchell, G.A.Ozin:J.Phys.Chem.**88**, 1425 (1984).

42. W.Schulze, H.U.Becker, R.Minkwitz, K.Manzel:Chem. Phys.Lett.**55**,59(1978);D.P.Dilella, M.Moskovits: J.Chem.Phys.**72**,2267(1980); D.P.Dilella, K.V.Taylor and M.Moskovits:J.Phys.Chem.**87**,524(1983); M.Moskovits,D.P.Dilella and W.Limm:J.Chem.Phys. **80**,626(1984);M.Moskovits:Chem.Phys.Lett.**118**, 111(1985).

43. D.P.Dilella,R.H.Lipson,M.Moskovits, and K.Taylor, Proceedings of the eighth Raman Conference (Bordeaux,France,1982);Metal Bonding and Interactions

in High Temperature Systems,edited by J.L.Gole and W.Stwalley,ACS Symposium Series No.179,1982.

44. K.Balasubramanian,J.Phys.Chem.**93**,6585(1989).

45. P.Jeffrey Hay and Willard R.Wadt,J.Chem.Phys. **82**,270(1984).

46. P.Jeffrey Hay and Willard R.Wadt,J.Chem.Phys. **82**,299(1984).

47. Charles W.Bauschlicher,Jr.and Stephen P.Walch, J.Chem.Phys.**76**,1033(1981).

48. Jean Demuynck,Marie-Madeleine Rohmer,Alain Strich, and Alain Veillard,J.Chem.Phys.**75**,3443(1981).

49. H-P.Cheng and D.E.Ellis, J.Chem.Phys.**94**,3737(1990).

50. Jan Andzelm, Elzbieta Radzio, and Dennis R.Salahub, J.Chem.Phys.**83**,4573(1985).

51. K.S.Pitzer,Acc.Chem.Res.**12**,271(1979).

52. K.Balasubramanian and K.S.Pitzer, Adv.Chem.Phys.**67**, 287(1987).

53. Gregory A.Bishea and Michael D.Morse.J.Chem.Phys.**95**, 8779(1991).

54. K.D.Bier,T.L.Haslett,A.D.Kirkwood, and M. Moskovits, J.Chem.Phys.**89**,6(1988).

55. D.P.Dilella,W.Limm,R.H.Lipson,M.Moskovits, and K.V.Taylor, J.Chem.Phys.**77**,5263(1982).

56. Martin Moskovits and Daniel P.Dilella,J.Chem.Phys. **72**,2267(1980).

57. D.P.Dilella,K.V.Taylor, and M.Moskovits,J.Phys.Chem. **87**,524(1983).

58. L.B.Knight,Jr.and R.W.Woodward,J.Chem.Phys.79,5820 (1983).

59. Kent M.Ervin,Joe Ho, and W.C.Lineberger,J.Chem.Phys **89**,4514(1988).

60. R.J.Van Zee,Y.M.Hamrick,S.Li and W.Weltner Jr.Chem. Phys.Lett.**195**,214(1992).

61. Lai-Sheng Wang,Han-Song Cheng and Jiawen Fan,J.Chem. Phys.**102**,9480(1995).

62. D.Dai and K.Balasubramanian, J.Chem.Phys.**98**,7098 (1993).

63. K.Balasubramanian, J.Chem.Phys.**91**,307(1989).

64. K.Balasubramanian and M.Z.Liao,J.Chem.Phys.**86**,5587 (1987).

65. Gordon R.Burton,Cangshan Xu, Caroline C.Arnold, and Daniel M.Neumark,J.Chem.Phys.**104**,2757(1995).

66. Hanae Haouari,Huaiming Wang, Robert Craig, John R.Lombardi,and D.M.Lindsay.J.Chem.Phys.**103**,9527 (1995).

67. Huaiming Wang, Robert Craig, Hanae Haouari,John R.Lombardi,and D.M.Lindsay,J.Chem.Phys.**105**,xxx(1996).

CHAPTER II. THEORY

II.2 The Jahn-Teller Effect

1. Herzberg,G.;"Molecular Spectra and Molecular structure",D.Van Nostrand,Inc:New York,1966;Chapter 1.p.40-51.

2. Englman,R.;"The Jahn-Teller Effect in Molecules and crystals", Wiley-Interscience:New York, 1972.

3. Bersuker,I.B.; "The Jahn-Teller Effect and Vibronic Interaction in Modern Chemistry", Plenum press: New York, 1983.

II.3 RAMAN Spectroscopy

II.3.1 Instrumentation

1. John R.Ferraro and Kazuo Nakamoto,Introductory Raman Spectroscopy,(Academic Press, inc ,1994).p.95.

2. Max Diem, Introduction to Modern vibrational spectroscopy, (Wiley, New York.1993), p. 109.

3. J.R.Lombardi.Encyclopidia of applied physics.15,509 (1996).

4. J.Michael Hollas, Modern Spectroscopy, (John Wiley &Sons, New York, 1993), P.64.

5. D.P.Shomaker,C.W.Garland, J.W.Nibler, Experiments in Physical Chemistry (McGraw-Hill, New York,1989).p.451.

II.3.3 Raman Excitation Spectroscopy

1. Thomas G.Spiro and Paul Stein, Ann. Rev.Phys .Chem. **28**,501(1977).

CHAPTER III. EXPERIMENTAL

1. D.M.Lindsay,F.Meyer,and W.Harbich, Z.Phys. **D12**, 15(1989).

2. W.Harbich,S.Fedrigo,F.Meyer,D.M.Lindsay, J.Lignieres J.C.Rivoal,and D.Kreisle,J.Chem.Phys. **93**,8535(1990).

3. R.Keller, in the Physics and Technology of Ion Sources, edited by I.G.Brown (Wiley, New York, 1989),Chap.7.

4. K.Besocke,S.Berger,W.O.Hofer,andU.Littmark, Radiat.Eff.**66**,35(1982).

5. G.A.Ozin and M.Moskovits, Cryochemistry, edited by Martin Moskovits and Geoffry A.Ozin (Wiley, New York,1976).

6. Beat Meyer, Low Temperature Spectroscopy (American Elsevier Publishing Company,Inc, New York,1971).

7. Eric Whittle, David A.Dows, and George C.Pimental. Matrix Isolation Method for the Experimental Study of Unstable Species(1954).

8. APD Cryogenics Inc.

CHAPTER IV.TRANSITION METAL DIMERS

IV.1 Raman spectra of mass-selected tantalum dimers in argon matrices:site effects

1. Beat Meyer, Low Temperature Spectroscopy (American Elsevier Publishing Company,Inc, New York, 1971).

2. Z.Hu, Bo.Shen,J.R.Lombardi, and D.M.Lindsay. J.Chem.Phys.**96**,8757(1992).

3. Z.Hu,Q.Zhou,J.R.Lombardi and D.M.Lindsay, Physics and Chemistry of Finite Systems: From Clusters to Crystals, Vol.II,969-976. 1992 Kluwer Academic Publishers.

IV.2 Raman spectra of mass-selected nickel dimers in argon matrices.

1. Z.Hu, B.Shen, Q. Zhou,S. Deosaran, J.R.Lombardi, D.M. Lindsay, W.Harbich, J.Chem.Phys.**95**,2206(1991).

2. Z.Hu, B.Shen, Q. Zhou,S. Deosaran, J.R.Lombardi, D.M. Lindsay,Proc.SPIE 1599,**65**(1992).

3. Z.Hu, Q. Zhou, J.R.Lombardi and D.M.Lindsay, in physics and chemistry of finite systems: From Clusters to Crystals, ed. by P.Jena, S.N.Khanna and B.K.Rao (Kluwer Academic Publishers, Dordrecht, 1992), pg.969.

4. Z.Hu, J-G.Dong,J.R.Lombardi, D.M. Lindsay, J.Chem. Phys.**97**,9263(1993).

5. Z.Hu, J-G.Dong,J.R.Lombardi, D.M. Lindsay, J.Chem. Phys.**97**,8811(1992).

6. Z.Hu, B.Shen, Q.'Zhou,S. Deosaran, J.R.Lombardi,D.M. Lindsay.J.Chem.Phys.**96**,8757(1992).

7. D.G.Leopold and W.C.Lineberger,J.Chem.Phys.**85**,51 (1986).

8. J.Dong, Z.Hu, R.Craig, J.R.Lombardi and D.M.Lindsay, J.Chem.Phys.**101**,9280(1994).

9. M.Moskovits and J.E.Hulse, J.Chem.Phys.**66**,3988(1977).

10. T.C.De Vore, A.Ewing, H.F.Franzen and V.Calder,Chem. Phys.Lett.**35**,78(1975).

11. Handbook of Physics and Chemistry, ed. by R.C.Weast(Chemical Rubber, Cleveland, 1989).

12. C.Cossé, M.Fouassier, T.Mejean, M.Tranquille, D.P.Dilella and M.Moskovits, J.Chem.Phys.**73**,6076 (1980).

13. G.Herzberg, Spectra of Diatomic Molecules (Van Nostrand,New York,1950).

14. J.Ho, M.L.Polak, K.M. Ervin, and W.C.Linberger, J.Chem.Phys.**99**,8542(1993).

15. W.C.Lineberger (private communication, 1995).

16. T.L.Haslett and M.Moskovits, J.Molec.Spectrosc. **135**,259(1989).

17. E.A.Rohlfing and J.J.Valentini,J.Chem.Phys. **84**,6560(1986).

18. T.H.Upton andW.A.Goddard, J.Am.Chem.Soc.**100**, 5659(1978).I.shim,J.P.Dahl and H.Johansen, Int.J.Quantum Chem.15,311(1979).J.O.Noell, M.D.Newton, P.J.Hay, R.L.Martin and F.W.Bobrowicz, J.Chem.Phys.**73**,2360(1980).

19. E.M.Spain and M.D.Morse, J.Chem.Phys.**97**, 4641(1992).

20. J.C.Pinegar, J.D.Langenberg, C.A. Arrington, E.M.Spain and M.D.Morse, J.Chem.Phys.**102**,666(1995).

21. Z.Hu, J-G.Dong, J.R.Lombardi, D.M.Lindsay and W.Harbich, J.Chem.Phys.**101**,95(1994).

22. A.M.James, P.Kowalczyk.R.Fournier and B.Simard, J.Chem.Phys.**99**,8504(1993).

IV.3 Spectroscopy of mass-selected rhodium dimers in argon matrices

1. M.D.Morse, Chem.Rev. **86**, 1049(1986).

2. S.R.Langhoff and C.W.Bauschlicher, Ann.Rev.Phys.Chem.**82**,5584(1985).

3. D.R.Salahub, in Ab Initio Methods in Quantum Chemistry II, edited by K. P. Lawley (Wiley, New York, 1987), p. 447.

4. I.Shim, Mat. Fys. Meddr. Danske. Vidensk. Selsk.16 Res. Dep.Of Neils Bohr Fellows **41**,147(1985).

5. K.Balasubramanian and D.Liao, J.Phys.Chem.**93**, 3989(1989).

6. F.Illas, J Rubio, J Canellas, and J.M.Ricart, J. Chem.Phys.**93**,2603(1996).

7. M.Harada and H.Dexpert, J.Phys.Chem.**100**, 565(1996).

8. D.L.Cocke, and K.A.Gingerich, J.Chem.Phys.**60**, 1958(1974).

9. Z.Hu, B.Shen, Q.Zhou, S.Deosaran, J.R.Lombardi, and D.M.Lindsay and W.Harbich, J.Chem.Phys.**95**, 2206(1991).

10. Z.Hu, B.Shen, J.R.Lombardi, and D.M.Lindsay, J.Chem.Phys.**96**,8757(1992).

11. Z.Hu, B.Shen, Q.Zhou, S.Deosaran, J.R.Lombardi, and D.M.Lindsay, Proc. SPIE **1599**,65(1991).

12. A.J.L.Hanlan and G.A.Ozin, Inorg.Chem.**16**,2848(1977). G.A.Ozin and A.J.L.Hanalan, Inorg.Chem.**18**,1781(1979).

13. G.Herzberg, *Spectra of Diatomic Molecules*(van Nostrand, Princeton, 1945).

14. Z.Hu, J.-G.Dong, J.R.Lombardi, and D.M.Lindsay, J.Chem.Phys. **101**, 95(1994), 65(1991).

IV.4 Raman spectrum of ruthenium dimers in argon matrices

1. Jian-Guo Dong, Zhendong Hu, Robert Craig, John R.Lombardi, and D.M Lindsay, J.Chem.Phys. **101**,9280(1994).

2. Huaiming Wang, Hanae Haouari, Robert Craig, John Lombardi and D.M.Lindsay,J.Chem.Phys.**104**,3420 (1996).

3. Huaiming Wang, Hanae Haouari, Robert Craig, John Lombardi and D.M.Lindsay, J.Chem.Phys.submitted for publication.

4. G.Sprintschink,H.Sprintschink,P.Kirsch, and D.G. whitten, J.A.C.S., **98**,2337(1976).

5. A.R.Miedma amd K.A.Gingerich,J.Phys.B,**12**,2081(1979)

6. F.A.Cotton, and I.Shim,J.A.C.S.,**104**,7025(1982).

7. K.K.Das and K.Balasubramanian, J.Chem.Phys. **95**,2568(1991).

8. H.Chen,M.Krasowski and G.Fitzgerald, J.Chem.Phys. **98**,8710(1993).

9. A.Goursot,L.Pedocchi, and B.Coq,J.Phys.Chem.**98**, 8747(1994).

10. M.Harada, H.Dexpert,J.Phys.Chem.**100**,565(1996).

11. Z.Hu,B.Shen, J.R.Lombardi and D.M.Lindsay, J.chem.Phys.**96**,8757(1992)

12. Z.Hu,B.Shen, J.R.Lombardi and D.M.Lindsay, J.chem. Phys.,**96**,8757(1992);Z.Hu,B.shen,Q.Zhou, S.Deosaran,

J.R.lombardi, and D.M.Lindsay, Proc.SPIE **65**,1599,(1991).

13. G.Herzberg, Spectra of Diatomic Molecules Van Nostrand, Princeton,(1945).

14. C.Kittel, Introduction to Solid State Physics Fifth Edition, John Wiley, and Sons, N.Y.

15. H.S.Johnston Gas Phase Reaction Rate theory, The Ronald Press,N.Y.(1966), p.72; see also L.Pauling, J.A.C.S.,**69**,542(1947).

16. Joe Ho, kent M.Ervin, Mark L.Polak, Mary K.Gilles, and W.C.Lineberger, J.Chem.Phys.**95**,4845(1991).

17. W.Schulze,H. U.Becker,P.Minkwitz,K.Manzel,Chem. Phys.Lett.55(1978),**59**.

IV.5 Bonding in transition metal dimers.

1. L.M.Russon,S.A.Heidecke,M.K.Birke,J.Conceicao,M.D. Morse, and P.B.Armentrout.J.Chem.Phys.**100**,4747(1993).

2. Dennise R.Salahub in Ab Initio Methods in Quantum Chemistry-II (Ed.K.P.Lawley),Wiley, New York, 1987.

CHAPTER V. TRANSITION METAL TRIMERS

V.1 Trimer review

1. Huaiming Wang,Robert Craig,Hanae Haouari,Jian-Guo Dong, Zhendong Hu,Alberto Vivoni,John R.Lombardi, and D.M.Lindsay,J.Chem.Phys.**103**,3289(1995).

2. Martin F.Jarrold and Kathleen M.Creegan,Chem.Phys.Letters,**166**,116(1989).

3. G.A.Bishea and M.D.Morse, J.Chem.Phys.**95**,5646(1991).

4. K.K Das and K.Balasubramanian, J.Mol.Spectry.**140**, 280(1990).

5. K.Balasubramanian,J.Chem.Phys.**87**,6573(1987).

6. K.Balasubramanian,J.Chem.Phys.**90**(1988)6310;**91**(1989) 307.

7. K.M.Ervin,J.Ho and W.C.Lineberger, J.Chem.Phys.**89**,4514(1988).

8. S.Taylor,G.W.Lemire,Y.Hamrick,Z.Fu and M.D.Morse, J.Chem.Phys.**89**,5517(1988).

9. K.Balasubramanian and D.W.Liao,J.Phys.Chem. **93**,3989(1989).

10. G.A.Ozin and A.L.J.Hanlan,Inorg.Chem.**18**,1781(1979).

11. D.L.Cocke and K.A.Gingerich,J.Chem.Phys.**60**,1958 (1974).

12. B.Simard,P.A.Hackett,A.M.James and P.R.P.Langridge-Smith,Chem.Phys.Letters **186**,415(1991).

13. I.Shim and K.A.Gingerich,J.Chem.Phys**78**,563(1983).

14. Z. Hu, B.Shen, Q.Zhou, S.Deosaran, J.R.Lombardi, D.M.Lindsay, and W.Harbich, J.Chem.Phys.**95**, 2206(1991).

15. Z.Hu, B.Shen, Q.Zhou, S.Deosaran, J.R.Lombardi, and D.M. Lindsay, Proc.SPIE 1599, **65**(1992).

16. Z.Hu, Q.Zhou, J.R.Lombardi, and D. M. Lindsay, in Physics and Chemistry of Finite Systems: From Clusters to Crystals, edited by P.Jena, S.N. Khanna, and B.K Rao(Kluwer Academic, Dordrecht, 1992), p. 969.

17. Z.Hu, J-G.Dong, J.R.Lombardi, and D.M.Lindsay, J.Phys.Chem.**97**,9263(1993).

18. Z.Hu, J-G.Dong, J.R.Lombardi, and D.M.Lindsay , J.Chem.phys.**97**,8811(1992).

19. Z.Hu, B.shen, J.R.Lombardi, D.M.Lindsay, J.Chem.Phys.**96**,8757(1992).

20. J-G.Dong, Z.Hu , R.Craig, J.R.Lombardi and D.M.Lindsay, J.Chem.Phys.**101**,9280(1994).

21. Z.Hu, J-G.Dong, J.R.Lombardi, D.M. Lindsay , J.Chem.Phys.**101**,95(1994).

22. Dingguo Dai and K.Balasubramanian, Chem.Phys.Lett. **195**,207(1992).

23. Kalyan K.Das and K.Balasubramanian,J.Chem.Phys. **93**,625(1990).

24. D.G.Dai, K.K.Das and K.Balasubramanian,Chem.Phys. Letters.**184**,589(1991).

25. K.Balasubramanian,J.Chem.Phys.**91**,307(1989).

26. Dingguo Dai and K.Balasubramanian,J.Chem.Phys. **98**,7098(1992).

27. Dingguo Dai and K.Balasubramanian,Chem. Phys.Letters.**231**,352(1994).

28. K.Balasubramanian and M.Z.Liao, Chem.Phys.Letters. **127**,313(1988).

29. K.Balasubramanian and M.Z.Liao,J.Chem.Phys. **86**,5587(1987).

30. Stephen P.Walch, and Charles W.Bauschlicher,Jr.and Stephen R.Langhoff J.Chem.Phys.**85**,5901(1986).

31. Stephen P.Walch, J.Chem.Phys.**86**,5082(1986).

32. Stephen P.Walch, J.Chem.Phys.**87**,6776(1987).

33. Stephen P.Walch and Charles W.Bauschlicher,Jr. J.Chem.Phys.**83**,5735(1985).

34. Hanae Haouari,Huaiming Wang, Robert Craig,John R.Lombardi, and D.M.Lindsay, J.Chem.Phys.**103**, 9527(1995).

35. H.Wang,R.Craig, H.Haouari,Y.Liu,J.R.Lombardi, and D.M.Lindsay. submitted to J.Chem.Phys.

36. G.Delacretaz,E.R.Grant,R.L.Wetten,L.Woste and J.W.Zwanziger,Phys.Rev.Letters**56**,2598(1986).

37. M.D.Morse,J.B.Hopkings.P.R.P.Langridge-Smith and R.E.Smalley, J.Chem.Phys.**79**,5316(1983).

38. E.A.Rohlfing and J.J.Valentini,Chem.Phys.Letters **126**,113(1986).

39. W.H.Crumley,J.S.Hayden and J.L.Gole,J.Chem.Phys.**84**, 5250(1986).

40. A.D.P.Dilella,K.V.Taylor and M.Moskovits, J.Chem.Phys.87(1983)524. M.Moskovits,Chem.Phys. Letters.**118**,111(1985).

41. D.G Truhlar,T.C.Thompson and C.A.Mead, Chem.Phys.Letters,**127**,287(1986).T.C.Thompson,D.G Truhlar, and C.A.Mead J.Chem.Phys.**82**,2392(1985).

42. J.W.Zwanziger,R.L.Wetten and E.R.Grant,J.Phys. Chem.**90**,3298(1986).

43. M.D.Morse, Chem.Phys.Letters,**133**,8(1987).

44. K.D.Bier,T.L.Haslett, A.D.Kirkwood and M.Moskovits, J.Chem.phys.**89**,6(1988).

45. R.Englman, The Jahn-Teller Effect in Molecules and Crystals (Wiley-Interscience 1972).

46. G.Herzberg,Molecular spectra and molecular structure, III.Electronic spectra and electronic structure of polyatomic molecules.pg40.(D.Van Nostrand company,Inc.)

47. P.Y.Cheng and M.A.Duncan,Chem.Phys.Lett,**152**,341 (1988).

48. M.Moskovits and D.P.Dilella,J.Chem.Phys.**72**,2267 (1980).

49. R.J.Van Zee,Y.M.Hamrick, S.Li and W.Weltner Jr.Chem. Phys.Lett.**195**,214(1992).

50. Dingguo Dai,K.Balasubramanian,Chem.Phys.Lett.**195**,207 (1992).

51. L.B .Knight,Jr. and R.W.Woodward,J.Chem.Phy.**79**,5820 (1983).

52. D.R.Herschbach and V.W.Laurie.J.Chem.Phys,**35**,458 (1961).

52. J.C.Weisshaar,J.Chem.Phys.**90**,1429(1989).

53. Bregory A.Bishea and Michael D.Morse,J.Chem.Phys.**95**, 8779(1991).

54. H.Hua Wang and Emily A.Carter.J.Phys.Chem.**96**, 1197(1991).

55. Muller,U.; Sattler,K.;Xhie.J.;Venkateswaran,N.; Raina, G.J.Vac.Sci.Technol.B 1991, **9**, 829.

56. K.Balasubramanian.J.Chem.Phys.**91**,307(1989).

57. J.A.Howard and R.Sutcliffe and B.Mille, Surface Science **156**,214-227(1985) .

V.2 Resonance Raman spectrum and excitation profiles of mass-selected zirconium trimers

1. K. Balasubramanian and Ch. Ravimohan, J.Chem.Phys. **92**,3659(1990).

2. C.W. Bauschlicher,Jr., H. Partridge, S.R. Langhoff, and M. Rosi, J.Chem.Phys.**95**,1057(1991).

3. Z.Hu, Q.Zhou, J.R. Lombardi, and D.M. Lindsay, Physics and Chemistry of Finite Systems: From Clusters to Crystals, Vol. II, 969, P.Jena et.al.(eds), Kluwer Academic Publishers, The Netherlands.

4. D.Dai and K.Balasubramanian, Chem.Phys.Lett.,**231**,4 (1994).

5. D.Dai and K.Balasubramanian, Chem.Phys.Lett.**193**, 565(1992).

6. Z.Hu, B.Shen, Q.Zhou, S.Deosaran, J.R.Lombardi,D.M. Lindsay and W.Harbich, J.Chem.Phys.**95**,2206 (1991).

7. Z.Hu, B.Shen, Q.Zhou, S.Deosaran, J.R.Lombardi and D.M.Lindsay, Proc. SPIE **1599**,65(1992).

8. Z.Hu, Q.Zhou, J.R.Lombardi and D.M.Lindsay, in Physics and Chemistry of Finite Systems: from Clusters to Crystals, ed. by P. Jena, S. N. Khanna and B. K. Rao (Kluwer Academic Publishers, Dordrecht, 1992), pg. 969.

9. Z.Hu, J.-G. Dong, J.R.Lombardi and D.M.Lindsay, J. Phys.Chem.**97**,9263(1993).

10. Z.Hu, J.-G. Dong, J.R.Lombardi and D.M.Lindsay, J.Chem.Phys.**97**,8811(1992).

11. Z.Hu, B.Shen, J.R.Lombardi and D.M.Lindsay, J. Chem.Phys.**96**,8757(1992).

12. G.Herzberg, Infrared and Raman Spectra of Polyatomic Molecules,D.VanNostrand, Princeton (1945).

13. G.A.Ozin and D.F.McIntosh, J.Phys.Chem.**90**,5756 (1986).

14. I.B.Bersuker, The Jahn-Teller Effect and Vibronic Interactions in Modern Chemistry,Plenu Press, NY (1983).

15. Ulf Sassenberg (private communication, 1996).

V.3 Spectroscopy of mass-selected niobium trimers in argon matrices

1. Huaming Wang, Robert Craig, Hanae Haouari, J-G.Dong, Zhendong Hu, Alberto Vivoni, John R.Lombardi and D.M. Lindsay, J.Chem.Phys.**103**,3289(1995).

2. Hanae Haouari, Huaming Wang, Robert Craig, John R.Lombardi and D.M.Lindsay, J.Chem.Phys.**103**,9527 (1995).

3. D.P.Dilella,W.Limm,R.H.Lipson,M.Moskovits,andK. V.Taylor;J.Chem.Phys.**77**,5263(1982).

4. K.D.Bier,T.L.Haslett, A.D.Kirkwood,and M.Moskovits ; J.Chem.Phys.**89**,6(1988).

5. Martin Moskovits and Daniel P.Dilella;J.Chem. Phys,**72**,2267(1979).

6. R.J.Van Zee,Y.M.Hamrick,S.Li and W.Weltner Jr ; Chem.Phys.Lett,**195**,214(1992).

7. Gregory A.Bishea and Michael D.Morse;J.Chem. Phys,**95**,8779(1991).

8. Gregory A.Bishea, Caleb A.Arrington, Jane M.Behm and M.D.Morse; J.Chem.Phys.**95**,8765(1991).

9. Martin F.Jarrold and Kathleen M.Greegan; International Journal of mass spectrometry and ion processs, **102**,161(1990).

10. Z.Hu,Q.Zhou,J.R.Lombardi, and D.M.Lindsay, Physics and Chemistry of Finite Systems: From Clusters to Crystals,edited by P.Jena et.al.(Kluwer, the Netherlands,1994),Vol.II,p.969.

11. Z.Hu,B.Shen,Q.Zhou,S.Deosaran,J.R.Lombardi,D.M. Lindsay,andW.Harbich,J.Chem.Phys.**95**,2206(1991).

12. Z.Hu,B.Shen,Q.Zhou,S.Deosaran,J.R.Lombardi,D.M. Lindsay,Proc.SPIE ,1599,**65**(1992).

13. Z.Hu,Q.Zhou,J.R.Lombardi, and D.M.Lindsay, in Physics and Chemistry of Finite Systems: From Clusters to Crystals,edited by P.Jena,S.N.Khanna, and B.K.Rao(Kluwer, the Dordrecht,1992), p.969.

14. Z.Hu,J-G.Dong, J.R.Lombardi, and D.M.Lindsay, J.Chem.Phys.**97**,9263(1993).

15. Hu,J-G.Dong, J.R.Lombardi, and D.M.Lindsay, J.Chem.Phys.**97**,8811(1992).

16. Hu,B.Shen,J.R.Lombardi,and D.M.Lindsay, J.Chem.Phys.**96**,8757(1992).

17. Thomas G.Spiro and Paul Stein, Ann.Rev.Phys. Chem.**28**,501(1977).

18. Dingguo Dai,K.Balasubramanian,Chem.Phys.Lett, **231**,352(1994).

19. M.D.Morse,Chem.Rev.**86**,1049(1986).

20. M.M.Kappes, chem.Rev.**88**,369(1988).

21. H.Sellers,J.Phys.Chem.**94**,1338(1990).

22. S.K.Loh,Li Lian, and P.B.Armentrout,J.Am.Chem.Soc. **111**,3167(1989).

23. M.B.Knicklbein and S.Yang, J.Chem.Phys.**93**,5760(1990).

24. A.R.Gee,D.C.O'Shea, and H.Z.Cummins,Solid State Commun.4,43(1965).

25. G.herzberg,Infrared and Raman Spectra of Polyatomic Molecules (Van Nostrand, Princeton, 1945).

26. E.B.Wilson, Jr.,J.C.Decius, and P.C.Cross, Molecular Vibrations(McGraw-Hill,New York,1971).

CHAPTER VI. TRANSITION METAL TETRAMER

1.Absorption and Raman spectroscopy of mass-selected Tantalum tetramers in argon matrices.

1. Z.Hu, B.Shen, Q Zhou, S.Deosaran, J.R.Lombardi,D.M. Lindsay and W.Harbich, J.Chem.Phys.**95**,2206(1991).

2. Z.Hu, B.Shen, Q.Zhou, S.Deosaran, J.R.Lombardi and D.M.Lindsay, Proc.SPIE **1599**,65 (1992).

3. Z.Hu, Q.Zhou, J.R.Lombardi and D.M.Lindsay, in Physics and Chemistry of Finite Systems: from Clusters to Crystals, ed. by P. Jena, S.N.Khanna and B. K. Rao (Kluwer Academic Publishers, Dordrecht, 1992), pg. 969.

4. Z.Hu, J.-G. Dong, J.R.Lombardi and D M.Lindsay, J. Phys.Chem.**97**,9263(1993).

5. Z.Hu, J.-G. Dong, J.R.Lombardi and D.M.Lindsay, J.Chem.Phys.**97**,8811(1992).

6. Z.Hu, B.Shen, J.R.Lombardi and D.M.Lindsay, J. Chem.Phys.**96**,8757(1992).

7. C.S.Venkateswaran, Proc. Ind. Acad. Sci.,**2A**,260 (1935).

8. H.S.Gutowsky and C.J.Hoffman, J.Am.Chem.Soc.**72**, 5751(1950).

9. L.R.Maxwell, S.B.Hendricks,and V.M.Mosley, J.Chem.Phys.**3**,699(1935).

10. C.D.Thomas and N.S.Gingrich, J.Chem.Phys.**6**,659 (1938).

11. F.J.Kohl, O.M.Uy, and D.Carlson, J.Chem.Phys.**47**, 2667(1967).

12. V.E.Bondybey and J.H.English, Chem.Phys.**73**,42, (1980).

13. M.Morse (private communication 1995).

14. G.A.Ozin and D.F.McIntosh, J.Phys.Chem.**90**,5756 (1986).

15. E.C.Honea,A.Ogura,C.A.Murray,K.Raghavachari,W.O. Sprenger,M.F.Jarrold, and W.L.Brown, Nature, **366**,41 (1993).

16. R.J.VanZee,C.A.Baumann, and W.Weltner, J.Chem.Phys. **82**,3912(1985).

17. G.Herzberg, Infrared and Raman Spectra of Polyatomic Molecules, D.VanNostrand, Princeton (1945).

18. I.B.Bersuker The Jahn-Teller Effect and Vibronic Interactions in Modern Chemistry,Plenum Press, N.Y. (1984).